



NTNU – Trondheim
Norwegian University of
Science and Technology

Analysis of Explosion Load Effects in Pipe-racks

Explosion simulation and its respective
structural response on pipe-racks on a
offshore topside module

Aiwei Su

Marine Technology

Submission date: May 2012

Supervisor: Bernt Johan Leira, IMT

Norwegian University of Science and Technology
Department of Marine Technology

Preface

This paper represents the work conducted in the spring semester of 2012, as a part of TMR4900; Master Thesis at the Institute of Marine Technology, Department of Marine Structures at NTNU (The Norwegian University of Science and Technology).

I would like to thank my supervisor Prof. Bernt J. Leira for modifying the project text on the basis of the initial scope of project as proposed by Aker Solutions (Aker Engineering and Technology) in Oslo, and also for his valuable support and guidance throughout the work process. I would also like to extend my thanks to the contact persons at Aker Solutions; Anne Bolstad and Øyvind Andersen for coming up with suggestions on the topic descriptions and the overall scope of project. They have also been helpful in providing me with necessary structural drawings, and answering questions I've had along the way.

Finally I would like to thank key personnel at the library at the Marine Technology Center for their help with locating relevant literature.

The workload of this thesis turned out to be manageable within the time scope of the spring semester. The completed thesis is roughly separated into three parts; The first part being a literature study where previous work done by various sources are presented. The second part is a modeling and analysis part where the pre-processing work is described in detail. The third part is a result and discussion part where the post-processing work is presented. Emphasis in the second and third part of this project, has been on familiarization with the modeling and analysis capabilities in Abaqus/CAE Standard and the explicit package (Abaqus/Explicit), together with post-processing and visualization of results using Python and Matlab scripting.

Aiwei Su, Trondheim. May 28, 2012

Abstract

An explosion on a typical offshore installation is a critical, however rare accidental event which may result in damage and loss of property, and in the worse case loss of lives. Top-side sections on an offshore installation which are exposed to an explosion blast should be designed to withstand such an event in a way that further escalation of the damage on personnel or property is avoided. There is however limited information on the modeling and analysis procedures for dealing with such events, and most classification rules on this subject give limited information and guidelines on the practical implementation of such effects for general analysis purposes. This thesis has been an investigation on these matters.

The basis of this Master thesis has been on a pipe rack structure from one of Aker Solutions' top-side projects. It has been assumed that this structure is exposed to an accidental hydrocarbon explosion, and the resulting structural response has been investigated. A parameter study has been performed by varying blast load levels and durations. The effects due to the weight of the piping on the structure have also been studied. The main task of this thesis has been to compare simplified, static analysis models against dynamic analysis models as to calculate dynamic amplification factors (DAF), the purpose of this is to better understand the dynamic behavior of the structure due to the blast loading. The intention is that the dynamic amplification factors are to be used further by the engineers at Aker Solutions for dimensioning and designing of similar structures.

Results showed that the blast loads as used in the analyses did not cause any structural responses within the material's plastic range. Further on, it was found that the magnitude of dynamic amplification is depending on both the blast duration *and* the weight of the pipes on the pipe rack. Typical results indicated that this dynamic amplification was reduced with increased blast duration.

Sammendrag

En eksplosjon på en offshore-installasjon er en kritisk, men sjelden ulykkeshendelse som kan føre til store ødeleggelser, skade på struktur og i det verste tilfellet tap av liv. Top-side seksjonen på en offshore-installasjon som kan være eksponert for eksplosjonsulykker bør designes på en slik måte at eskalering av allerede påført skade på struktur eller personell unngås. Det er desverre begrenset informasjon å finne om konkrete modellering og analyseprosedyrer, og de fleste klasseregler på dette området er svært generelle og gir begrenset informasjon og veiledning omkring den praktiske implementeringen av slike eksplosjonslaster for generelle analyser. Gjennom arbeidet med denne oppgaven har den praktiske implementeringen av eksplosjonslaster i forhold til dynamiske analyser blitt undersøkt.

Utgangspunktet for denne oppgaven har vært et rørstativ fra et av Aker Solutions' top-sideprosjekter. Det har blitt antatt at strukturen har blitt eksponert for en hydrokarboneksplosjon, og den resulterende strukturelle responsen har blitt undersøkt. Et parameterstudie har blitt utført gjennom å variere eksplosjonslast og varighet. Effekten av å ha forskjellig vekt på rørene på stativet har også blitt undersøkt. Hovedfokuset i oppgaven har vært å beregne dynamisk amplifikasjonsfaktorer (DAF), med den hensikt å øke forståelsen for hvordan strukturen responderer på eksplosjoner. Disse faktorene vil videre kunne brukes av ingeniører hos Aker Solutions for dimensjonering og design av liknende strukturer. Resultater viste av eksplosjonslastene som brukt i analysene ikke førte til strukturell respons innenfor materialets plastiske område, videre ble det også påvist at mengden dynamisk amplifikasjon er sterkt avhengig av både eksplosjonsvarighet og rørvekten på stativet. Typiske resultater indikerte av den dynamiske amplifikasjonen ble redusert med økt eksplosjonsvarighet.

Contents

1	Introduction	1
1.1	Explosion incident event tree	1
1.2	General introduction on explosion/blast loads	2
1.3	Deflagrations and detonations	3
2	Interaction between blast and structure	6
2.1	Reflection load	6
2.2	Dynamic pressure	9
2.3	Load on a structure	11
3	Structural response	12
3.1	Dynamic analysis	12
3.1.1	SDOF-methods	13
3.1.2	MDOF-methods	14
3.2	Geometric non-linearity	14
3.3	Damping	15
3.4	Solution methods for non-linear analyses	18
3.4.1	Implicit integration method	18
3.4.2	Explicit integration method	18
4	Blast loads on topside structural elements	19
4.1	Mitigation schemes	21
4.2	Pipe rack system	22
4.3	Pressure distribution and magnitude	26
4.4	Ductility Level Analysis	28
5	Analysis by Abaqus	30
5.1	Modeling of geometry	31
5.2	Material settings	31
5.3	Structural elements	33
5.4	Model mesh	36
5.4.1	Mesh sensitivity (Convergence study)	36

5.4.2	CPU-time	39
5.5	Mass model	40
5.6	Load model	42
5.7	Boundary conditions	45
5.8	Geometric non-linearity	45
5.9	Damping model	45
5.10	Step settings	50
5.10.1	Self-weight	50
5.10.2	Blast	53
5.10.3	Post-blast	53
5.10.4	Incrementation settings	53
5.11	Post-processing	54
5.11.1	Field-Output settings in Abaqus	54
5.11.2	Integration and section points in Abaqus	56
5.11.3	Scripting in Abaqus and Matlab	57
6	Analysis results	58
6.1	Eigenmodes and eigenfrequencies	58
6.2	Static analyses	59
6.3	Dynamic analyses with simplified blast load model	62
6.4	Dynamic Amplification Factors (DAF)	66
6.4.1	Stress (Von-Mises) at critical locations	66
6.4.2	Reaction Forces (Support Reactions)	78
7	Discussion of results	84
7.1	Static and dynamic analyses	84
7.2	DAF for critical locations on the pipe rack	85
7.2.1	Using the upper bound (Method A)	86
7.2.2	Averaging over all elements, use the upper bound (Method B)	87
7.2.3	Averaging over all elements, use curve fit techniques (Method C)	89
7.2.4	Summary	93
7.3	DAF for support reactions	94
7.3.1	Using the upper bound (Method A)	94
7.3.2	Averaging over all nodes, use the upper bound (Method B)	94
7.3.3	Averaging over all nodes, use linear curve fit (Method C)	95
7.3.4	Summary	100
8	Conclusion and further work	102
8.1	Conclusion	102
8.2	Recommendations for future work	103
	Bibliography	105

A Piping weight	A. 1
B Response range corresponding to eigenmodes	B. 1
C Pipe span chart	C. 1
D Python Script for extracting RF (Magnitude)	D. 1
E Python Script for extracting RF (X, Y and Z-direction)	E. 1
F Variation of DAF against blast duration.	F. 1
G Variation of DAF against piping weight (arrangement).	G. 1
H Variation of V.M stresses along path/beam.	H. 1
I Matlab script: Read in data and calculate DAF.	I. 1

List of Figures

- 1.1 Explosion event tree. From the lecture notes by J.Amdahl. TMR 4195 Design of Offshore Structures, 2009. 2
- 1.2 Characteristic shape of the pressure diagram for a) shock wave (detonation), and b) pressure wave (deflagration)[1]. 3
- 1.3 Simplified pressure diagram for a) shock wave (detonation), and b) pressure wave (deflagration)[1]. 4
- 1.4 Important factors to be considered when idealising a blast load with respect to the assumed structural response [2]. 5

- 2.1 Reflection coefficients for different values of the overpressure, as functions of the angle of incidence[1]. 7
- 2.2 Schematic representation of the disturbance of the blast for a box shaped structure [1]. 8
- 2.3 A schematic representation of the pressure variation through time is shown for a finite reflective surface [1]. 9
- 2.4 Drag coeffecients given for various simple structural shapes [1]. 10
- 2.5 A schematic representation of the pressure variation through time is shown for a finite reflective surface [1]. 11

- 3.1 Simple beam subjected to a static load [3]. 13
- 3.2 The SDOF method implemented on a stiffened plate blast response problem [4] 14
- 3.3 Variation of damping ratio with respect to response or natural frequency [5]. 17

- 4.1 Typical topside module arrangement [6]. 20
- 4.2 Figure showing the importance of proper ventilation as to reduce the effects of an explosion[4]. 21
- 4.3 Importance of correct positioning of equipment in case of an explosion event [4]. 21
- 4.4 Blast scenario with pressure release. Dynamic pressure attacking perpendicular on the pipe rack. 22
- 4.5 PDMS (Plant design manager system) CAD representation of the processing area and the pipe rack position. Figure provided by Aker Solutions. . 23

4.6 Isolated view of the pipe rack and neighbouring structural elements, with dynamic pressure attacking perpendicular to the span of the pipe rack. 24

4.7 The pipe rack is welded directly to the upper deck girders as shown. The pipe rack is also connected to the primary structure (column) as shown marked with green. 24

4.8 www.reliner.com, showing a typical pipe bracket for the offshore industry. 25

4.9 PDMS (Plant Design Manager System) 3D representation of a part of the pipe rack with pipes and U-brackets. Visualization provided by Aker Solutions. 25

4.10 The weight of a pipe is assuming to be represented as point loads on the structure. 26

4.11 Simplified pressure diagram as provided from Aker Solutions for the dynamic pressure. According to Aker Solutions, the under-pressure will have an absolute value of about 10% of the initial over-pressure. 27

5.1 Stress-strain capacity table, provided by Aker Solutions (from project scope) 32

5.2 Stress-strain capacity curve, provided by Aker Solutions (from project scope) 32

5.3 Euler-Bernoulli beam formulation [7]. 33

5.4 Timoshenko beam formulation accounts for the additional shear angle [7]. 33

5.5 Bending of Timoshenko beam [8]. 34

5.6 Force and moment equilibrium for an infinitesimal segment of the beam. 35

5.7 Figure showing the eigen modes for a particular beam with both ends clamped. 36

5.8 Showing the variation in global seeding for three different kind of seeding densities. 37

5.9 Showing the two beams used in the stress convergence study. 38

5.10 Mesh sensitivity for beam 1 and 2. Blast duration 50 ms, 0.2 bar drag pressure. 39

5.11 Variation in CPU time for different mesh sizes. A trend line was created based on these data, a power function can be derived from these. This function gives the required CPU time (y) for a given input x (mesh size). 40

5.12 Inertia properties (point masses) assigned to represent piping weight . . . 41

5.13 Illustration of piping arrangement 1, 2 and 3. 42

5.14 Line load applied on the beam elements in Abaqus 43

5.15 Amplitude toolset (tabular feature) in Abaqus 44

5.16 Triangular pressure load profile corresponding to the input given in the amplitude toolset (see also diagram provided by Aker Solutions in figure 4.11. Td is the duration of the blast, it is assumed to be between 50 and 200 ms) 44

5.17 Fixed boundary conditions (in all 6 DOFs) are added to the connections between pipe rack and the rest of the structure 45

5.18 Figure illustrating the damping effect (stiffness proportional damping) for the lowest eigenmode, position: element 899, Section point (SP) 13. Von-Mises stress variation [Pa] over blast and post-blast domain. 47

5.19 Figure illustrating the damping effect (stiffness proportional damping) for the lowest eigenmode, position: element 899, Section point (SP) 13. Von-Mises stress variation [Pa] over blast domain only. 48

5.20 Figure illustrating the damping effect (stiffness proportional damping) for the lowest eigenmode, position: Node 152. Reaction force [N] in the blast direction (Y-direction) over blast domain only. 49

5.21 Stress variation for element 424, 50 ms blast duration, 1 second post-blast step. Stresses given for 4 integration points. Linearly applied structural self-weight and piping weight. 51

5.22 Stress variation for element 424, 50 ms blast duration, 1 second post-blast step. Stresses given for 4 integration points. Instantaneously applied structural self-weight and piping weight as for piping arrangement 1. . . . 52

5.23 Figure illustrating the effect of aliasing on a sinusoidal curve [9]. 54

5.24 Figure illustrating the effect of aliasing for element 424. Aliasing effects cause a misleading representation of the post-blast response. 55

5.25 Numbering of integration points for output [10]. 56

5.26 Section points for rectangular hollow section (RHS profile), beam in space. The four standard section points are 1, 5, 9 and 13 [10]. 56

6.1 High stress area for the cases with pipe rack including piping arrangements 1,2 and 3. 60

6.2 High stress area for the case with pipe rack only, no piping weight applied. 61

6.3 Illustration of the structural response during blast and post-blast. 62

6.4 Stress (High stress areas marked red. Boundary conditions are marked green. 63

6.5 Dynamic response with respect to Von-Mises stresses on element 614 due to change in piping arrangement (Green curve represents arrangement 3, blue curve is the pipe rack without piping weight). The characteristic response peak is seen during the blast for all three cases. 64

6.6 Variation of reaction force in Y-direction (blast-direction) for 4 selected nodes at end connections. 65

6.7 The difference between method 1 and method 2 for extracting stresses for calculating the DAF. 67

6.8 An example of maximum dynamic stress extraction from the blast step. Section points 1 and 5 (red and blue curve represent the highest stresses during the blast step). 68

6.9 Variation of DAF with respect to blast duration for method 1 and 2. . . 69

6.10 The locations of the 12 selected elements to be used for the extended DAF calculations. 69

6.11 An example of DAF values obtained from the 50 ms blast case, for arrangement 1. The DAFs are calculated for four section-points separately, in addition to the average of all section points. 70

6.12 Plot of the variation of DAF with respect to blast duration, for all 4 section points for all 12 elements (0.4 bar, arrangement 3). The high DAFs represented by the response from element 689 and 702 are clearly expressed by the graph. 70

6.13 By removing the contribution from element 689 and 702, a more general picture of the response is seen. It should be emphasized that the response expressed by these DAFs represents 91.7% of the total number of DAFs for this particular piping arrangement. 71

6.14 Plots of the variation of DAF with respect to blast duration for all section points, for the different piping arrangements. Blast drag pressure 0.2 bar. It is shown from these figures that the magnitude of the DAF decreases with increasing blast duration. It should be noted that the data points for element 689 and 702 have been removed in this figure. 72

6.15 Plots of the variation of DAF with respect to blast duration for all section points, for the different piping arrangements (neglecting the DAFs from element 689 and 702). Blast drag pressure 0.4 bar. It should be noted that most DAF values are below 2, with exceptions of some elements in the 50 ms blast case. It is shown from these figures that the DAF decreases with increasing blast duration. 73

6.16 The following figure illustrates the scattering of data points for DAFs as line plots. The largest concentration of data points are located roughly between 0.5 and 2. The extreme DAF points only represent a small number of points. Please note that the range of scattering is largest for the 50 ms blast case. When looking at the 50 ms 0.2 bar blast case, 90.6% of the DAFs are below 2. For the 50 ms 0.4 bar blast case, 85.4% of the DAFs are below 2. 75

6.17 The following figure illustrates the scattering of data points for DAFs as line plots. The once four DAFs for each element is now reduced to one averaged DAF, this reduced the size of the scattering range of data points. Once again, it should be emphasized that the majority of DAFs are below the value of 2. 76

6.18 The following scatter plots illustrate the scattering of data points for DAFs (averaged section points). These plots do not contain the data points from element 689 and 702. 77

6.19 The variation of DAF plotted against piping weight (arrangement) as a scatter plot. The figure illustrates the scattering of data points. These plots do not contain the data points from element 689 and 702. 78

6.20 Location and node numbering for the extraction of reaction forces. 79

- 6.21 Coordinate system with respect to the direction of the blast, and the direction of the gravity. 80
- 6.22 Variation of DAF (based on reaction force in X-direction) with respect to blast duration. Please note that most DAFs are below 10, with the exception of the DAF for nodes 65, 95, 71 and 158. 81
- 6.23 Variation of DAF (based on reaction force in Y-direction) with respect to blast duration. The Y-direction is the direction of the blast. The majority of the DAFs are found to be below 1.5. 82
- 6.24 Variation of DAF (based on reaction force in Z-direction) with respect to blast duration. The Z-direction is the direction of the gravity. Please note that the majority of the DAFs are below 1.5. 83

- 7.1 Showing the response stress peak observed under blast. The figure also show that the differences between the lowest and highest stresses (Delta peak stress) remain almost constant for the different piping weights during the blast. This indicates that the stress response *during* the blast may be independent of the piping weight. 85
- 7.2 Upper bound values for DAF, method A. 0.2 bar blast pressure (not including data points from element 689 and 702). 86
- 7.3 Upper bound values for DAF, method A. 0.4 bar blast pressure (not including data points from element 689 and 702). 87
- 7.4 Upper bound values for DAF, method B. 0.2 bar blast pressure. 88
- 7.5 Upper bound values for DAF, method B. 0.4 bar blast pressure. 88
- 7.6 Variation of DAF with respect to blast duration, method C. Please note that this graph does not include the averaged data points from element 689 and 702. 89
- 7.7 Variation of DAF with respect to blast duration, method C. The following graph includes the averaged data points from element 689 and 702. 90
- 7.8 Variation of DAF with respect to arrangement (piping weight), method C. The following graph does not include the averaged data points from element 689 and 702. 91
- 7.9 Variation of DAF with respect to arrangement (piping weight), method C. The following graph includes the averaged data points from element 689 and 702. 92
- 7.10 According to method A, the DAF value can be taken directly from the upper bound. 94
- 7.11 According to method B, the DAF value can be taken directly from the upper bound from the averaged DAF over all nodes. 95
- 7.12 Linear least squared curve fit for the data points of RF1 (Reaction force in X-direction), DAF vs. blast duration. 96
- 7.13 Linear least squared curve fit for the data points of RF2 (Reaction force in Y-direction; direction of blast), DAF vs. blast duration. 96

7.14 Linear least squared curve fit for the data points of RF3 (Reaction force in Z-direction; direction of gravity), DAF vs. blast duration. 97

7.15 Linear least squared curve fit for the data points of RF1 (Reaction force in X-direction), DAF vs. piping arrangement. 98

7.16 Linear least squared curve fit for the data points of RF2 (Reaction force in Y-direction; direction of gravity), DAF vs. piping arrangement. 99

7.17 Nonlinear least squared curve fit for the data points of RF3 (Reaction force in Z-direction; direction of gravity), DAF vs. piping arrangement. 99

A.1 Piping weight recalculated as concentrated masses in Excel. A. 1

C.1 Span chart provided by Aker Solutions C. 1

F.1 The following graph shows the variation of DAF for the first section points with respect to blast duration, using method 1 to extract the stresses. Stress is taken for one element per case only F. 1

F.2 The following graph shows the variation of DAF for the first section points with respect to blast duration, using method 2 to extract the stresses. Stress is taken for one element per case only F. 2

G.1 Averaged DAF plotted against piping weight (arrangement) for all elements. 0.2 bar blast drag pressure. G. 1

G.2 Averaged DAF plotted against piping weight (arrangement) neglecting the data points for element 689 and 702. 0.2 bar blast drag pressure. G. 2

G.3 Averaged DAF plotted against piping weight (arrangement) for all elements. 0.4 bar blast drag pressure. G. 2

G.4 Averaged DAF plotted against piping weight (arrangement) neglecting the data points for element 689 and 702. 0.4 bar blast drag pressure. G. 3

H.1 Integrated Von-Mises stress along path, horisontal beam 1. H. 1

H.2 Integrated Von-Mises stress along path, horisontal beam 2. H. 2

H.3 Von-Mises stress variation along path, horisontal beam 1. H. 3

H.4 Von-Mises stress variation along path, horisontal beam 2. H. 4

List of Tables

- 1.1 Definition of response domains by various sources 4
- 3.1 Damping ratios for different structural systems 17
- 4.1 Occurrence events on the North Sea Platforms in the UK, Norwegian and Dutch sector for 25 years (1973-97) [11] 28
- 4.2 Ductility values for design of topside offshore installations 29
- 4.3 Damage levels - Ductility ratios 29
- 5.1 Approximate global sizes with its corresponding mesh size for the pipe rack beam model 37
- 5.2 Damping constants used for the investigation of the damping effect on the structural response 46
- 6.1 Results from the static simplified model with 0.2 bar drag pressure for two different section points. 60
- 6.2 Results from the static simplified model with 0.4 bar drag pressure for two different section points. 60
- 7.1 DAF for 0.2 bar drag pressure (DAF vs. blast duration). The values in parentheses are the DAF accounted for element 689 and 702. 93
- 7.2 DAF for 0.4 bar drag pressure (DAF vs. blast duration). The values in parentheses are the DAF accounted for element 689 and 702. 93
- 7.3 DAF for different piping arrangements found by method C. Arrangement 1 being the heaviest loaded condition. The values in parentheses are the DAFs accounted for element 689 and 702. 93
- 7.4 DAF values for support reactions (reaction forces) in X-direction. The values in parentheses are the DAF for 0.4 bar drag pressure. 100
- 7.5 DAF values for support reactions (reaction forces) in Y-direction (direction of the blast). The values in parentheses are the DAF for 0.4 bar drag pressure. 100

7.6 DAF values for support reactions (reaction forces) in Z-direction (direction of the gravity). The values in parentheses are the DAF for 0.4 bar drag pressure. 100

7.7 DAF values for support reactions (reaction forces) in X-direction. The values in parentheses are the DAFs for 0.4 bar drag pressure. 101

7.8 DAF values for support reactions (reaction forces) in Y-direction. The values in parentheses are the DAFs for 0.4 bar drag pressure. 101

7.9 DAF values for support reactions (reaction forces) in Z-direction. The values in parentheses are the DAFs for 0.4 bar drag pressure. 101

Nomenclature

P_s	incident peak overpressure
t_p	positive phase duration
i_s	impulse
P_r	reflection pressure
P_D	dynamic (drag) pressure
t_s	time in which P_r decreases to P_s and P_D
S	characteristic dimension of a surface exposed to a blast
U	velocity
c_0	velocity of sound in air
p_0	atmospheric pressure
C_D	drag coefficient
ρ_s	air density within a blast
$u_s(t)$	velocity of combustion products
k_{lm}	load mass transformation factor
x	maximum plastic displacement
x_{el}	maximum elastic displacement
μ	ductility ratio, coefficient of kinetic friction
σ	nominal (engineering) stress
σ_{true}	true (cauchy) stress
ϵ	nominal (engineering) strain
ϵ_{true}	true (cauchy) strain
σ_{Mises}	Von Mises stress
σ_y, σ_f	yield stress, stress in y-direction
σ_{ij}	stresses in the principle directions $i=j=1,2,3$
E	Young's modulus
I	area moment of inertia
F_D	structural damping force
F_E	internal elastic force
g	structural damping factor
c_i	characteristic constant for the i th damping mechanism
\dot{u}	velocity vector

N	normal pressure between body and surface
C	damping matrix
M	mass matrix
K	stiffness matrix
α	mass proportional damping constant
β	stiffness proportional damping constant
ζ	damping ratio
ω_i	natural frequency for the i th eigenmode
ω_d	damping stress
D^{el}	the material's <i>current</i> elastic stiffness
$\dot{\epsilon}$	strain rate
t	time
$r(t)$	response given time t
γ	shear angle
θ	rotation angle of beam cross-section
\tilde{M}	bending moment
\tilde{F}_s	shear force
u	axial displacement
w	deflection of beam axis
ϵ_x	axial (normal) strain
γ_{xz}	shear strain in xz-direction
G	shear modulus
τ_{xz}	shear stress in xz-direction
ρ	material density
k	shear correction factor
κ	curvature
\tilde{q}	transverse distributed load
\tilde{m}	distributed external moment
f_s	sampling frequency
f_{max}	maximum frequency of signal
$Rdyn_i$	dynamic response for element or node i
$Rstat_i$	static response for element or node i

Abbreviations

<i>API</i>	American Petroleum Institute
<i>DNV</i>	Det Norske Veritas
<i>FEA</i>	Finite element analysis
<i>FEM</i>	Finite element method
<i>CAD</i>	Computer aided design
<i>RHS</i>	Rectangular hollow section
<i>GUI</i>	Graphical user interface
<i>DOF</i>	Degrees of freedom
<i>GBS</i>	Gravity based structure
<i>TLP</i>	Tension leg platform
<i>C – 3PO</i>	See-Threepio
<i>R2 – D2</i>	Artoo Detoo
<i>MDOD</i>	Multi-degree of freedom
<i>SDOF</i>	Single-degree of freedom
<i>CFD</i>	Computational fluid dynamics
<i>ERP</i>	Explosion relief panel
<i>DAL</i>	Design accidental load
<i>FLACS</i>	Flame accelerator simulator (CFD-Software)
<i>ODB</i>	Output database
<i>SP</i>	Section point
<i>RF</i>	Reaction force
<i>DAF</i>	Dynamic amplification factor

Chapter 1

Introduction

1.1 Explosion incident event tree

An explosion on a typical offshore installation is the result of several incidents which together create a chain reaction leading up to the final explosion. An accidental release of a gas or liquid, for instance due to a leakage might ignite immediately, creating a fire. However if the gas or liquid release is within a confined space, it may lead to formation of a combustible fuel-air cloud, which after ignition will create a hydrocarbon explosion.

The primary objectives for assessing blast scenarios and to provide blast resistant designs are [12]:

- (a) Personnel safety
- (b) Controlled shutdown
- (c) Financial considerations

Blast resistant design should provide a level of safety for persons in a building that is no less than that for persons outside the building in the event of an explosion. Preventing cascading events due to the loss of control of process units not involved in an accident is another important objective in blast resistant design. A blast incident in one processing area should not be allowed to affect the safe operation or shutdown of other units or areas.

Preventing or minimizing financial losses is another objective of blast resistant design. Good blast resistant design should, depending on the size and location of the blast utilize the ductility of the material and cause a limited degree of damage to the structure, such that it can be either repaired or have a section replaced.

The total explosion event tree is illustrated below:

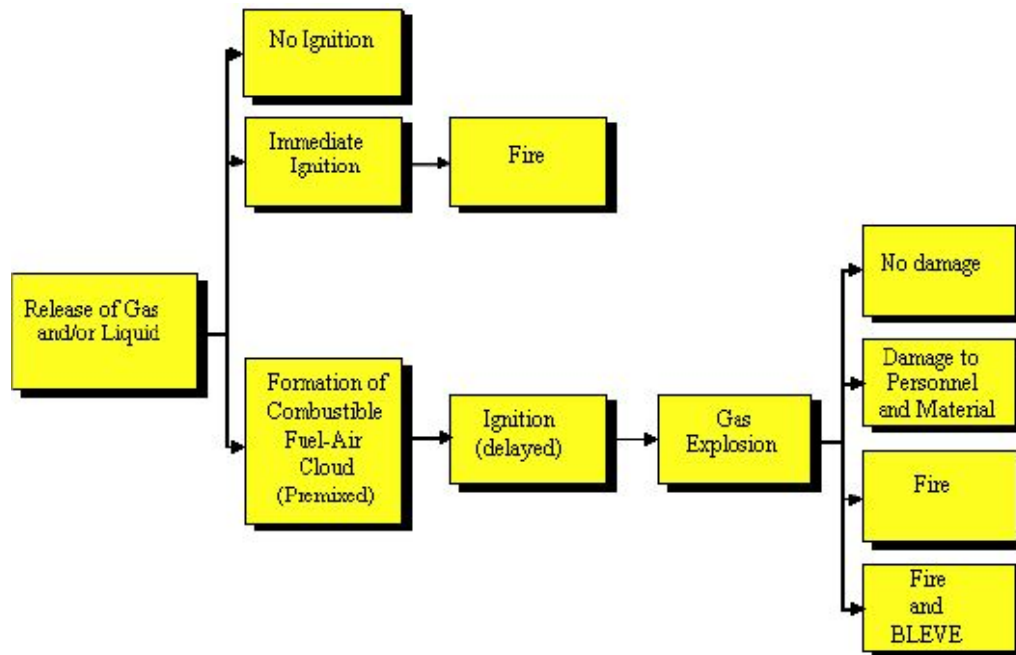


Figure 1.1: Explosion event tree. From the lecture notes by J.Amdahl. TMR 4195 Design of Offshore Structures, 2009.

1.2 General introduction on explosion/blast loads

An explosion is a rapid increase in volume and release of energy in an extreme manner, usually with the generation of high temperatures and pressure gases. A shock or pressure wave is created practically instantaneously after an explosion, which is referred to as a *blast*. This blast will move at high speed through surrounding air, often in supersonic speed. If the explosion takes place within a confined space, the effects and damages can often be extensive. Debris (fragments) from an explosion will fly at high velocity and impose further damage to the surroundings and in the worst case cause injury or death. An explosion load is characterized by the following parameters[1]:

- Shape of shock or pressure wave
- Rise time
- Maximum pressure (incident peak overpressure), P_s
- Positive phase duration, t_p
- Impulse, $i_s = \frac{1}{2} \cdot P_s \cdot t_p$

The shape of the shock or pressure wave is dependent on several factors[4]:

- Type of fuel and oxidizer

- Size and fuel concentration of the combustible cloud
- Location of ignition point
- Strength of ignition source
- Size, location and type of explosion vent areas
- Location and size of structural elements and equipment
- Mitigation schemes

1.3 Deflagrations and detonations

Explosions are separated into two types; (a) detonations and (b) deflagrations. Deflagrations are characterized by pressure waves moving in subsonic speeds (typically < 1000 m/s), while detonations are more extreme and represent shock waves moving in the supersonic range (1000-2000 m/s)[4]. A typical gas explosion is of the deflagration type, while an explosion of condensed explosives (or a very powerful gas explosion) is in the detonation range.

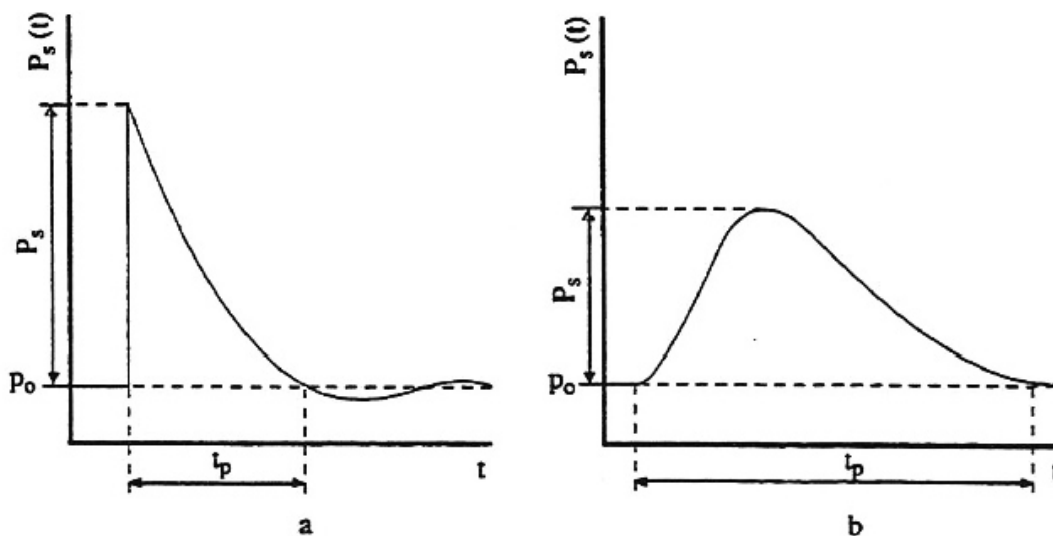


Figure 1.2: Characteristic shape of the pressure diagram for a) shock wave (detonation), and b) pressure wave (deflagration)[1].

A detonation is characterized by an instantaneous pressure rise (no rise time), and often a negative pressure after t_p (positive phase duration). The maximum value of this negative pressure does not normally play any important role, since this pressure is of a magnitude much smaller than the positive peak overpressure. A deflagration is characterized by

a rise time, and a slower decrease to zero within the positive phase duration time. A common simplification of the shape of the pressure diagrams is to linearize the variation, as shown in figure 1.3.

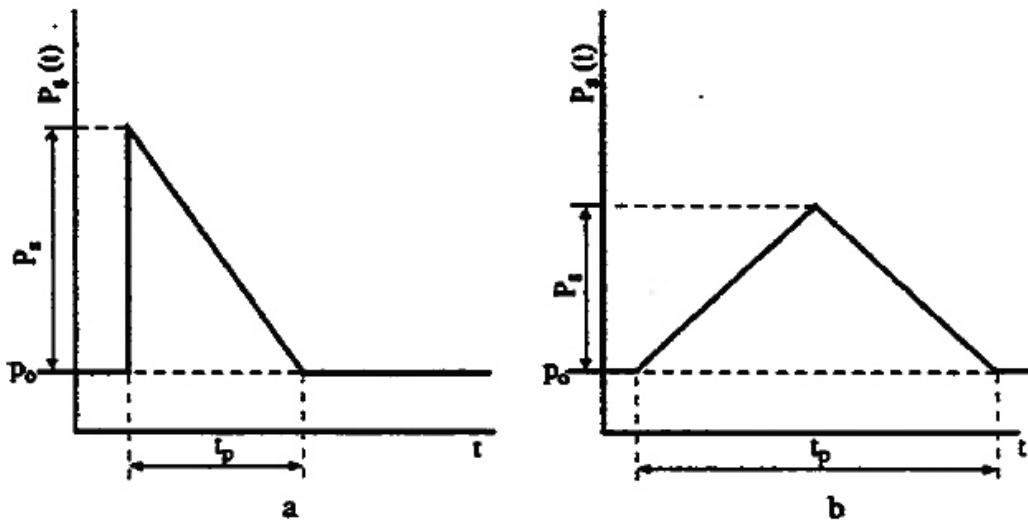




Figure 1.3: Simplified pressure diagram for a) shock wave (detonation), and b) pressure wave (deflagration)[1].

When idealizing a blast load, it is suggested by many sources to study the ratio between the blast duration and the structural eigenperiod. Three different domains, classified as respectively impulsive, dynamic and quasi-static can be defined with respect to the value of this ratio. The definitions of the different domains are summarized in table 1.1.

Source	Impulsive domain	Dynamic domain	Quasi-static domain
Amdahl J. [4]	$\frac{t_d}{T} \leq 0.3$	$0.3 \leq \frac{t_d}{T} \leq 3.0$	$\frac{t_d}{T} \geq 3.0$
ERS [2]	$\frac{t_d}{T} \leq 0.4$	$0.4 \leq \frac{t_d}{T} \leq 2.0$	$\frac{t_d}{T} \geq 2.0$

Table 1.1: Definition of response domains by various sources

It is seen that a great amount of simplifications on the representative pressure history can be done when dealing with the "quasi-static" domain, however for an impulsive or dynamic domain, the requirements on the accuracy of the blast load representation are much higher. Reference is made to the Blast and Fire Engineering Project for Topside Structures (Work Package No. BR1/BR2 [2]), and the table as presented in figure 1.4.

FEATURE OF BLAST LOAD	NATURE OF BLAST LOAD		
	Impulsive $\tau/T < 0.4$	Dynamic $0.4 < \tau/T < 2.0$	Quasistatic $\tau/T > 2.0$
Peak Value	Preserving the exact peak value is not critical	Preserve peak value - increase/decrease in this quantity will result in a similar increase/decrease in response	
Duration	Preserving the exact load duration is not critical	Preserve load duration since in this range it is close to the natural period of the structure. Even slight changes may affect response.	Load duration is not too important if response is purely elastic, but it becomes significant when response is plastic
Impulse	Accurate representation of the impulse is important, with negative impulse included in some cases	Accurate representation of the impulse is not too critical, however, better results would be achieved if some attempt were made to estimate this quantity	Accurate representation of the impulse is not important
Rise Time	Preserving rise time is not important	Preserving rise time is very important, not doing so can significantly affect response	
General Shape	General shape of idealised load is a right-angle triangle of the form : 	General shape of idealised load is a triangle of the form :  A tri- or tetra-linear form can be used to more accurately represent the rise and decay of the load, predicting slightly better response	

The table summarises the findings of this report including contributions submitted from other organisations. The aim is to highlight the important factors to be considered when idealising a blast load so that reasonable predictions of response can be achieved.

Figure 1.4: Important factors to be considered when idealising a blast load with respect to the assumed structural response [2].

Chapter 2

Interaction between blast and structure

When a blast meets a structure or an obstacle, it will be disturbed. The disturbance causes the loading on the obstacle to differentiate from the time-pressure path of the undisturbed blast, taking a much more complex form which in turn is heavily dependent on the shape of the structure and direction of the blast wave relative to the structure. Two effects from blast and structure interaction are important to mention, these are *reflections* and *dynamic pressures*.

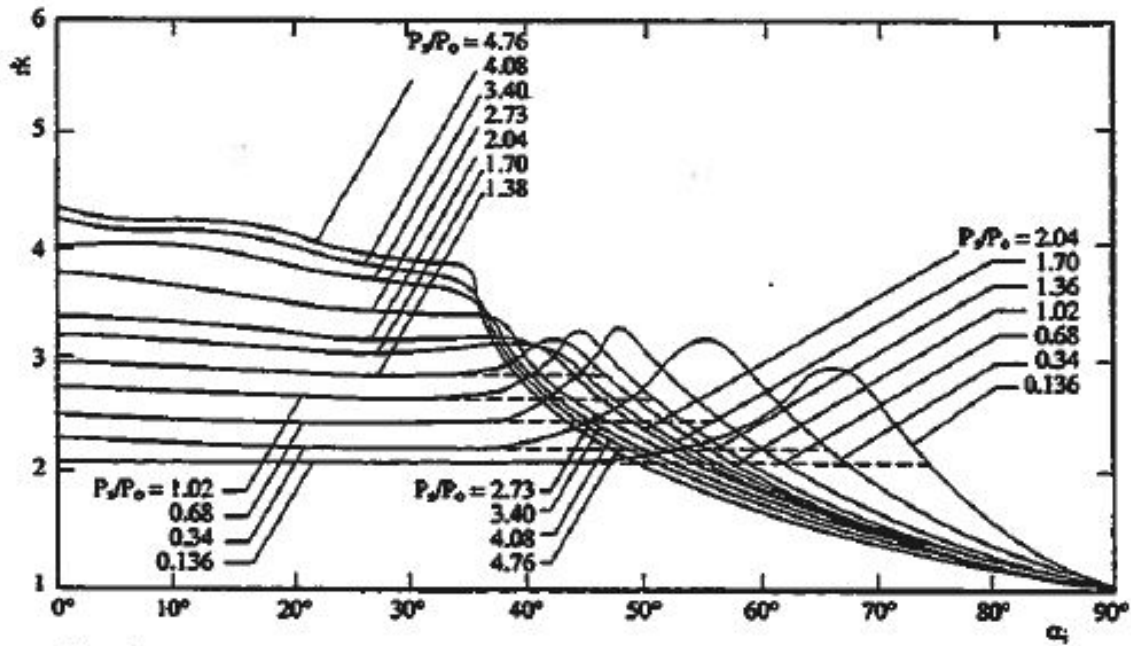
2.1 Reflection load

When a blast wave hits a surface, it will be reflected, and a wave moving in the direction opposite to the incident wave is created. This causes the reflection surface to be loaded by an overpressure, a reflection load P_r of the reflected wave. This overpressure is larger than the peak overpressure P_s of the incident wave, and a reflection coefficient is used to account for this effect:

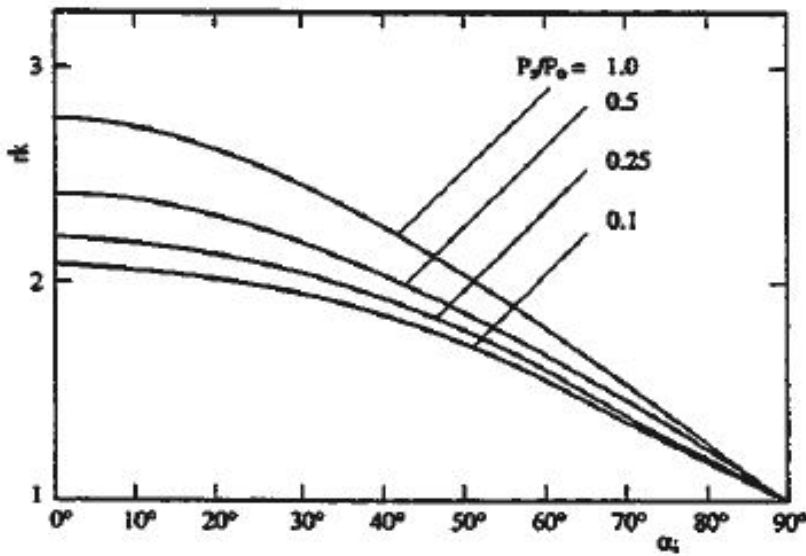
$$rk = \frac{P_r}{P_s} \quad (2.1)$$

The value of this coefficient is dependent on several factors, including the angle of incidence between the wave-front and the reflected surface (0-90 deg) and the type of wave (shock wave or pressure wave). Figure 2.1 shows the reflection coefficients for different values of the overpressure, as functions of the angle of incidence.

A simplified schematic representation of the disturbance of the blast caused by a box shaped structure is shown in fig 2.2



a: Shock wave



b: Pressure wave

Figure 2.1: Reflection coefficients for different values of the overpressure, as functions of the angle of incidence[1].

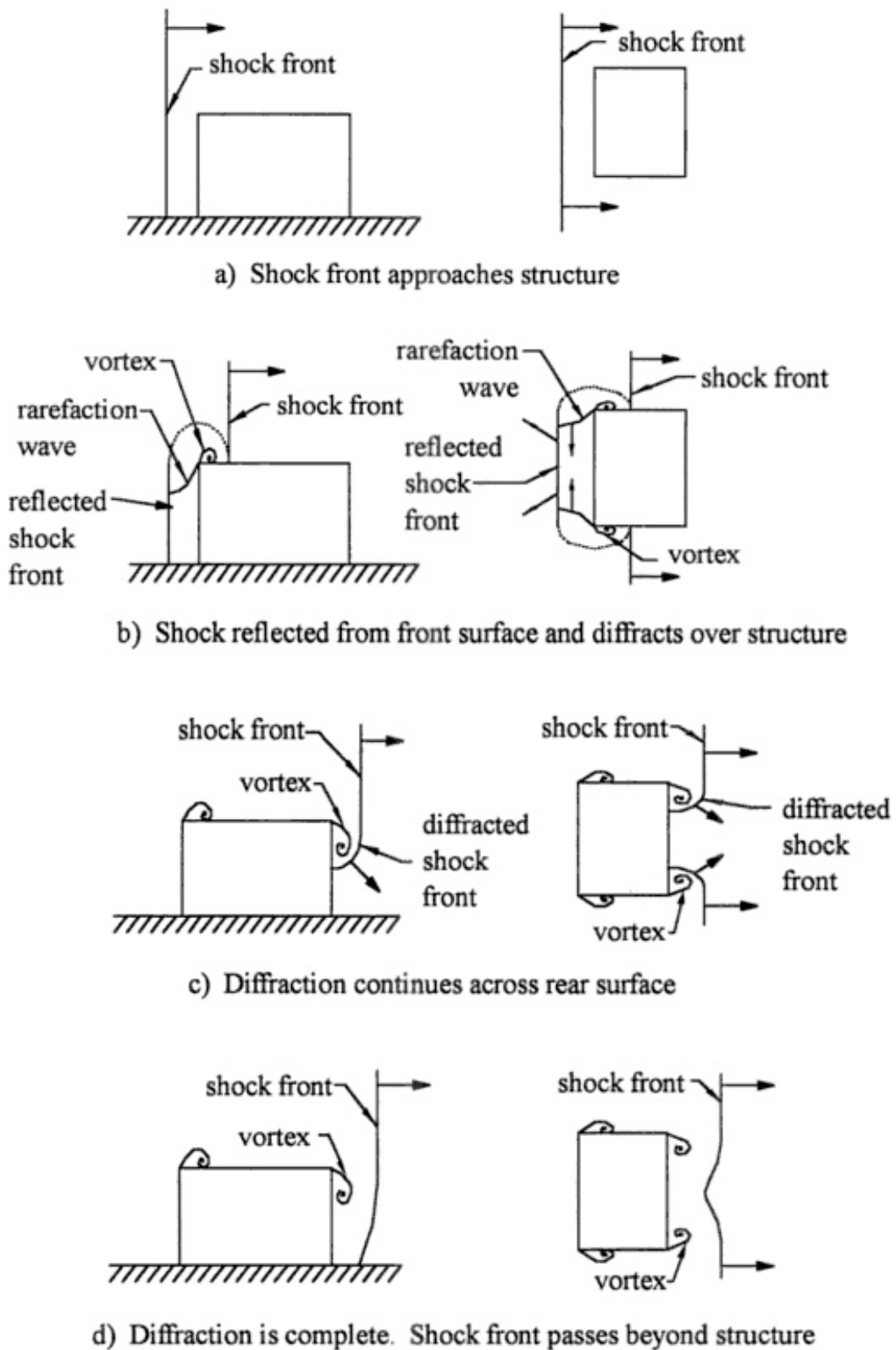


Figure 2.2: Schematic representation of the disturbance of the blast for a box shaped structure [1].

The reflection pressure is often added together with the incident peak overpressure P_s and the dynamic pressure P_D . The time in which the reflected pressure starts to decrease to P_s and P_D is denoted t_s .

$$t_s = \frac{3 \cdot S}{U} \quad (2.2)$$

Where S is the characteristic dimension of the surface, while U is the velocity determined by:

$$U = c_0 \sqrt{1 + \frac{6 \cdot P_s}{7 \cdot p_0}} \quad (2.3)$$

in which c_0 is the velocity of sound in air ($\pm 340m/s$), and p_0 is the atmospheric pressure.

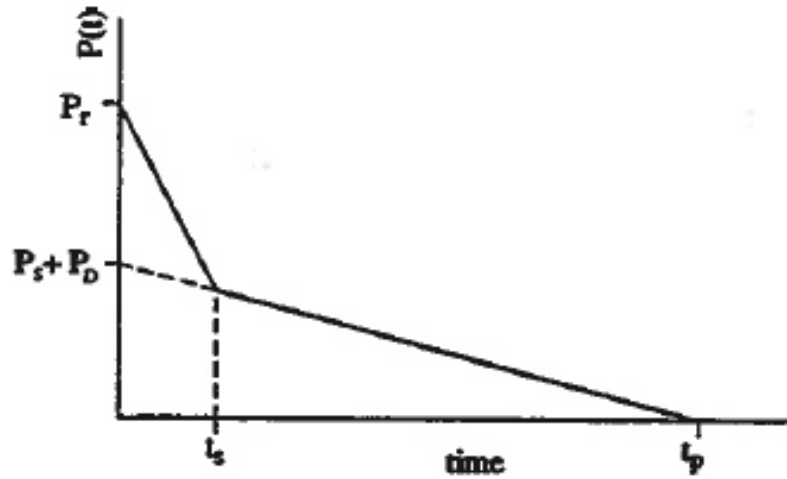


Figure 2.3: A schematic representation of the pressure variation through time is shown for a finite reflective surface [1].

2.2 Dynamic pressure

A blast will, when meeting a structure or an obstacle create a dynamic load on the structure. This is caused by air displacement in the direction of the blast-wave. The air displacement from a blast is referred to as an *explosion wind*, and causes a dynamic pressure given by the following formula [1]:

$$P_D = C_D \cdot 0.5 \cdot \rho_s \cdot u_s(t)^2 \quad (2.4)$$

whereby: C_D is the so-called drag coefficient, which is dependent on the shape of the structure (projected area) and its orientation relative to the blast front. Figure 2.4 shows the different values of C_D given for various simple structural shapes.

ρ_s is the air density within the blast ($kg \cdot m^3$), and $u_s(t)$ is the velocity of the air particles (combustion products) ($m \cdot s^{-1}$)

Table 1. Coefficients C_D . Taken from [2]










Shape	Figure	C_D
Long Straight Cylinder		1.20
Sphere		0.47
Cylinder		0.82
Disc		1.17
Cube		1.05
Cube		0.80
Oblong Box		2.05
Oblong Box		1.55
Strip		1.98

Figure 2.4: Drag coefficients given for various simple structural shapes [1].

It should be noted that the dynamic pressure exerts the dominant blast effect on open frame structures, framed structures with frangible cladding, and on small structures or components such as poles, stacks etc.

2.3 Load on a structure

It is often common to differentiate between three types of extreme conditions when dealing with blast wave interactions on a structure. Situation (A) in fig 2.5 represents a case where the blast wave runs over a large surface without hindrance. The load on the surface will for this case be taken equal to the overpressure P_S of the incident wave.

In case (B), the blast wave is on a path perpendicular to a surface of very large dimensions. There will be minimal rarefaction effects from the edges, and the load on the surface can be taken as the overpressure from the reflected blast wave P_r .

For case (C) we are dealing with an object of small dimensions, the rarefaction progresses so quickly that any reflection can be neglected. Furthermore, one can assume that the pressure difference between the front and back part of the part is so small that only the dynamic pressure P_D is considered. It should be noted that in most structures, a combination of these three cases must be considered.

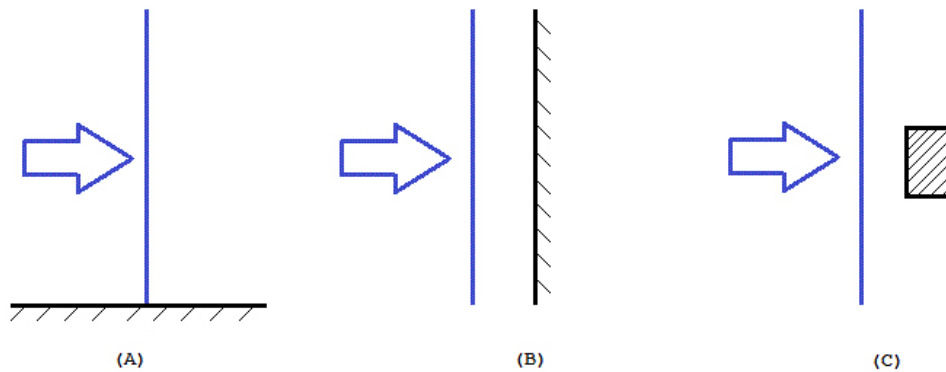


Figure 2.5: A schematic representation of the pressure variation through time is shown for a finite reflective surface [1].

Chapter 3

Structural response

When a structure is exposed to a dynamic (transient) load, such as a blast load, it will react to this load by deforming. Structures can also vibrate; this is a phenomenon which is governed by its own natural periods of vibration. Because of the extensive magnitude of a blast load compared to the loads which the structure is designed to withstand under normal operating conditions (dead-, live- and wind loads etc.), together with the small probability that a structure will be exposed to such a load during its life-time, it is therefore not economical to design a structure for this type of load. Consequently, it is possible to accept, in practice, a certain degree of damage in the form of ductility. The definition of ductility will be addressed later in this paper (see section 4.4). For severe blast cases, the study of plastic deformations will be necessary, hence linear elastic theory will not be sufficient.

Studying the change in deformations, strains and the maximum stresses over the explosion time history will be the main task during a dynamic blast assessment.

3.1 Dynamic analysis

Structural dynamic analyses are required to assess certain blast problems. Because both load and response vary with time, it is evident that a dynamic problem does not have a single solution as with a static problem. Instead, one must establish a response history covering all the relevant phenomena which are of interest in the study.

A characteristic feature of a dynamic analysis is illustrated in fig 3.1. If a simple beam is subjected to a static load p , its internal forces are in equilibrium with the present load. On the other hand, if the load $p(t)$ is added dynamically, the mass and stiffness of the structure play a role in the distribution of the internal forces in it. The internal moments and shears in the beam must equilibrate not only with the externally applied force $p(t)$, but also the inertia forces resulting from the accelerations of the beam. It should be noted

that if motions are so slow that the inertia forces are negligibly small, one can treat the problem as a static problem; however this is usually not the case with a blast problem.

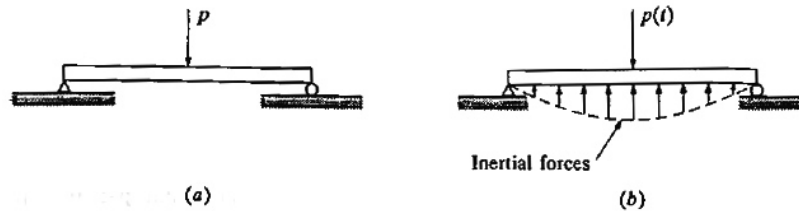


Figure 3.1: Simple beam subjected to a static load [3].

A structural dynamic analysis will be dependent on whether the system is being treated as a single-degree of freedom (SDOF) system, or a multi-degree of freedom (MDOF) system. The response of a SDOF system can be evaluated directly from the solution of a single differential equation of motion, while the MDOF system is made complicated due to the necessity of discretization. A numerical solution of a MDOF system equation can be found using non-linear finite element method.

3.1.1 SDOF-methods

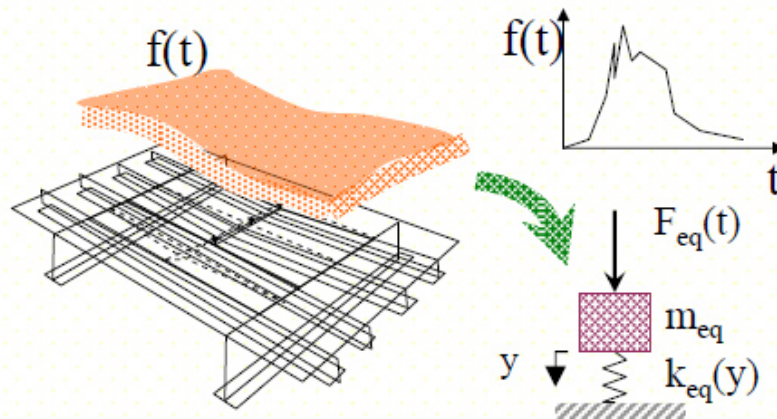
SDOF-methods, such as Biggs' method is commonly used to assess the blast response in an early design stage, and allows for easy hand calculations. This method is based on simplifying the structural problem into a mass-spring system without damping, and includes a load-mass transformation factor to account for various boundary and load conditions [4]. These transformation factors are based on approximations to classical beam and plate theory for deflections in the elastic range and plastic hinge or yield-line theory in the plastic range. Biggs' method can be easily adopted for dynamic analysis of structural topside components such as floor plates and blast walls subjected to blast loads[2].

The SDOF system represented in fig 3.2 can be expressed with the following formula [4]:

$$k_{lm}M\ddot{y} + Ky = F(t) \quad (3.1)$$

Whereas k_{lm} is the load-mass transformation factor.

A numerical approach based on the Rayleigh-Ritz method is also applicable. This method represents a versatile way to formulate a load-deflection curve using deflection functions. The assumed mode of deflection can be described by one or more component deflections or modes with unknown magnitudes which, when combined, approximate the exact displaced shape. Structural models with composite members like stiffened plates can be easily analysed using this method [2].



Dynamic equilibrium:

$$m_{eq} \ddot{y}(t) + \cancel{c_{eq} \dot{y}(t)} + k_{eq}(y) = F_{eq}(t)$$

Figure 3.2: The SDOF method implemented on a stiffened plate blast response problem [4]

It is shown that SDOF-methods as mentioned above provide an accurate estimate of the blast response for stiffened plates. The accuracy of the method is dependent on how good the resistance function represents the real situation.

3.1.2 MDOF-methods

For scenarios such as a topside frame structure being exposed to a blast load, the problem can no longer be simplified as a SDOF-system, and more advanced methods have to be implemented. The most common method is to use the Finite Element Method (FEM)/Finite Element Analysis (FEA), utilizing its ability to handle complicated geometries and boundaries.

3.2 Geometric non-linearity

Geometric non-linearity effects are due to the presence of large strain, small strains but finite displacements/and or rotations, and loss of structural stability. Slender structures such as bars may experience large displacements and rotations with small strains [13], in which geometric non-linear effects have to be accounted for if one is to obtain accurate results. Due to the nature of a large-displacement problem, an updated reference state is

needed for the structure (updated geometry), and stress-equilibrium is thus calculated on the basis of the latest reference state.

3.3 Damping

When exposing a non-conservative dynamic system to an external force, the presence of damping forces causes a dissipation of energy in the system which eventually causes a reduction in vibration amplitude, and ultimately stops the motion. If the energy in a non-conservative system is to be kept at a constant level, an external source must supply energy to the system at a rate equal to the rate of energy dissipation.

The most common types of damping are:

- Structural damping (hysteretic damping)
- Viscous damping
- Coulomb damping (dry friction damping)

Structural damping (Hysteretic damping) is due to internal friction, or friction at connections between elements of a structural system. For an elastic system (a system vibrating so that the induced stresses are within the elastic range), the i th structural damping force $F_{D,i}$ is proportional in magnitude to the internal elastic force $F_{E,i}$ (i.e. the forces caused by stressing of the structure), and opposite in direction to the velocity vector \dot{u}_i . This expression is expressed by:

$$F_{D,i} = i \cdot g \cdot F_{E,i} \quad (3.2)$$

whereas g is a constant (structural damping factor) and i is the unit imaginary number [14] [15].

Viscous damping is found in many engineering systems such as shock absorbers, hydraulic dashpots and sliding of a body on a lubricated surface. This kind of damping is generally used for systems which are vibrating or moving in a fluid, being air, oil or similar. The i th viscous damping force is expressed as:

$$F_{D,i} = c_i \cdot \dot{u}_i \quad (3.3)$$

whereas c_i is a characteristic constant for the i th damping mechanism, and \dot{u}_i is the velocity vector [14]. For free vibrations of a one DOF system with a viscous model, the amplitudes will decay exponentially.

Coulomb damping or dry friction is due to the motion of a body on a dry surface. This results in a damping force which is constant, only dependent on the normal pressure N

between the moving body and the surface, and μ , the coefficient of kinetic friction. The Coulomb damping force is expressed by:

$$F_D = \mu \cdot N \quad (3.4)$$

In the ABAQUS code, a classic viscous damping model called Rayleigh damping is used to represent the effect of damping. It should be emphasized that Rayleigh damping is only a generalization of the damping properties of a real structure, and it is used in order to avoid the need to form a damping matrix based on the physical properties of the real structure. The formulation of this damping matrix is based on assuming proportionality to the mass and stiffness matrices through equation 3.5:

$$C = \alpha \cdot M + \beta \cdot K \quad (3.5)$$

here α is the mass proportional damping constant, and β is the stiffness proportional damping constant.

Relationships between modal equations and orthogonality conditions allow this equation to be rewritten as equation 3.6 [16]

$$\zeta_i = \frac{\alpha}{2\omega_i} + \frac{\beta\omega_i}{2} \quad (3.6)$$

Here ζ_i is the damping ratio and ω_i is the natural frequency of the i th mode.

The Rayleigh damping model assumes that the damping ratio depends upon the frequency through the two constants that are usually chosen based upon matching the system damping to the experimental values at two of the system's natural frequencies [17].

The first term in equation 3.6 is a mass damping term. The α factor introduces damping forces caused by the absolute velocities of the model and so simulates the idea of the model moving through a viscous "ether" (a permeating, still fluid, so that any motion of any point in the model causes damping), in analogy to the viscous damping equation 3.3. This damping factor defines mass proportional damping, in the sense that it gives a damping contribution proportional to the mass matrix for an element. The second term in equation 3.6 is a stiffness term. The stiffness proportional damping constant in ABAQUS introduces damping proportional to the strain rate. β is interpreted as defining viscous material damping in ABAQUS, which creates an additional "damping stress," σ_d proportional to the total strain rate. This is expressed in equation [15].

$$\sigma_d = \beta D^{el} \dot{\epsilon} \quad (3.7)$$

whereas $\dot{\epsilon}$ is the strain rate. Further wise, it should be noted that D^{el} is defined as the material's current elastic stiffness in both ABAQUS Standard and the Explicit module.

Figure 3.3 illustrates the contribution from the mass and stiffness damping terms to the total damping ratio. Generally speaking, the mass proportional Rayleigh damping α , damps the lower frequencies, while the stiffness proportional Rayleigh damping β , damps the higher frequencies.

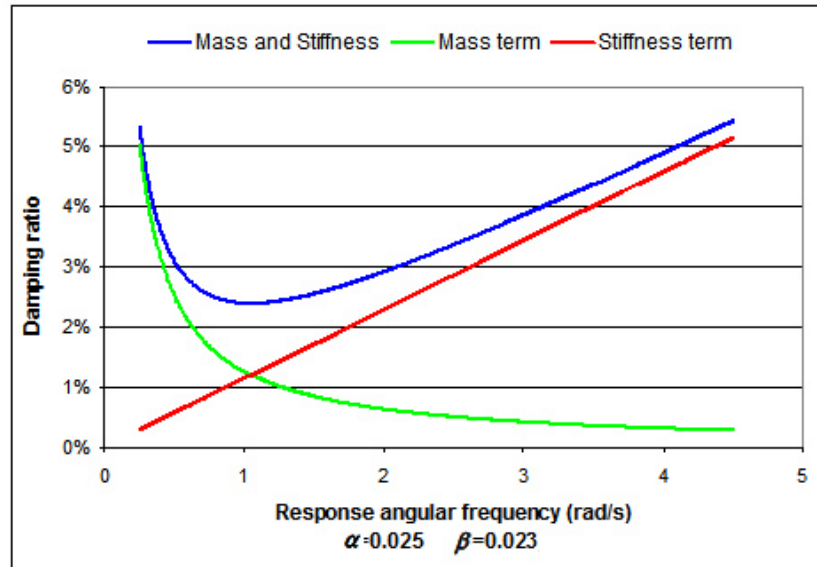


Figure 3.3: Variation of damping ratio with respect to response or natural frequency [5].

Simple variations of Rayleigh damping are the mass-proportional damping ($\beta=0$) and stiffness proportional damping ($\alpha=0$). During an early screening phase, for any MDOF systems of a certain complexity, it is difficult to determine meaningful values of the two damping constants α and β . In practice, it is therefore more common to "tune" in the damping properties to provide a certain level of damping (often given as percent of critical damping) based on known values for damping ratios from similar structures. The constants can then be calculated on the basis of this. Table 3.1, provides an overview over approximate values for ζ , the viscous damping ratio for common materials.

Type of system	ζ , damping ratio (% of critical)
Reinforced steel [18]	0.3-1
Unclad welded steel structures (e.g. steel stacks) [19]	0.3
Unclad bolted steel structures [19]	0.5
Steel material (bare structure) [20]	0.1-0.2

Table 3.1: Damping ratios for different structural systems

Further discussion upon damping in Abaqus are found in section 5.9.

3.4 Solution methods for non-linear analyses

In FEA (Finite Element Analysis), direct numerical integration methods are used to find approximate solutions to the non-linear response problems. These are considered standard solution methods in e.g Abaqus CAE. The direct numerical integration methods are separated into two methods; implicit and explicit methods.

3.4.1 Implicit integration method

Implicit methods imply that the displacements at the new time step, $t + \Delta t$, are expressed by the velocities and accelerations at the new time step, in addition to the historical information at previous time steps. Many of the implicit methods are unconditionally stable for linear systems; there is no mathematical limit on the size of the time increment that can be used to integrate a linear system. The method can be expressed with equation 3.8.

$$r(t + \Delta t) = f \{r(t), \dot{r}(t + \Delta t), \ddot{r}(t + \Delta t), \dot{r}(t), \ddot{r}(t), \dots\} \quad (3.8)$$

The implicit integration method is the basis solution method for Abaqus CAE, i.e the Abaqus (Standard) Implicit Package.

3.4.2 Explicit integration method

The explicit scheme is based on obtaining the displacements at a new time step, $t + \Delta t$ by the displacements, velocities and accelerations of previous time steps, as seen in equation 3.9 [21].

$$r(t + \Delta t) = f \{r(t), \dot{r}(t), \ddot{r}(t), r(t - \Delta t), \dot{r}(t - \Delta t), \ddot{r}(t - \Delta t), \dots\} \quad (3.9)$$

It should be noted that the central difference operator, which is the most commonly used explicit operator for stress analysis applications in the Abaqus Explicit Package (Abaqus/Explicit), is only conditionally stable; the stability limit being approximately equal to the time for an elastic wave to cross the smallest element dimension in the model [22]. The applications for explicit methods are thus limited to problems of very short durations, i.e impulse load problems or similar.

Chapter 4

Blast loads on topside structural elements

A topside module is a large, pre-built unit that includes accommodation, production and drilling zones which is typically built separate from the rest of the substructure, which can be either a TLP, jacket, FPSO or Semi-submersible. The topside module will be installed on top of the rest of the substructure during the late phase of assembly.

A typical topside module is designed as a bearing system consisting of a system of trusses, beams and stiffened plates. The purpose of the structure is to support as much equipment as possible while keeping the overall self-weight to a minimum, the design should also withstand unique load combinations which include both the pre-service conditions (fabrication and installation) and the in-service conditions (environmental, functional and live-loads). Accidental loads such as blast loads are treated separately, as these often require extensive non-linear structural and CFD analyses.

The typical arrangement of a topside module is shown on fig 4.1. A topside module can be looked on as a compact process plant, and it should be noted that the module is separated into zones, spread over several deck levels. A structural steel framing supports the entities of the process areas which consist of: the wellhead area at which pipes carrying hydrocarbon fluids from the reservoir terminate; the production separators in which these fluids are separated; and the compression facilities at which the gases from the separators are compressed, dried, purified and prepared for export.

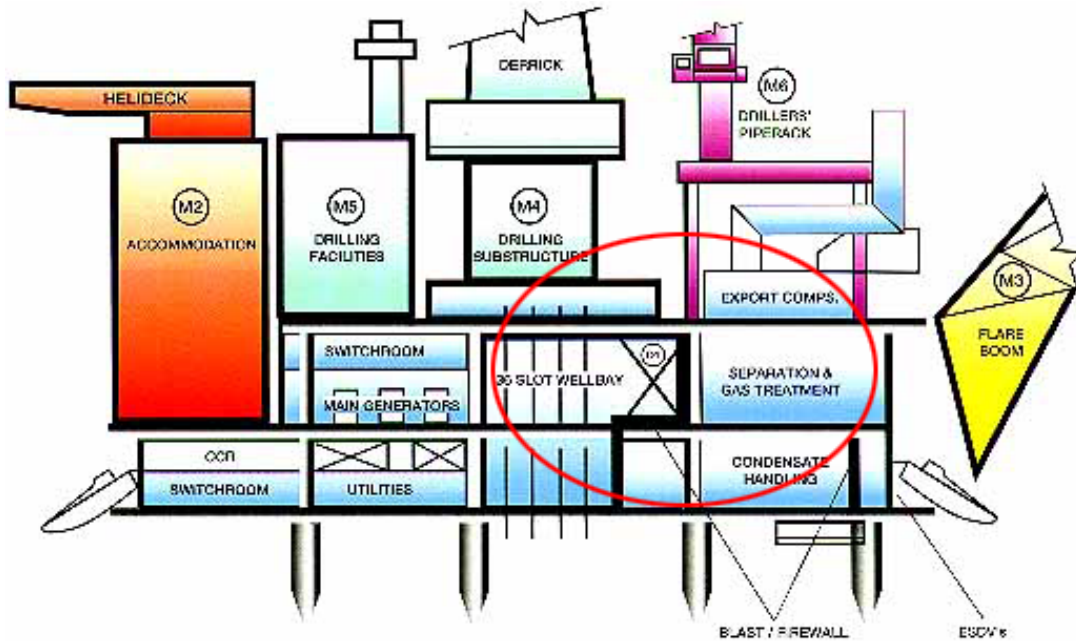


Figure 4.1: Typical topside module arrangement [6].

One of the worst scenarios that can occur on an offshore installation is a hydrocarbon explosion. In an unconfined area, the pressure waves from the blast are emitted in all possible directions in a matter of milliseconds, capable of travelling over long distances and creating widespread damage. In a confined area, there is a large risk of increased over pressures which are capable of causing extensive localized damage to both equipment and structure. Entities having large surfaces such as walls will attract high loads from an explosion. For small entities such as piping lines or cable trays, the effect of blast pressure is at minimum, but the blast waves may drag and pull these entities off the supports, leading to possible rupture which may escalate the initial event [23].

Normal safety conventions require the installation of blast walls (corrugated or stiffened plates) around these respective areas [24], in which the purpose is to minimize the damage of a possible explosion event.

One should bear in mind that the topside module is an extremely complex structural system, consisting of structural members, piping, equipment, cables and other appurtenances that can obstruct the free movement of the pressure waves. To be able to calculate the response for such a complex case, it is necessary to do simplifications. It should be emphasized that these simplifications should be done in such a way that a certain level of conservatism is ensured.

4.1 Mitigation schemes

The magnitude of the damage caused by a blast can be reduced by simple mitigation schemes easily implemented in an early design phase of a topside module. These mitigation schemes are especially important for enclosed spaces, such as in a process area. Ventilation openings and special designed release ducts can easily help reducing the level of overpressure from an explosion as seen in fig 4.2, effectively leading the pressure wave towards a safe direction where it can be left to escape.

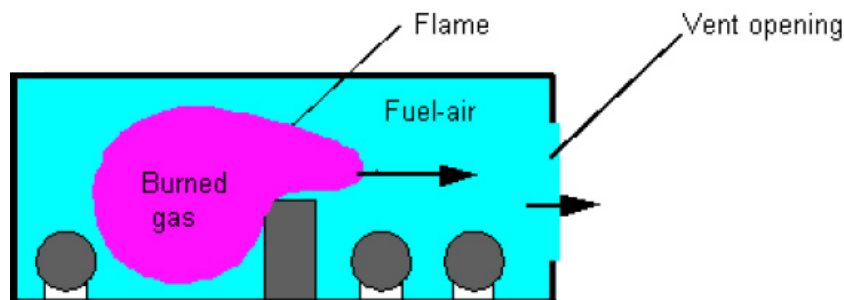


Figure 4.2: Figure showing the importance of proper ventilation as to reduce the effects of an explosion[4].

The placement of any structural component or equipment relative to the blast may also reduce the damage imposed to these objects. If obstacles are placed in such a way that they leave an escape route for the pressure wave toward the vent areas, the localized damage within the confined space may be reduced dramatically.

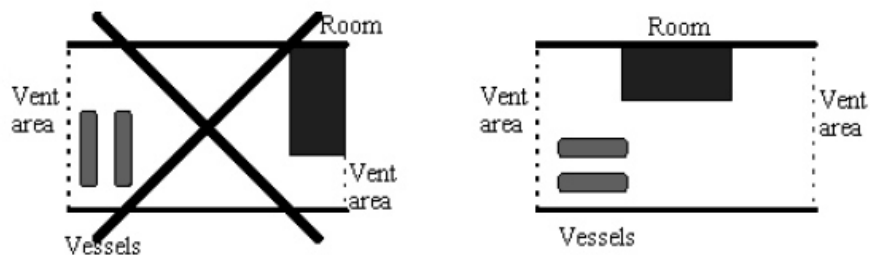


Figure 4.3: Importance of correct positioning of equipment in case of an explosion event [4].

Other mitigation systems include ERP (Explosion Relief Panels) and water deluge systems [25].

4.2 Pipe rack system

A pipe rack is a structure designed to support metallic pipes and cables going from one area of the topside module to another. The major pipe racks on a typical offshore topside are concentrated around the processing areas, going from one processing unit to another, supporting the pipes which transport either hydrocarbons, gases or other chemicals used for processing and production.

A conventional offshore pipe rack is a steel-based truss structure welded together by RHS (Rectangular hollow section) profiles. Due to the ease of production, all welded RHS connections have eccentricities. Investigations by [11] on topside structures exposed to explosions, showed that the ductility of joints played a prominent role as a key of safety element that can be translated to performances of a structural system. The effects of connection eccentricities will not be assessed in this paper, but may be an area of investigation as a part of a further work. In this paper, a structural model without node eccentricities at the connections is analysed.

A pipe rack is welded directly on the primary topside framing structure. For the blast scenario as proposed by Aker Solutions, the main span of the pipe rack is perpendicular to the dynamic pressure from the blast (See figure 4.4). Strictly speaking, this is considered an undesirable position, as the pressure is attacking perpendicular to the span of the pipe rack structure.

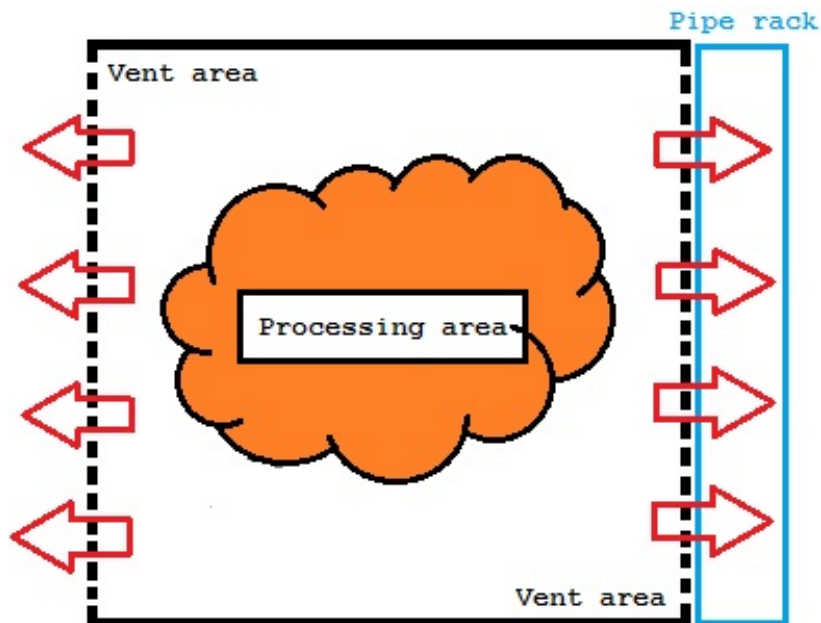


Figure 4.4: Blast scenario with pressure release. Dynamic pressure attacking perpendicular on the pipe rack.

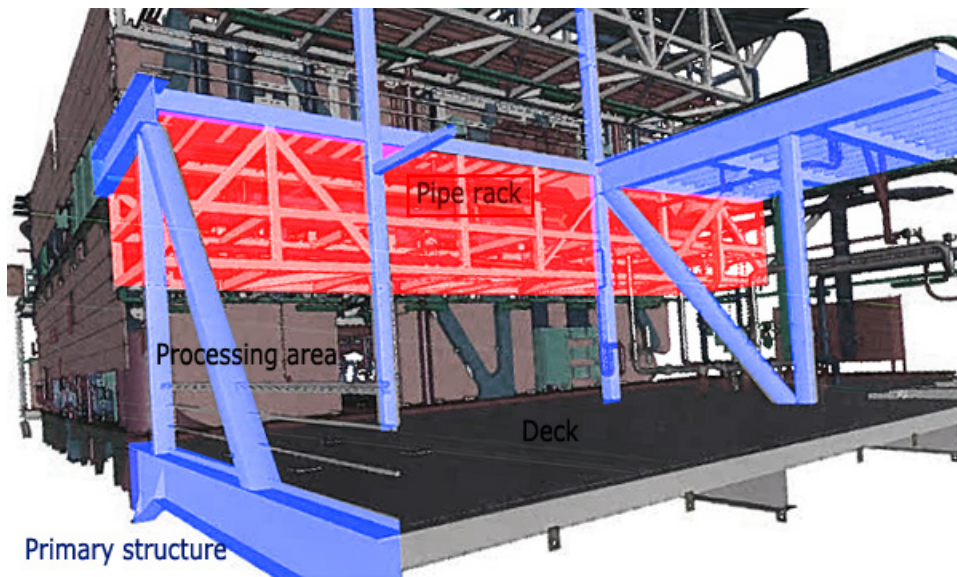


Figure 4.5: PDMS (Plant design manager system) CAD representation of the processing area and the pipe rack position. Figure provided by Aker Solutions.

All pipes are connected to the pipe rack by special U-brackets, this is shown in figure 4.9 and 4.8. For larger pipes, special brackets are used.

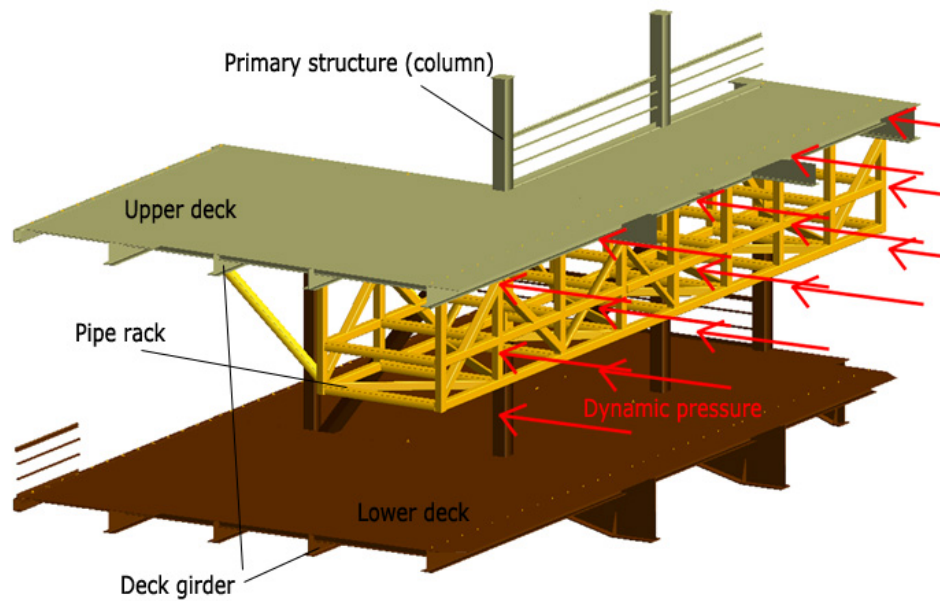


Figure 4.6: Isolated view of the pipe rack and neighbouring structural elements, with dynamic pressure attacking perpendicular to the span of the pipe rack.

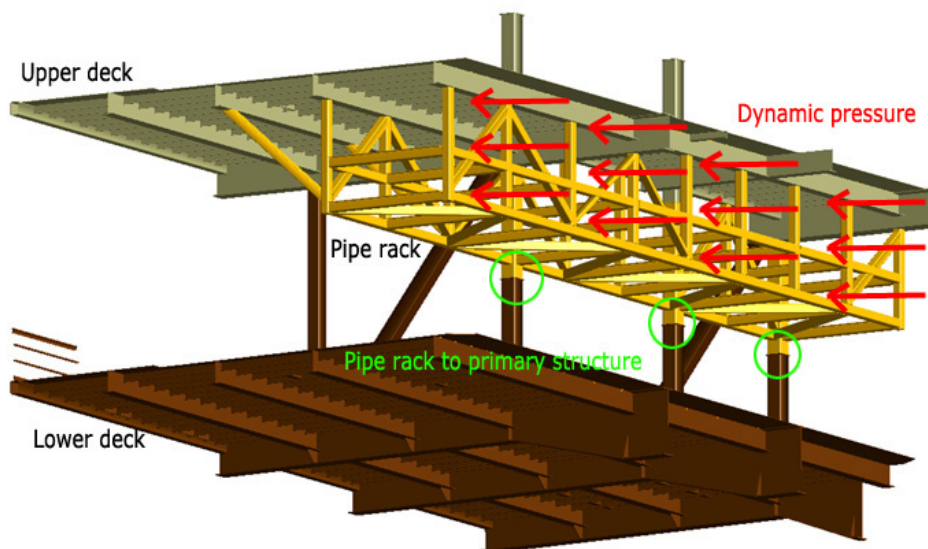


Figure 4.7: The pipe rack is welded directly to the upper deck girders as shown. The pipe rack is also connected to the primary structure (column) as shown marked with green.

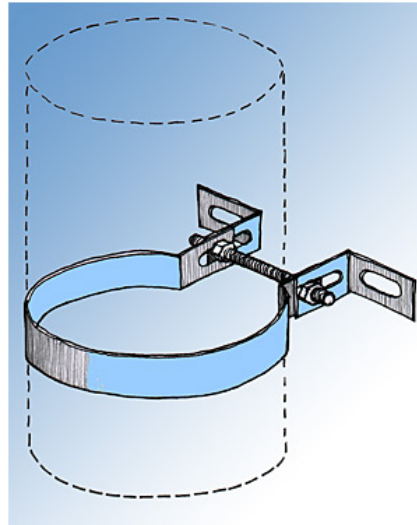


Figure 4.8: www.reliner.com, showing a typical pipe bracket for the offshore industry.

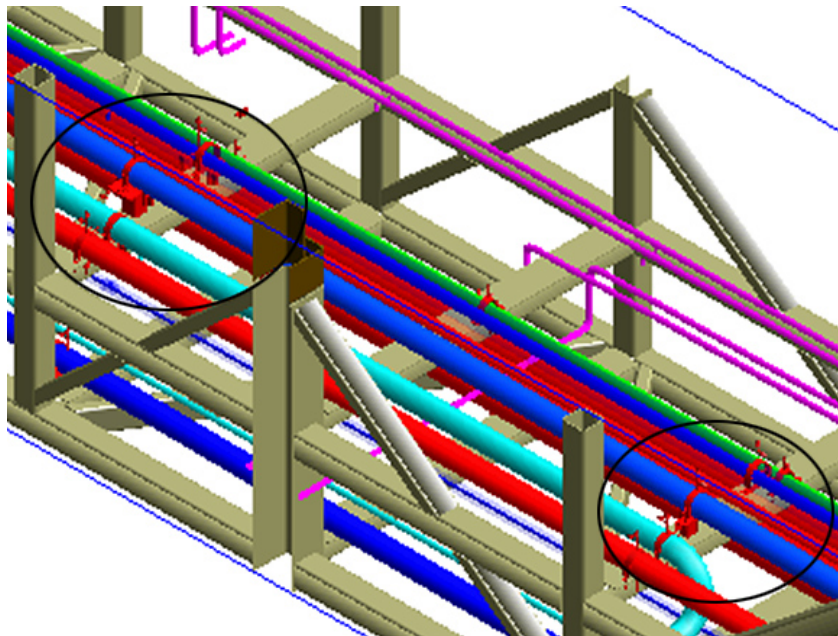


Figure 4.9: PDMS (Plant Design Manager System) 3D representation of a part of the pipe rack with pipes and U-brackets. Visualization provided by Aker Solutions.

Due to the fastening method of the pipes using simple brackets, it should be reasonable to assume that these pipes do not contribute significantly to the overall stiffness and structural integrity of the pipe rack system. The weight of the pipes on the pipe rack structure on the other hand, will be of an importance. Because the number of pipes, including their dimensions and weights will be subjects to changes through the project, simplifications on the piping weight and arrangement has been done. For all analyses, the arrangements as shown in figure 5.13 are used.

Approximate weights of the main pipes have been calculated using a weight table given by Aker Solutions (see appendices A and C). The pipe weight will be distributed over the span of the pipe rack, assuming the weight to be represented by a point mass (inertia) on the corresponding horizontal brace.

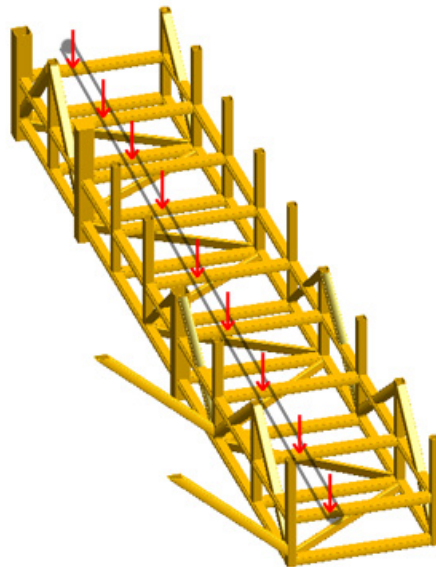


Figure 4.10: The weight of a pipe is assuming to be represented as point loads on the structure.

4.3 Pressure distribution and magnitude

The pipe rack consists of a truss system of RHS (rectangular hollow section) profiles which is of small dimensions compared to the actual blast. As previously mentioned in section 2.2 and 2.3, the reflection pressure can therefore be neglected, and the only relevant pressure to be taken account for in the analysis will be the dynamic pressure P_D . This is a simplification also suggested by [26] for the analysis of blast responses on primary steelwork such as isolated columns and beams.

As suggested by [27], the explosion pressure distribution can be considered uniformly distributed for components and sub-structures. This applies for a pipe rack.

A simplified pressure diagram shown in figure 4.11 has been provided by Aker Solutions. For explosion scenarios, Aker assumes the duration to be in the range of 50-200 ms.

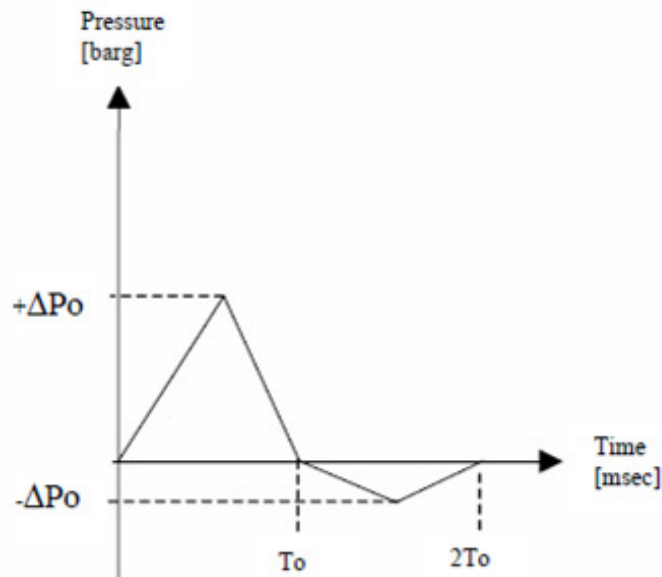


Figure 4.11: Simplified pressure diagram as provided from Aker Solutions for the dynamic pressure. According to Aker Solutions, the under-pressure will have an absolute value of about 10% of the initial over-pressure.

As seen from section 2.2, the dynamic pressure is given as the following expression:

$$P_D = C_D \cdot 0.5 \cdot \rho_s \cdot u_s(t)^2 \quad (4.1)$$

If we assume a hydrocarbon gas explosion being in the deflagration range, the velocity of the combustion particles are to be assumed to be travelling in subsonic speed (less than 343 m/s). According to [28], typical combustion gases found on an offshore processing facility are ethane, propane, butane and methane. These have vapor densities in the range of roughly 0.5-2 kg/m³.

Predicting the magnitude of the different variables in the calculation of the dynamic pressure for a blast scenario is a complicated task. Tabulated values of the drag coefficient, C_D is only given for simple geometries such as a box or a cylinder. The velocity and the density of the combustion particles during a deflagration blast is very hard to determine as these depend on many factors. However, simplifications can be made as to give a first estimate. According to [29], the major portion of the loading on an open-frame structure

is the drag pressure contribution. The drag coefficient C_D for an individual member such as a I-beam or rectangle is about 1.5, however when the whole frame is considered it has been suggested to reduce C_D to 1.0. This is because various members shield one another to a certain extent from the effects of the full blast loading.

If we assume the explosion gas to be represented by $\rho_s = 0.5 \text{ kg/m}^3$, and with an air velocity just under subsonic (340 m/s), C_D equal to 1.0 we get a dynamic pressure of roughly 0.3 bar. The proposed design value (DAL) for the dynamic pressure as given by Aker Solutions is between 0.2 and 0.4 bar (These pressure values are obtained from blast analyses by an external risk consultant company using Gexcon's FLACS software). We see that simple hand calculations of the dynamic pressure, based on the assumed parameters give a reasonable value which is in the same magnitude as the one proposed by Aker.

Table 4.1 shows data obtained over a time period of 25 years (1973-97) from various blast events and the corresponding recorded overpressure level. These blast values are in the same range as provided by Aker.

Overpressure (bar)	≤ 0.2	0.2-1	1-2	≥ 2
All events (total 34)	24	8	2	0
Annual exceedance freq.	$2 \cdot 10^{-4}$	$4 \cdot 10^{-5}$ - $2 \cdot 10^{-4}$	$2 \cdot 10^{-5}$ - $4 \cdot 10^{-5}$	$\leq 2 \cdot 10^{-5}$

Table 4.1: Occurrence events on the North Sea Platforms in the UK, Norwegian and Dutch sector for 25 years (1973-97) [11]

4.4 Ductility Level Analysis

A ductile material is defined as a material which allows plastic deformation without losing its strength before fracture occurs, while a brittle material allows little or no plastic deformation. In general, structures must be designed to behave elastically under normal loading conditions (operational conditions), while plastic displacements are allowed during a blast scenario. A measure of the maximum plastic displacement is given by the ductility ratio defined by:

$$\mu = \frac{x}{x_{el}} \quad (4.2)$$

Where x is the maximum plastic displacement and x_{el} is the maximum elastic displacement. Two important levels of assessment are defined following the API (American Petroleum Institute) guidelines concerning blast load design, these are the so-called "Design Level analysis", and the "Ultimate Strength analysis" (Ductility Level analysis) [26]. The Design Level analyses are conventional linear elastic load cases similar to those used

routinely for design with the normal code based elastic failure criteria applied. For a Ductility Level analysis, critical ductility values μ are to be calculated and studied.

Ductility values that have been used for designing topside offshore installations are as follows according to [30]:

Structure type	Ductility value μ or deg
Load bearing panels	1 (BP and Exxon)
Beams and non-load bearing	5 (BP and Exxon)
Rotation beam-column	2 or 12 deg (BP and Exxon)
Secondary structures	1.5 (Brown and Root)
Blast wall	2.5 (Brown and Root)
Steel beam rotation (compact section)	20 or 12 deg (Mobil)
Plates rotation	20 or 12 deg (Mobil)

Table 4.2: Ductility values for design of topside offshore installations

Yasseri [31] proposed the following ductility criteria based on damage levels, shown in table 4.3.

Ranking/Damage level	Acceptable limits
High	$\mu \geq 6$
Substantial	$4 \leq \mu \leq 6$
Moderate	$2 \leq \mu \leq 4$
Light	$1 \leq \mu \leq 2$
Negligible	$\mu \leq 1$

Table 4.3: Damage levels - Ductility ratios

The damage levels from table 4.3 correspond to the following descriptions:

- (a) High: Beyond repair and total loss
- (b) Substantial: Repairable damage for main load bearing system but major loss for equipment with shutdown
- (c) Moderate: Repairable damage and interruption to production; resume production after inspection, repair and replacement
- (d) Light: Minimum repairs and no interruption to production
- (e) Negligible: No repairs required

Chapter 5

Analysis by Abaqus

Non-linear dynamic analyses are required to assess the blast response problems because of the dynamic nature of the blast load, together with the expected plastic response from the structure. The finite element (FEA) software Abaqus CAE (version 6.10-2) has been used for pre- and post processing. The Abaqus Implicit module has been used to analyse the static cases, while the Abaqus Explicit module has been used for the non-linear dynamic analyses. Abaqus is a versatile FEA software used throughout the world for stress, heat transfer, and other types of analysis in mechanical, structural, civil, biomedical, and related engineering applications. Abaqus CAE is capable of pre-processing, post-processing, and monitoring the processing stage of solving a FEM problem. It should be noted that the first stage can be done by other compatible CAD software as well, or even a text editor. However caution should be made with respect to exporting and importing models from other CAD software, as errors and compatibility-issues can arise if one deals with complex models or problems.

While Abaqus CAE supports automatic time incrementation within an implicit time integration algorithm (Hilber-Hughes-Taylor) for nonlinear dynamic analysis, the Abaqus Explicit Package uses the explicit time integration algorithm. Abaqus Explicit Package is thus more suitable for the analysis of brief transient dynamic events, such as the one being assessed in this paper. For a description on the incrementation settings used for the pipe rack blast model, reference is made to section 5.10.4.

It should be noted that two different models were made; one static model and one dynamic model. While these two models have the same geometry, boundary conditions, masses and mesh densities, the static model features a linear elastic material. The dynamic model has an elasto-plastic material assigned to the structure and a time-varying load model. Parameter studies based on varying the magnitude of the blast load, blast duration and the weight of the piping were performed, and a direct comparison between the static model and the more realistic dynamic model was done. The results were studied and a connection between these two models have been investigated through the calculation of

dynamic amplification factors.

5.1 Modeling of geometry

The pipe rack structure was modeled as wire elements with given sectional profiles corresponding to the correct dimensions as from the drawings provided by Aker Solutions. Five different RHS (Rectangular hollow section) profiles were used:

- RHS 200x200x8
- RHS 200x200x10
- RHS 200x100x8
- RHS 200x200x12.5
- RHS 350x350x12.5

Both beams and truss elements are used in two and three dimensions to model slender, rod-like structures in Abaqus CAE. Beam and truss elements represent structures in which the cross-section is assumed to be small compared to the length. The main difference between these two is that the beam element provides axial strength and bending stiffness, while the bending stiffness is neglected for the truss element [32]. For the analysis, all wire elements have been assigned beam section properties. The non-linear geometry (Nlgeom) setting has been applied to all elements.

5.2 Material settings

Elastic material properties have been assigned to the static analysis model, while material non-linearity has been accounted for in the dynamic model, by establishing an elasto-plastic material in Abaqus. The classical metal plasticity model in Abaqus is intended for applications such as crash analyses, metal forming, and general collapse studies [32]. It should also be noted that the plasticity model in Abaqus must be used in conjunction with the linear elastic material model, and that true (Cauchy) stress and log strain values are to be used [33].

Nominal stress (engineering stress) is calculated assuming the cross-sectional area not to change during deformation; this is a valid approach if the expected deformations are small. However for a case with large deformations, the change in cross-sectional area is significant and true (Cauchy) stress has to be implemented. We see from figure 5.2 that both nominal and true stresses are almost identical and linear elastic up to the yield strain. After this point, the true stress is larger than the nominal stress when the strain increases. This is due to the reduction of the cross sectional area due to deformation.

The equations that convert nominal stress to true stress are as follows [34]:

$$\sigma_{true} = \sigma(1 + \epsilon) \tag{5.1}$$

$$\epsilon_{true} = \ln(1 + \epsilon) \tag{5.2}$$

In the elasto-plastic non-linear material model, it has been suggested by Aker Solutions to use the table as from figure 5.1 and 5.2 for Carbon Steel grade S355.

fy = 355MPa		Log	Log		Plastic	
Nom strain	Nom stress	True strain	True stress	Plastic strain	Point	
ϵ_{nom}	σ_{nom}	ϵ	σ	ϵ_{pl}	No.	
0,00000	0,0	0,000000	0,0	0,000000		
Elastic limit	0,00169	355,0	0,001689	355,6	0,000000	0
	0,01652	365,6	0,016386	371,6	0,01462	1
	0,03135	376,2	0,030871	388,0	0,02902	2
	0,04618	386,8	0,045149	404,6	0,04322	3
	0,06101	397,4	0,059225	421,6	0,05722	4
	0,07585	407,9	0,073107	438,9	0,07102	5
	0,09068	418,5	0,086798	456,5	0,08462	6
	0,10551	429,1	0,100304	474,4	0,09805	7
	0,12034	439,7	0,113631	492,6	0,11128	8
	0,13517	450,3	0,126782	511,2	0,12435	9
Critical strain	0,15000	460,9	0,139762	530,0	0,13724	10

Figure 5.1: Stress-strain capacity table, provided by Aker Solutions (from project scope)

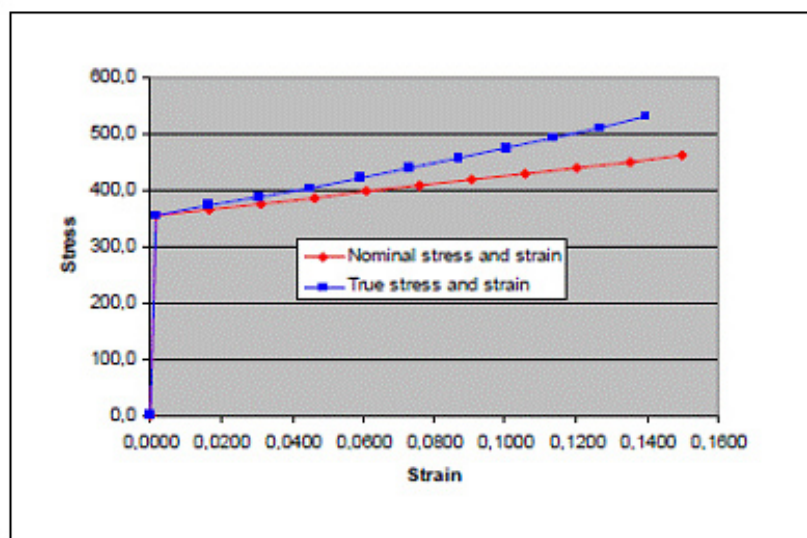


Figure 5.2: Stress-strain capacity curve, provided by Aker Solutions (from project scope)

5.3 Structural elements

It should be noted that while Abaqus/Implicit supports both Euler-Bernulli (B23, B23H, B33, and B33H) and Timoshenko (B21, B22, B31, B31OS, B32, B32OS) beam elements, Abaqus/Explicit supports the latter type only.

The Explicit linear beam element B31 has been assigned to the model. The B31 element is a 2-node linear beam in space based on the Timoshenko beam formulation. Unlike Euler-Bernoulli beam elements, Timoshenko beams also incorporate a first order correction for transverse shear deformation effects. The kinematic assumption from the Timoshenko beam theory says that a plane section originally normal to the centroid remains plane, but in addition also shear deformations occur. This is in contrast to Euler-Beam theory where the plane section normal to the midline is assumed remaining unchanged during deformation. An additional angle γ will be introduced in the Timoshenko beam theory due to the additional shear effect, this is defined as the shear angle. θ is the rotation angle of the normal. The slope of the midline for will be $w'(x) = \theta + \gamma$. Reference is made to figure 5.3 and 5.4 for a comparison between these two basic beam theories.

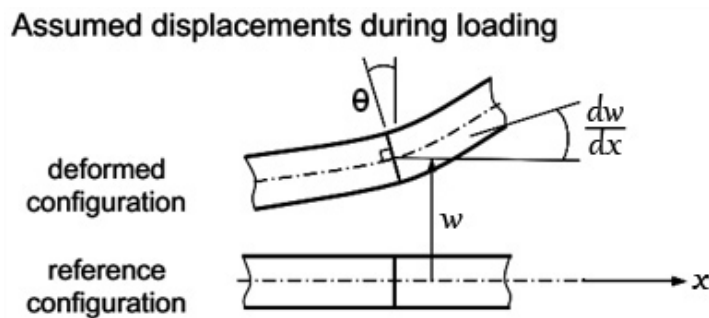


Figure 5.3: Euler-Bernoulli beam formulation [7].

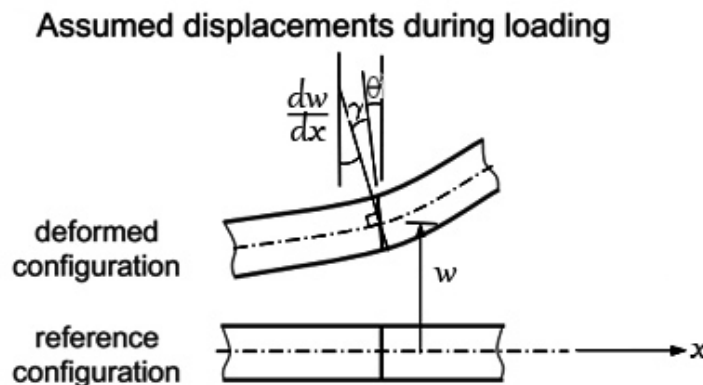


Figure 5.4: Timoshenko beam formulation accounts for the additional shear angle [7].

The effects of the shear contribution can be shown by deriving the bending moment \tilde{M} and \tilde{F}_s , the shear force in the cross section. This will be done following an approach as presented by Yao. W and Zhong. W [8].

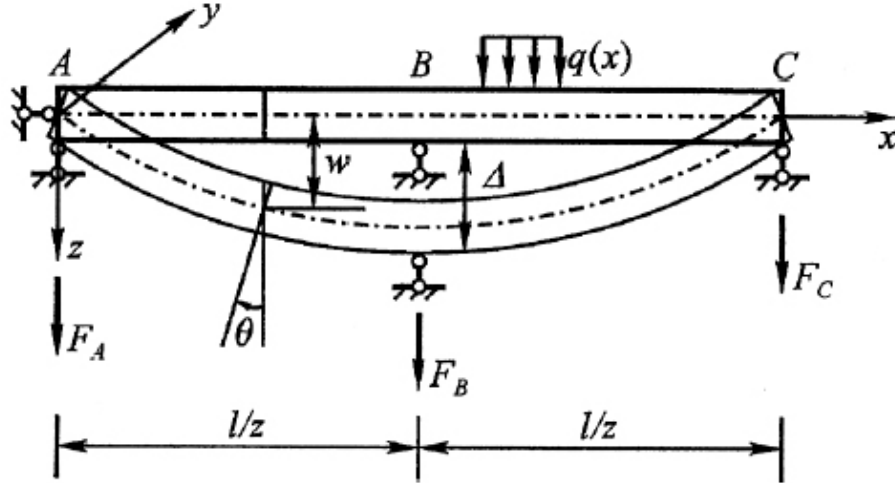


Figure 5.5: Bending of Timoshenko beam [8].

If the x -axis is defined along the undeformed beam axis, and the xz -plane is taken as the deflection plane as shown in figure 5.5, the displacements $\hat{u}(x, z)$ and $\hat{w}(x, z)$ at any point (x, z) on the beam can be described by two generalized displacements, i.e the deflection of the beam axis $\tilde{w}(x)$ and the rotational angle of the beam cross-section $\tilde{\theta}(x)$. These are expressed by the equations in 5.3.

$$\hat{u}(x, z) = -z\tilde{\theta}(x), \quad \hat{w}(x, z) = \tilde{w}(x) \quad (5.3)$$

By using the strain-displacement relation [35] the following strain components are obtained:

$$\epsilon_x = -z\frac{d\tilde{\theta}}{dx}, \quad \gamma_{xz} = \frac{d\tilde{w}}{dx} - \tilde{\theta} \quad (5.4)$$

If the stress-strain relation is used, and the effect of the stress quantities from σ_y is neglected, the two expressions are further rewritten:

$$-z\frac{d\tilde{\theta}}{dx} = \frac{1}{E}\sigma_x, \quad \frac{d\tilde{w}}{dx} - \tilde{\theta} = \frac{1}{G}\tau_{xz} \quad (5.5)$$

By multiplying the first equation in 5.5 by z on both sides and integrating over the cross-section area on both sides, and repeating this integration for the second equation, equation 5.6 and 5.7 are obtained.

$$-I \frac{d\tilde{\theta}}{dx} = \frac{1}{E} \int_A z \sigma_x dA = -\frac{1}{E} \tilde{M} \quad (5.6)$$

$$A \left(\frac{d\tilde{w}}{dx} - \tilde{\theta} \right) = \frac{1}{G} \int_A \tau_{xz} dA = \frac{1}{G} \tilde{F}_s \quad (5.7)$$

Here I is the moment of inertia about the y -axis of the cross-section of the beam, A is the cross-sectional area of the beam and E is the Young's modulus. G is the shear modulus. The final expressions for the bending moment \tilde{M} and the shear force \tilde{F}_s in the cross section are:

$$\tilde{M} = EI \cdot \tilde{\kappa}, \quad \tilde{F}_s = kGA \cdot \tilde{\gamma} \quad (5.8)$$

Whereas $\tilde{\kappa}(x) = \frac{\partial \tilde{\theta}}{\partial x}$, and $\tilde{\gamma} = \frac{\partial \tilde{w}}{\partial x} - \tilde{\theta}$.

When deriving these formulas, an assumption was made that the shear stresses over the cross-section remained constant. This is not correct in real-life, hence a shear correction factor k is introduced. This factor is dependent on the assumed shear stress distribution over a cross-section. It should be noted that $k \rightarrow \infty$ implies approaching the classic Euler-Bernoulli beam solution, where the shear stress contribution is neglected.

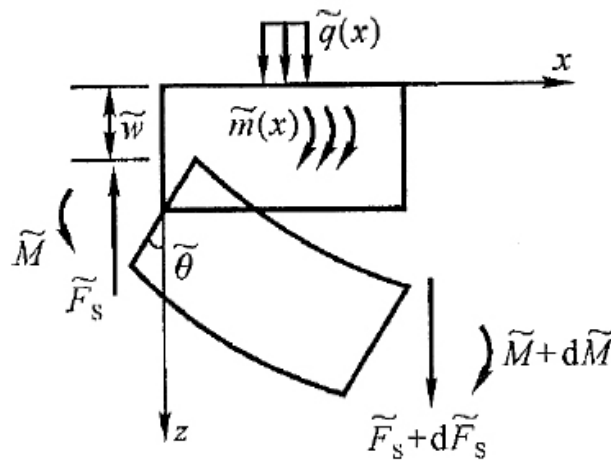


Figure 5.6: Force and moment equilibrium for an infinitesimal segment of the beam.

By further using moment and force equilibrium on an infinitesimal segment of the beam, the strong form of the equation of motion in terms of displacements can be derived. The final expression is given as equation 5.9. The transverse distributed load is represented by \tilde{q} , \tilde{m} is the distributed external moment. Reference is made to [8] for the full derivation.

$$\left. \begin{aligned} \frac{\partial}{\partial x} [kGA(\frac{\partial \tilde{w}}{\partial x} - \tilde{\theta})] + \tilde{q} &= \rho A \frac{\partial^2 \tilde{w}}{\partial t^2} \\ \frac{\partial}{\partial x} (EI \frac{\partial \tilde{\theta}}{\partial x}) + kGA(\frac{\partial \tilde{w}}{\partial x} - \tilde{\theta}) + \tilde{m} &= \rho I \frac{\partial^2 \tilde{\theta}}{\partial t^2} \end{aligned} \right\} \quad (5.9)$$

5.4 Model mesh

5.4.1 Mesh sensitivity (Convergence study)

When meshing the model, one need to consider the mode shapes that may be excited in the response, and choose a refinement of the mesh based on these observations. For a particular beam with both ends clamped as in figure 5.7, several eigenmodes are to be expected. The mesh resolution for this case, should be such that it can fully capture both the 1st and the higher 4th eigenmode.

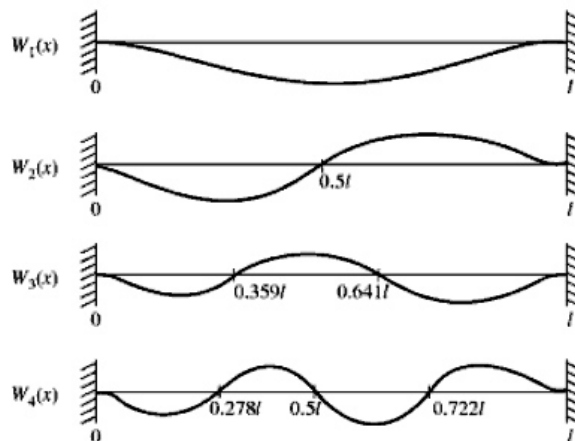


Figure 5.7: Figure showing the eigen modes for a particular beam with both ends clamped.

One should also bear in mind that designing the mesh for the static case may be different than designing the mesh for the dynamic case, where the response might be excited by high-frequency loads. In finite element modeling, a finer mesh will typically result in a more accurate solution. However, an increase in mesh density will also increase the computation time. A mesh sensitivity study has been performed on the beam model. The purpose is to study the stress sensitivity with respect to the stress distribution of a

part of the model, and to find an optimal mesh density which gives adequate results with the shortest CPU time as possible.

It should be noted that automatic global seeding has been used in Abaqus, which means that the mesh size is created automatically based on a maximum size criteria given as an *approximate global size*-input. Abaqus will mesh the model based on this input, and ensure that this criterion is met. For a beam model such as the pipe rack, automatic global seeding will give seeds of constant density, and thus an even mesh distribution over the global model.

Table 5.1 shows approximate global sizes with its corresponding mesh size (percent of whole beam length) for the pipe rack model:

Approximate global size (Automatic global seeding)	Approximate mesh size (% of whole beam)
0.4	13-14
0.3	8-11
0.2	7-8
0.1	3-4
0.07	2-3
0.04	1
0.01	less than 1

Table 5.1: Approximate global sizes with its corresponding mesh size for the pipe rack beam model

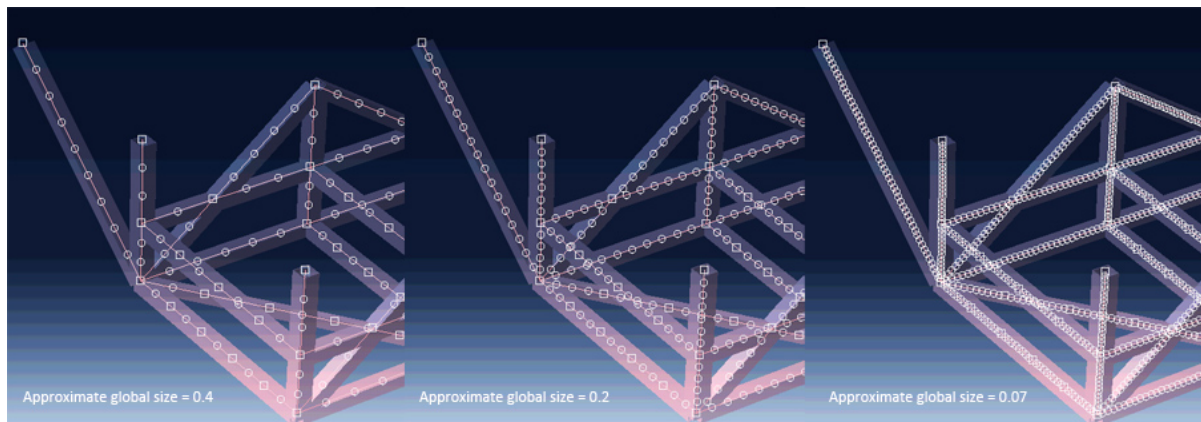


Figure 5.8: Showing the variation in global seeding for three different kind of seeding densities.

The mesh sensitivity study was done based on looking at two horizontal beam elements (see figure 5.9), and integrating the stress fields over the length of the elements. Due to

the dynamic analysis varying in time, a specific time step (time = 0.9763 s) was chosen. The stress field integration has been performed for all mesh density cases at the same time step. Reference is made to appendix H.

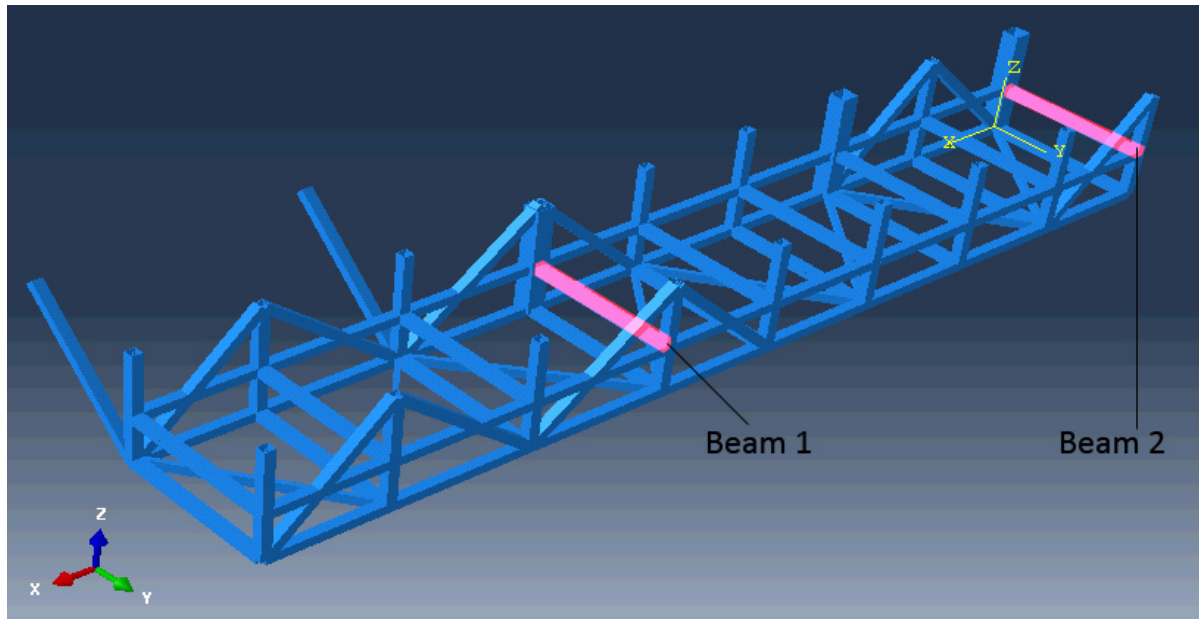


Figure 5.9: Showing the two beams used in the stress convergence study.

By studying figure 5.10, it is seen that the integrated stress will converge towards a fixed value for finer meshes. It is shown evidently, that mesh sizes 0.3 and 0.4 are unsuitable for such analyses as they will lead to overestimation of stresses compared to the converged value. For beam 1, mesh 0.3 and 0.4 give an overestimation of the integrated stress of roughly 20 to 30 percent. For beam 2, this overestimation is between roughly 50 and 100 percent. Such overestimated stress levels are not acceptable. The same figure also shows that a mesh size 0.1 will cause a slight underestimation of the stress level for both beam 1 and beam 2. Convergence is achieved for finer mesh less than 0.1. For detailed stress field plots for beam 1 and beam 2, please see appendix H.

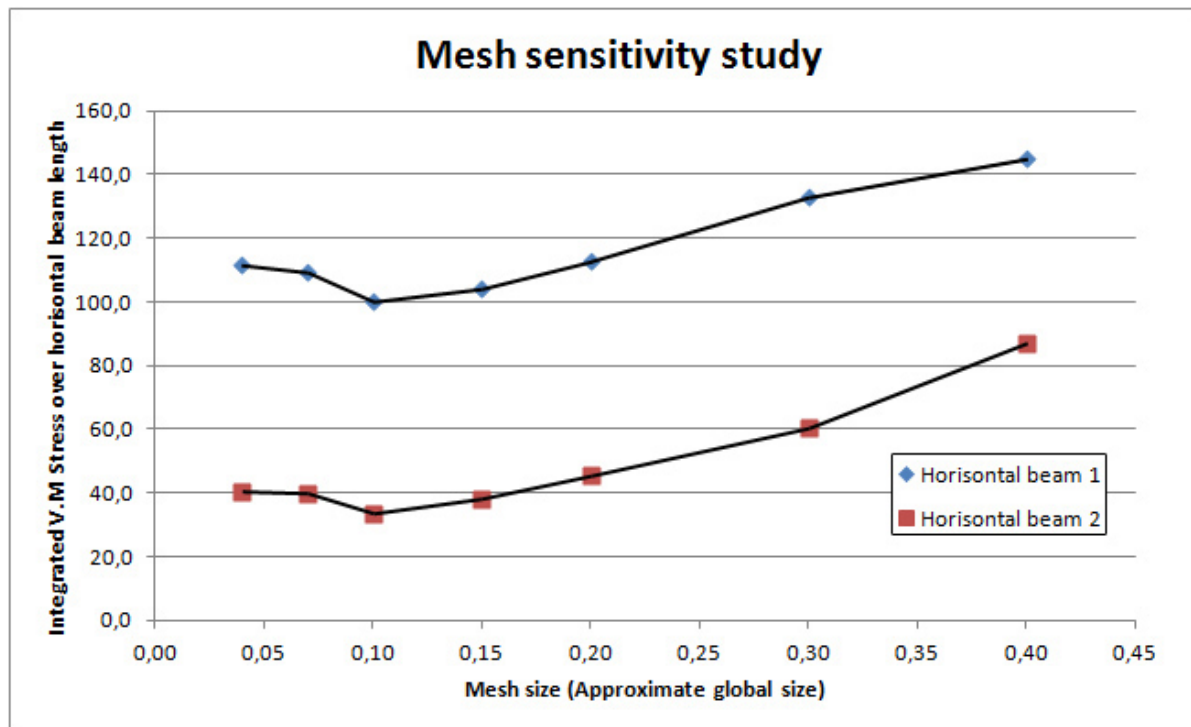


Figure 5.10: Mesh sensitivity for beam 1 and 2. Blast duration 50 ms, 0.2 bar drag pressure.

5.4.2 CPU-time

The CPU Time will increase for finer mesh in the model. Figure 5.11 shows the CPU time for a given mesh size for the *undamped* pipe rack beam model. Because a parameter study is to be performed, a large amount of analyses are to be run. It is therefore essential that the analysis model has a CPU time of such duration that effectiveness in each analysis run can be achieved, and still result in adequate results. It is previously shown in section 5.4.1 that mesh sizes below 0.2 are unsuitable to use for the model. From figure 5.11 it is seen that mesh sizes above 0.1 will cause a rapid increase in CPU time.

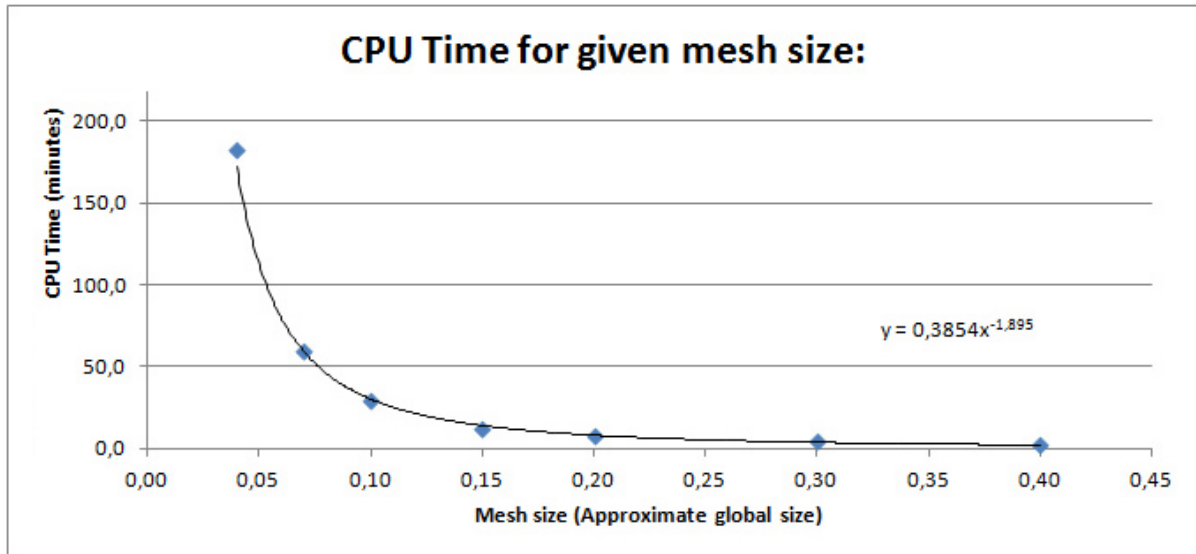


Figure 5.11: Variation in CPU time for different mesh sizes. A trend line was created based on these data, a power function can be derived from these. This function gives the required CPU time (y) for a given input x (mesh size).

Based on a consideration of a trade-off between computational time and relative accuracy of results, an approximate global size of 0.2 has been chosen to be used for the automatic global seeding in Abaqus. The yielded results are expected to be slightly conservative, as discussed in the previous section 5.4.1.

5.5 Mass model

The structural mass has been represented in Abaqus by applying gravity loads on all elements. The weight of the pipes attached to the pipe rack has been modelled by applying inertia (point masses) properties at prescribed points on the beam model. It should be noted that inertia (point masses) in Abaqus are specified as mass, and not weight [36]. Reference is given to appendix A for an overview of the inertia (point masses) used. It has been assumed that each pipe spans across the whole length of the pipe rack, thus distributing its weight evenly on each horizontal beam, this is visualized in figure 5.12.

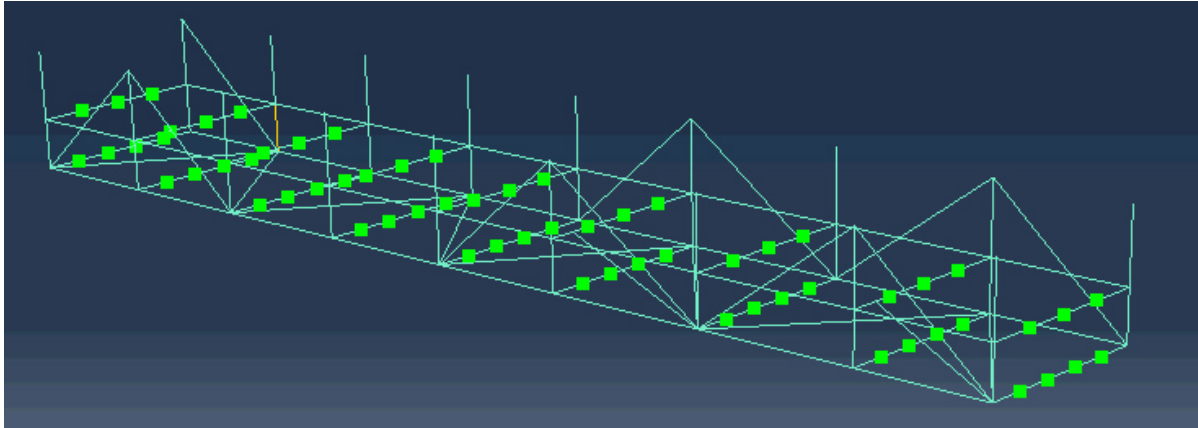


Figure 5.12: Inertia properties (point masses) assigned to represent piping weight

The piping arrangement on a pipe rack will vary, both with respect to the number of pipes, sizes and weights, and are prone to changes throughout a project. From a general perspective, the size of the pipes (including some requirements on spacing between them) limits the number of pipes which can be added to a pipe rack. Electrical wirings are present as well, but are negligible in an analysis due to small weight and size. To be able to solve the problem in the most general way, it is needed to generalize the problem; the effect on the change of piping will therefore be represented by several assumed piping configurations, hence named arrangement 1, 2 and 3. These are shown in figure 5.13. Arrangement 1 represents the heaviest loaded condition, with overall weight decreasing for 2 and 3 respectively.

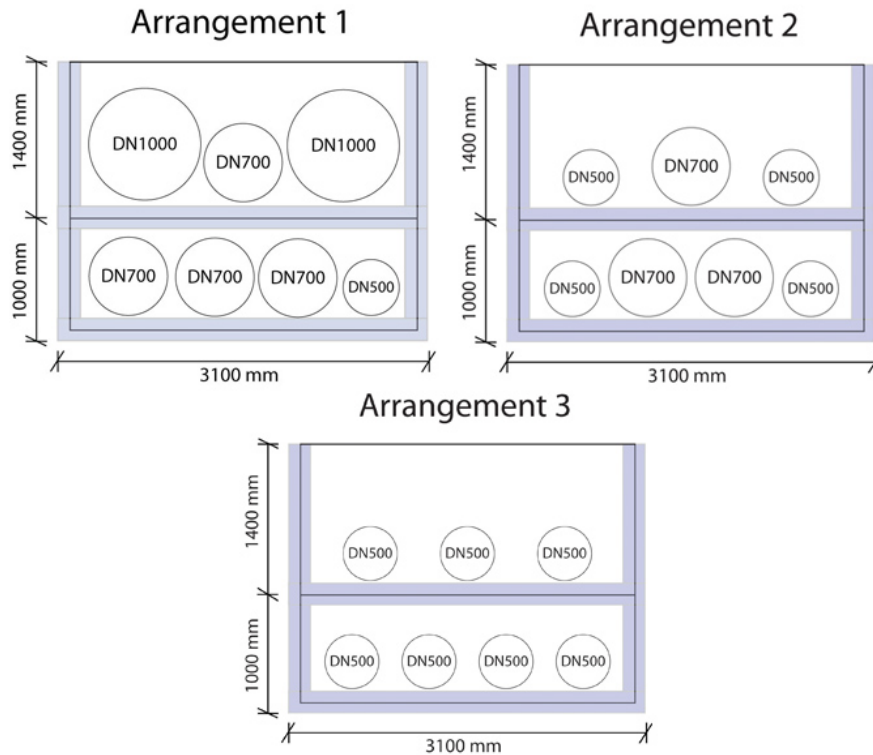


Figure 5.13: Illustration of piping arrangement 1, 2 and 3.

5.6 Load model

When using a wire element assigned with a profile, a uniform distributed load is applied in Abaqus using a line load. A line load is applied as a uniform load over the wire element (unit=N/m). Because the dynamic pressure is expressed in Pascals, it is multiplied with a characteristic element RHS profile height to obtain the correct line load. For this pipe rack, two type of RHS profiles are used; RHS200 and RHS350. Meaning that the cross-section height of the profiles are 200 and 350mm respectively.

- Dynamic pressure = 0.2 bar = $2 \cdot 10^4 \text{ Pa} \left(\frac{\text{N}}{\text{m}^2} \right)$
- Dynamic pressure = 0.4 bar = $4 \cdot 10^5 \text{ Pa} \left(\frac{\text{N}}{\text{m}^2} \right)$

The line loads corresponding to these pressures (on RHS350) are thus:

- Line load (0.2 bar) = $20\,000 \frac{\text{N}}{\text{m}^2} \cdot 0.35 \text{ m} = 7000 \frac{\text{N}}{\text{m}}$
- Line load (0.4 bar) = $40\,000 \frac{\text{N}}{\text{m}^2} \cdot 0.35 \text{ m} = 14\,000 \frac{\text{N}}{\text{m}}$

The line loads corresponding to these pressures (on RHS200) are:

- Line load (0.2 bar) = $20\,000 \frac{N}{m^2} \cdot 0.2\,m = 4000 \frac{N}{m}$
- Line load (0.4 bar) = $40\,000 \frac{N}{m^2} \cdot 0.2\,m = 8000 \frac{N}{m}$

The line load has been applied to the whole structure as shown in figure 5.14. Simplification on the effects of shielding has been taken account for by using a drag coefficient C_D equal to 1.0, as suggested in section 4.3.

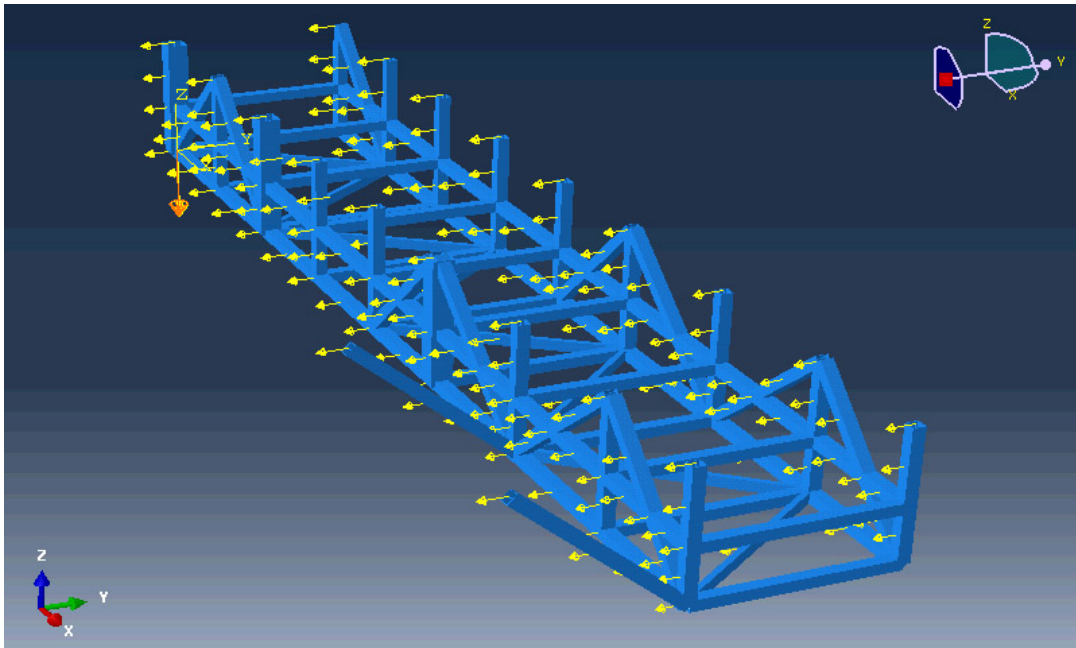


Figure 5.14: Line load applied on the beam elements in Abaqus

Because a dynamic analysis is time-dependent, it is necessary to create a time-varying load profile in Abaqus to correctly represent the effects of the blast load. The amplitude toolset in Abaqus has been used to define the pressure load profile for the dynamic analyses. By using the tabular feature, the load profile was defined by directly giving the input values for a profile amplitude corresponding to a specific time. This is illustrated in figure 5.15 for the pressure load profile for the 50 ms blast.

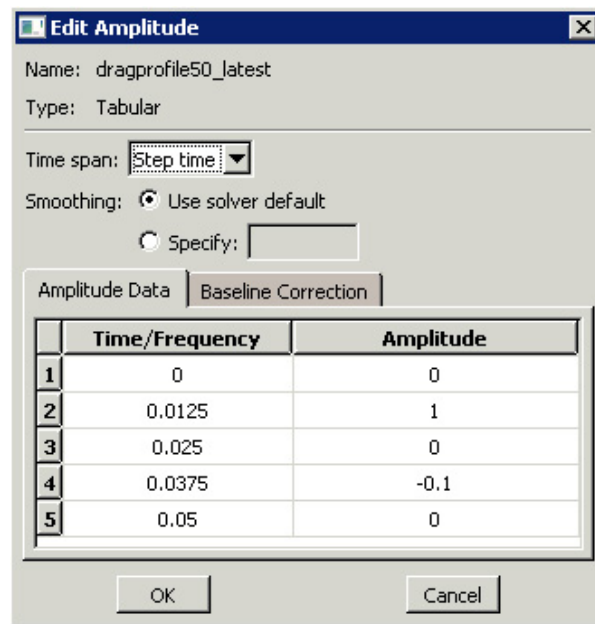
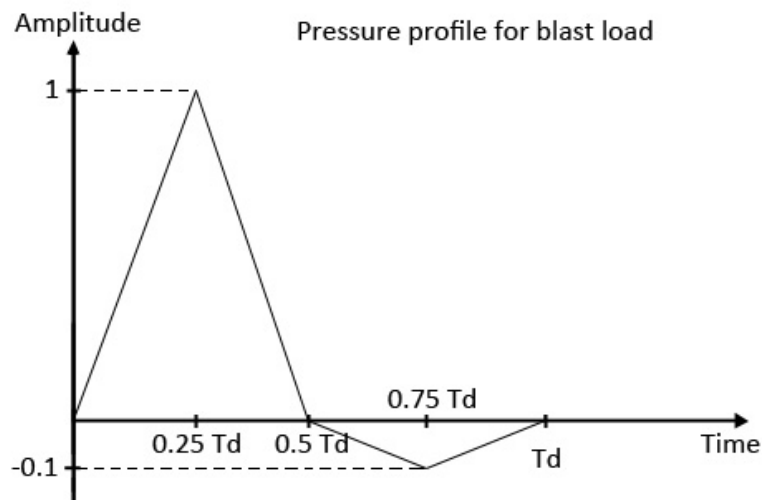


Figure 5.15: Amplitude toolset (tabular feature) in Abaqus

Figure 5.16: Triangular pressure load profile corresponding to the input given in the amplitude toolset (see also diagram provided by Aker Solutions in figure 4.11. T_d is the duration of the blast, it is assumed to be between 50 and 200 ms)

5.7 Boundary conditions

All structural elements welded directly to the girders on the deck above are assumed fixed in all 6 DOFs. For simplification, the three connections between pipe rack and the support beams are assumed fixed as well. An overview of the boundary conditions imposed to the model in Abaqus is found in figure 5.17.

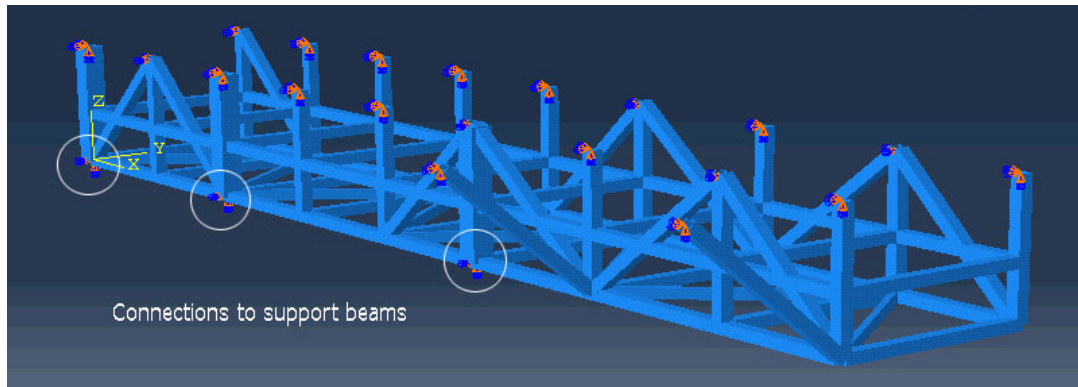


Figure 5.17: Fixed boundary conditions (in all 6 DOFs) are added to the connections between pipe rack and the rest of the structure

5.8 Geometric non-linearity

Non-linear geometric effects have been taken account for both in the static and dynamic analyses by turning on the "Nlgeom" feature in Abaqus CAE.

5.9 Damping model

General damping in Abaqus is represented by Rayleigh damping. To investigate the damping contribution from the stiffness and mass proportional damping term, the pipe rack model, 50 ms blast duration and 0.2 bar overpressure is analysed in ABAQUS/Explicit. Abaqus requires input for the mass and stiffness proportional damping coefficients α and β . By assuming stiffness proportional damping, the mass proportional damping constant (α) is set to zero in the rewritten Rayleigh damping expression (equation 3.6), the result is equation 5.10.

$$\zeta = \frac{\beta\omega}{2} \quad (5.10)$$

Solving for β yields:

$$\beta = \frac{2\zeta}{\omega} \quad (5.11)$$

Similarly the mass proportional damping term can be found by setting the stiffness proportional constant (β) to zero.

Solving for α yields:

$$\alpha = 2\omega\zeta \quad (5.12)$$

Table 5.2 shows damping constants calculated to study the damping effect (The natural frequency used in these calculations is taken as the eigenfrequency for the lowest eigenmode). By using these constants, analyses are run with both mass and a stiffness proportional damping model respectively. The results from the stiffness proportional damping analyses for an element are shown in figure 5.18. It should be noted that the damping effect from the mass proportional damping is of negligible magnitude.

Damping ratio, ζ (percent of critical)	α	β
0.1	0.029	1.39e-4
0.2	0.058	2.78e-4
0.3	0.086	4.16e-4
0.4	0.115	5.55e-4

Table 5.2: Damping constants used for the investigation of the damping effect on the structural response

When comparing the different stiffness proportional damping models over the blast *and* post-blast domain (see figure 5.18), it is seen that a damping ratio of 0.1 percent of critical damping gives the most significant damping effect among all stiffness proportional damping models. The global Von-Mises stress level from the maximum peak due to the blast loading in the post-blast domain will be reduced with roughly 70 percent compared with the no damping case, assuming 0.1 percent damping ratio. When 0.2 percent damping ratio is used, the reduction is around 50 percent compared to the case with no damping. Figure 5.19 shows that 0.4 percent of critical damping gives the largest damping effect when looking at the blast domain only. For this particular case, a reduction of roughly 7 percent on the Von-Mises stress is observed for the damped model compared to the undamped one.

Further wise, figure 5.20 illustrates the damping effect on the reaction force (support reaction) in the direction of the blast (Y-direction). The largest reduction in the reaction force between the non-damped model and the damped model is roughly 13.

It is shown through these investigations, that if no damping model is used, structural elements will oscillate forever due to the lack of energy dissipation in the computational model. Because of the many uncertainties of choosing a proper damping constant,

including the risk of producing non-conservative results, a choice was made to neglect damping in all dynamic analysis models presented in this paper. This argument is also backed up by investigations on explosion analyses by Hong and J.Y Richard [37]. According to their research, damping effects can be ignored in explosion analyses, if conservative stress levels are of interest. In addition, if the structural response happens to be plastic, Yandzio and Gough showed that in an inelastic analysis, the energy dissipated through plastic deformation is significantly greater than that dissipated by structural damping [38].

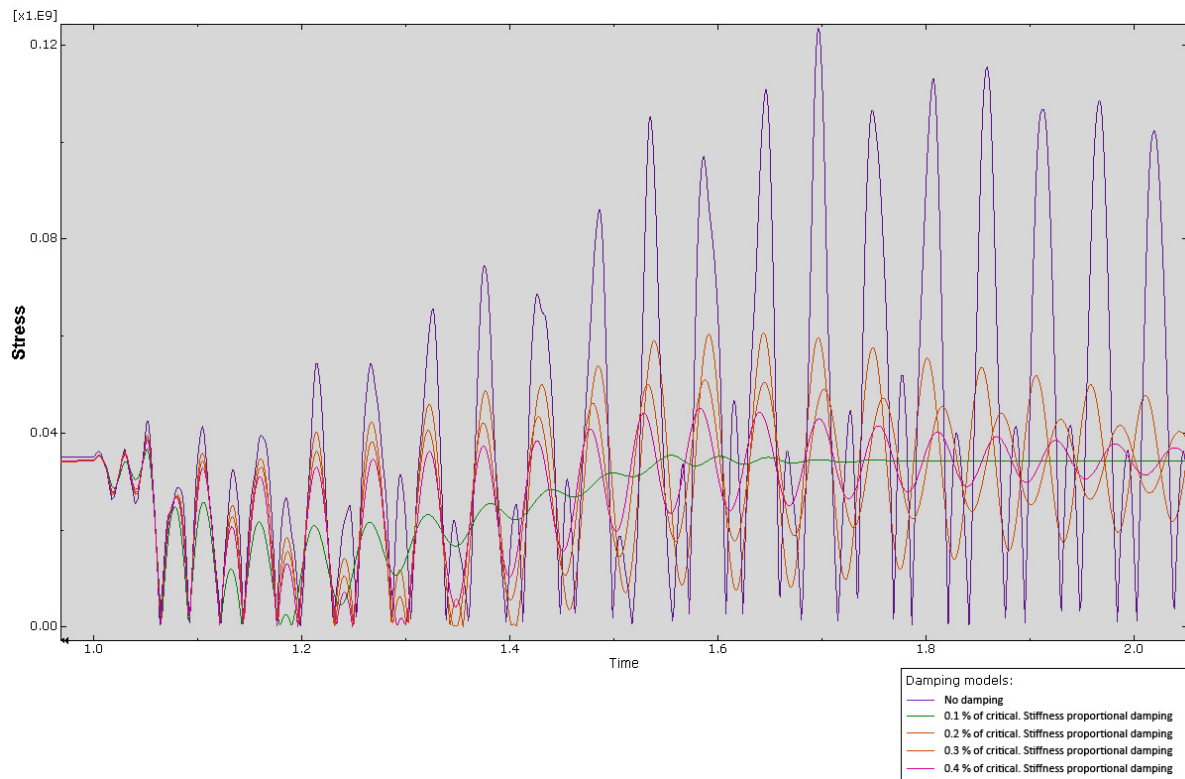


Figure 5.18: Figure illustrating the damping effect (stiffness proportional damping) for the lowest eigenmode, position: element 899, Section point (SP) 13. Von-Mises stress variation [Pa] over blast and post-blast domain.

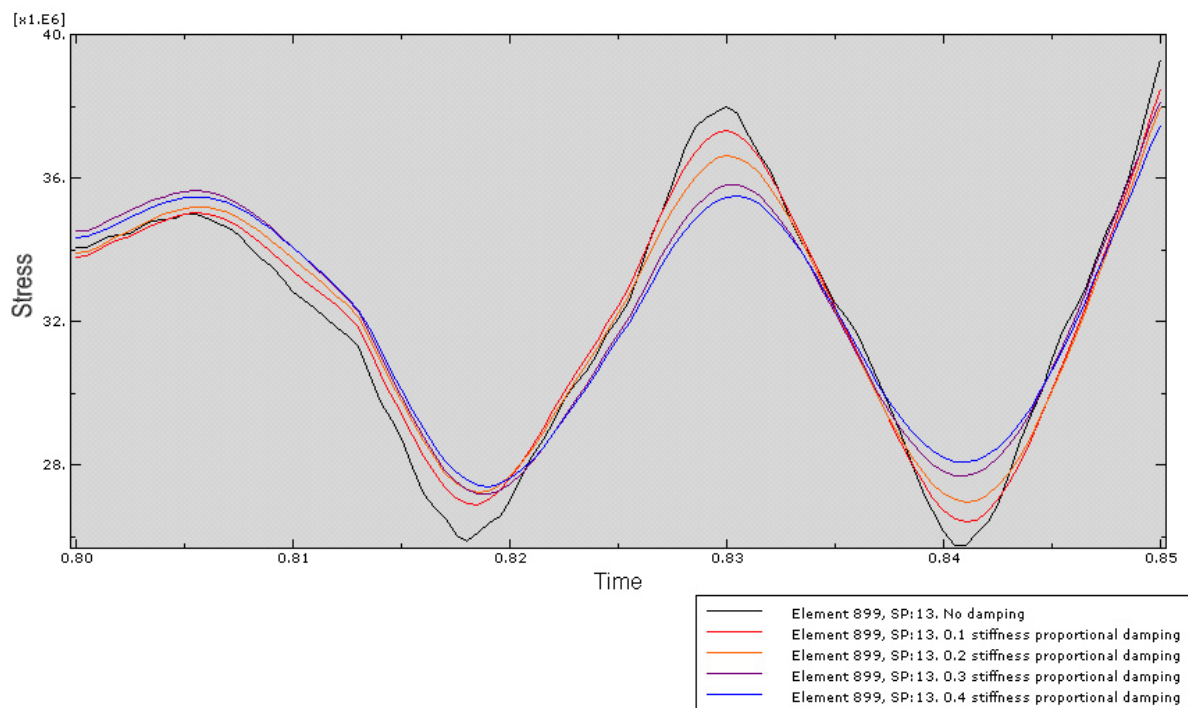


Figure 5.19: Figure illustrating the damping effect (stiffness proportional damping) for the lowest eigenmode, position: element 899, Section point (SP) 13. Von-Mises stress variation [Pa] over blast domain only.

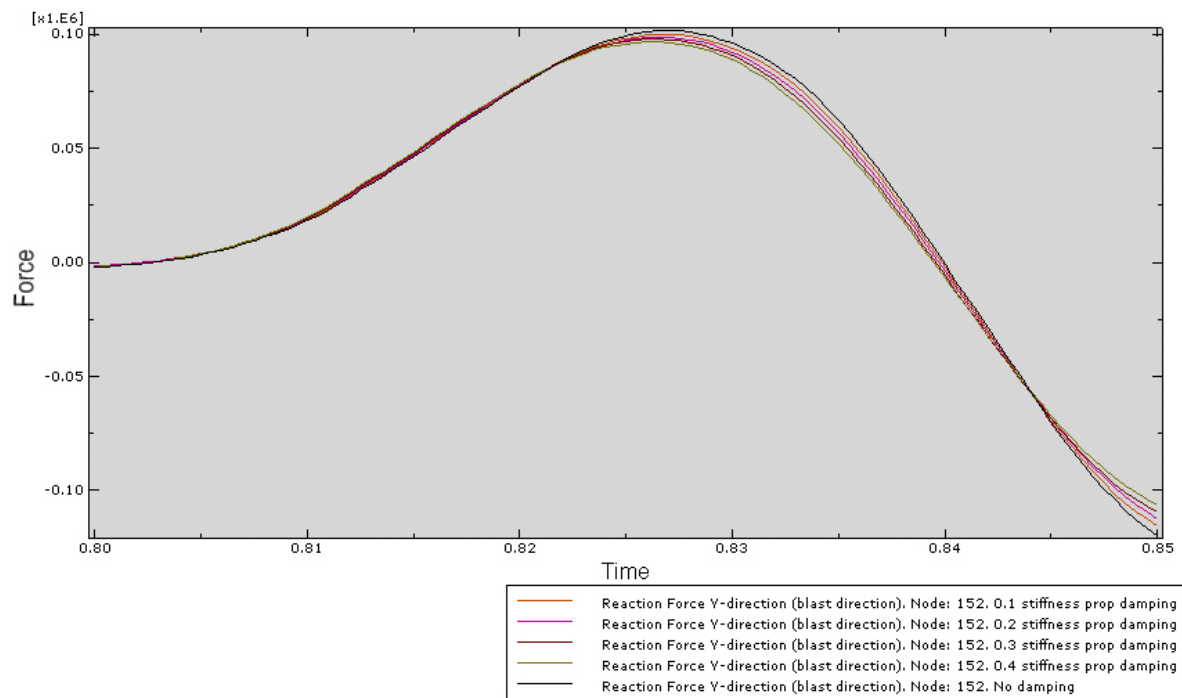


Figure 5.20: Figure illustrating the damping effect (stiffness proportional damping) for the lowest eigenmode, position: Node 152. Reaction force [N] in the blast direction (Y-direction) over blast domain only.

5.10 Step settings

Analysis steps in Abaqus are used to separate an analysis into manageable parts. Within each step, the user is free to control the different loading- and boundary condition parameters. The initial step is a standard step in Abaqus, which is created automatically at the beginning of the model's step sequence. This initial step cannot be renamed, edited, replaced, copied or deleted.

The initial step allows the user to define boundary conditions, predefined fields and other interactions that are applicable at the beginning of the analysis. For the pipe rack analyses, the boundary conditions are applied in the initial step, and will thus propagate through the rest of the steps in the analysis. In addition the initial step, 3 other steps are present in the analysis. These are:

1. Self-weight (gravity load, mass from pipes)
2. Blast (positive and neg. load amplitude). Different step duration depending on duration of blast (i.e 50, 100, 150 or 200 ms)
3. Post-blast (only gravity load is set active, no propagation of blast load from previous step)

5.10.1 Self-weight

The "Self-weight" step is where the gravity (structural self-weight of the structure) and piping weight is applied linearly on the structure using Abaqus' in-built *RAMP* function. This function uses 0.5 seconds to linearly increase the structural self weight up to a quasi-static stress level. This is illustrated in figure 5.21. If the structural weight is loaded instantaneously, the element will experience oscillatory stress variation before the initial blast is initiated. This will give a wrong representation of the stress variation during the actual blast, which is illustrated in figure 5.22. It is shown from the same figure that the oscillations will reach the maximum global amplitude earlier for the instantaneously applied self-weight and piping weight, than for the case with linear increase. Both methods however show a similar stress level for the maximum amplitude during post-blast.

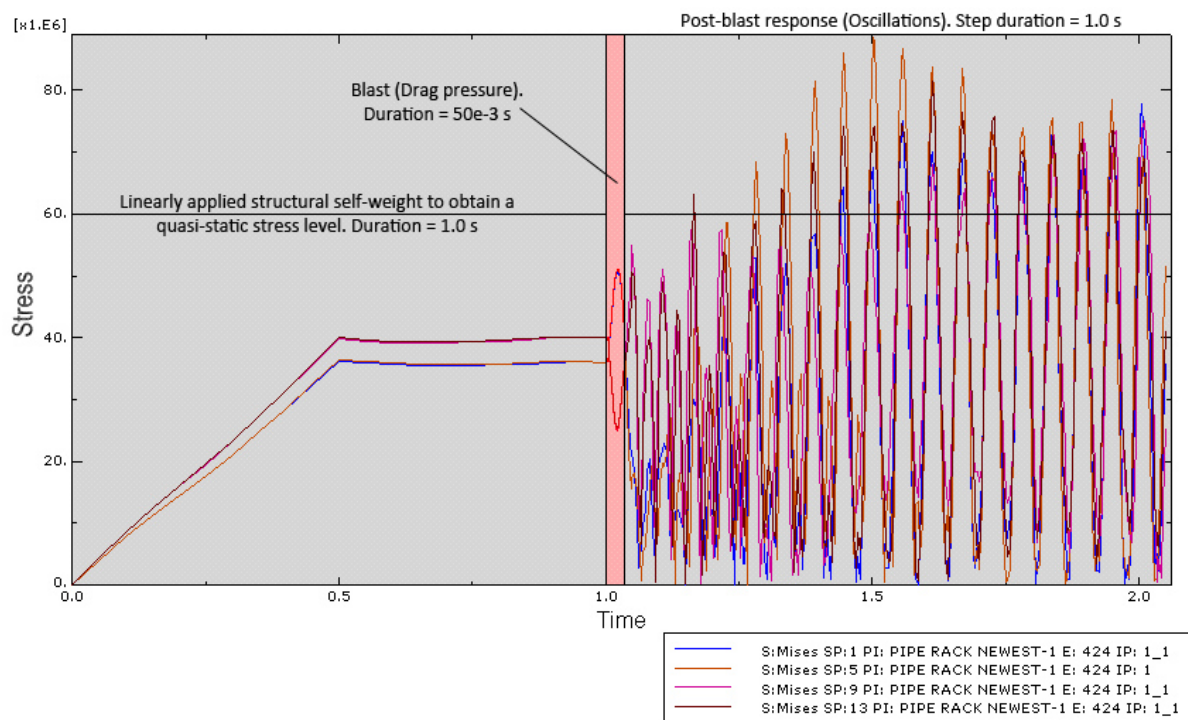


Figure 5.21: Stress variation for element 424, 50 ms blast duration, 1 second post-blast step. Stresses given for 4 integration points. Linearly applied structural self-weight and piping weight.

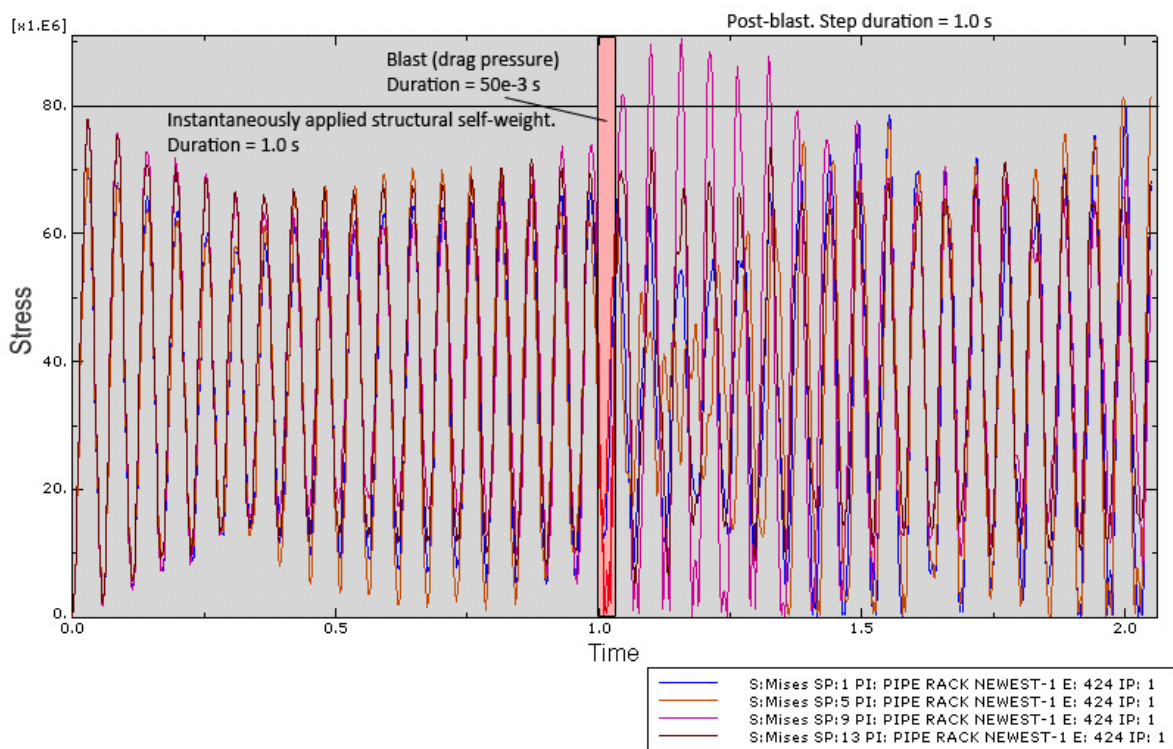


Figure 5.22: Stress variation for element 424, 50 ms blast duration, 1 second post-blast step. Stresses given for 4 integration points. Instantaneously applied structural self-weight and piping weight as for piping arrangement 1.

5.10.2 Blast

The "Blast" step is where the blast drag pressure is introduced. Reference is made to section 4.3 and 5.6 for a more detailed description of the load itself. The *amplitude tool set* (tabular feature) in Abaqus was used to define this amplitude profile. This amplitude takes account for both the positive and the negative part of the drag pressure profile. This step has the same duration as the blast itself, i.e 50, 100, 150 or 200 ms depending on which case that was being analysed.

5.10.3 Post-blast

The "Post-blast" step is a step without any loads imposed on the structure, but with the structural self-weight (gravity load) propagating from the previous steps. The purpose of this step is to study the post-blast response of the structure. An important aspect of this step is to ensure correct settings for the ODB-field output to avoid aliasing during signal processing. Reference is made to section 5.11.1.

Determining the length of the post-blast step is a topic of discussion. It is observed from results that the maximum response amplitude, e.g Von-Mises stresses are higher during the post-blast step than under the blast step. However, the structure's post-blast response is not important for calculating the DAF, which is the main scope of this thesis. For calculating stresses to determine DAF-values, the duration of the post-blast step has been decreased to keep the analysis time to a minimum. For the study of the damping effect on the response during post-blast, this step has been purposely increased to be able to fully capture this.

5.10.4 Incrementation settings

The incrementation settings in Abaqus are being set to the automatic configuration (*Automatic time incrementation*). This means that Abaqus/Explicit will automatically adjust the increment size when the analysis is proceeding depending on the stability limit [39].

Fixed time incrementation is supported by Abaqus/Explicit, but when this is used, Abaqus/Explicit will not check if the computed response is stable during the step. Validity of the response has to be checked for each analyses by carefully checking the energy history and other response variables, this is time consuming and rarely recommended [39].

5.11 Post-processing

5.11.1 Field-Output settings in Abaqus

The recording of the data during an analysis is done by sampling. In Abaqus CAE, this is controlled via the *Field-Output Editor*. To obtain a realistic representation of the response, and to avoid aliasing (i.e distortion of sampled result data), it is important to choose a sampling frequency which is high enough to cover all variations, but on the same time, be of such level that the size of the output file does not become unnecessary large.

The effect of distortion of data due to aliasing is illustrated in figure 5.23. The original sine wave has a maximum frequency of 1 kHz. In order to define the amplitude and phase of the original sine wave, it is necessary to use a sampling frequency of at least $2f_{max}$ (2 kHz), in which $2f_{max}$ is defined as the Nyquist sampling rate according to the Sampling Theorem [40]. The requirement is given as expression 5.13.

$$f_s > 2 \cdot f_{max} \quad (5.13)$$

here f_s is the sampling frequency, and f_{max} is the maximum frequency of the signal.

If a sampling rate of 3 kHz is used, which is above the required sampling rate, the data will be recorded without aliasing. The 1.1 kHz sampling rate however, is below the required rate, and the resulting curve becomes a misleading representation of the original sine wave.

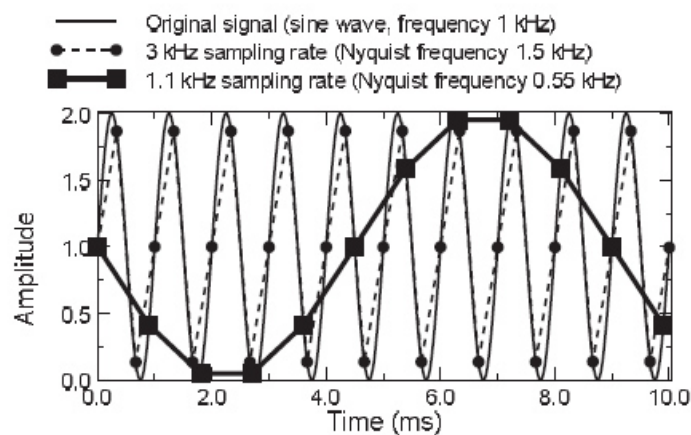


Figure 5.23: Figure illustrating the effect of aliasing on a sinusoidal curve [9].

The safest way to ensure that aliasing does not occur in Abaqus is to request output at each increment. However, this is often impractical as it may create very large output files.

Figure 5.24 shows the effect of aliasing (distortion of sampled data) for element 424. A low sampling rate may cause the maximum stress peak not to be accurately recorded; it may also give a very misleading representation of the high-frequency oscillations which characterizes the post-blast response.

The sampling rate (output rate) has been adjusted for each step in the analysis using the *Field Output Editor* in Abaqus CAE. The sampling rate for the *self-weight step* is low, as it is expected a linear increase of both stresses and displacements until it reaches the final quasi-static value. Further wise, the sampling rate has been increased for the blast and post-blast steps. This is to be able to accurately record the high-frequency variations of both stresses and displacements during both blast and post-blast.

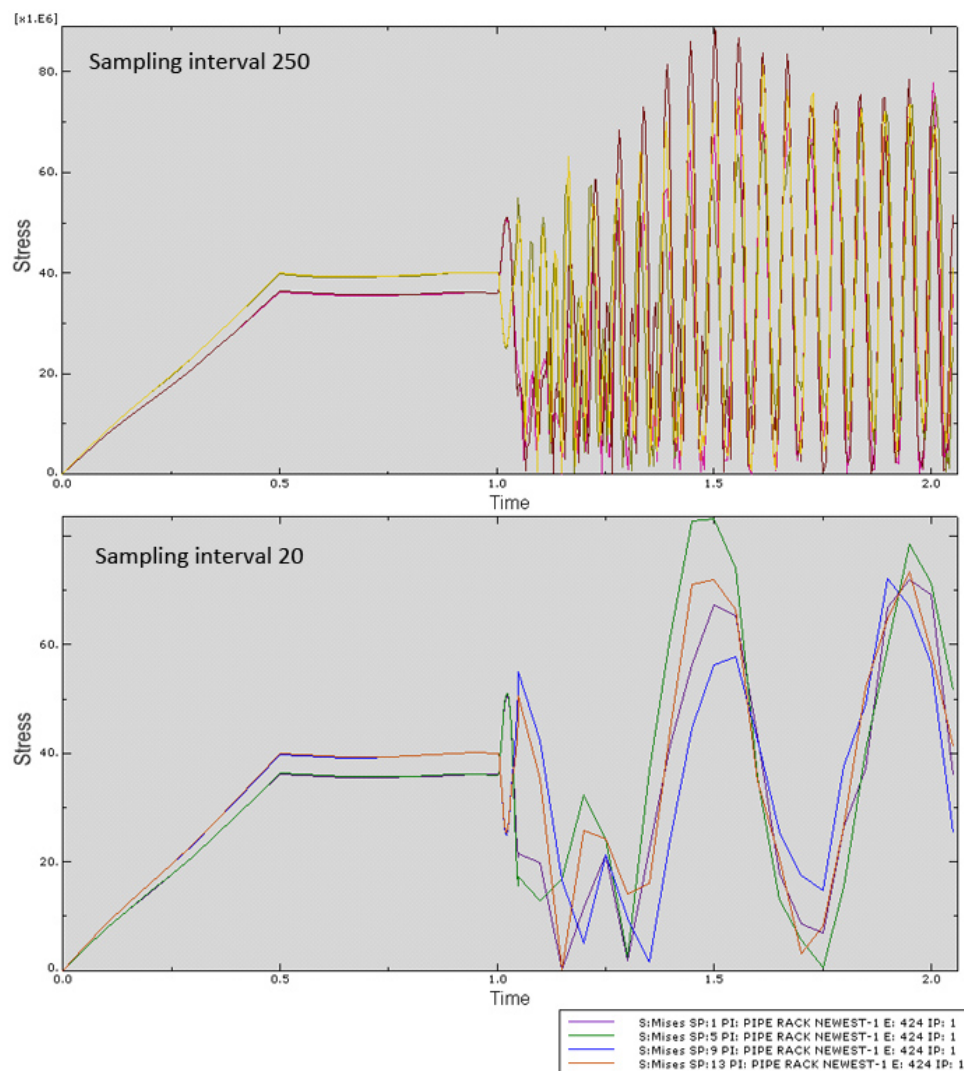


Figure 5.24: Figure illustrating the effect of aliasing for element 424. Aliasing effects cause a misleading representation of the post-blast response.

5.11.2 Integration and section points in Abaqus

Abaqus operates with two different definitions for output formats such as the stress; one being *integration point*, and the other one being *section point*. For the 2-noded linear B31 beam element used in this thesis, the integration point is defined as shown in figure 5.25.

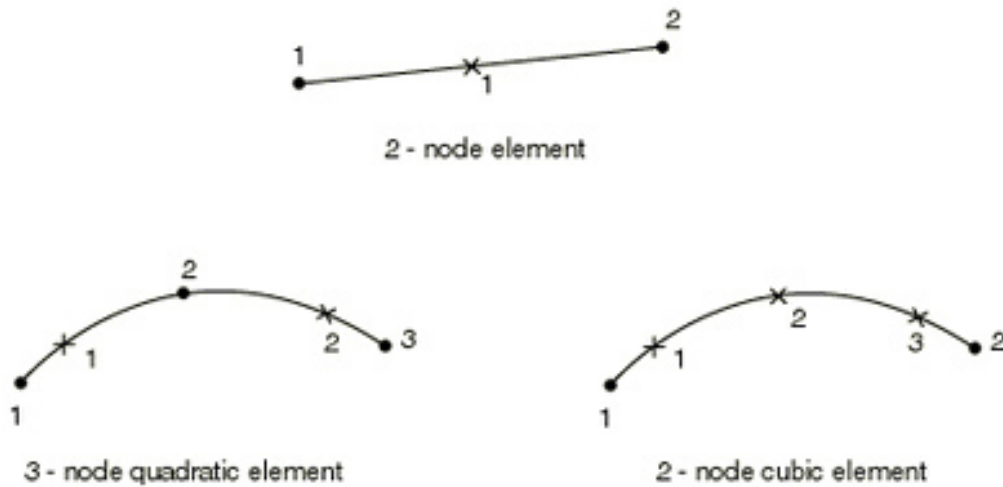


Figure 5.25: Numbering of integration points for output [10].

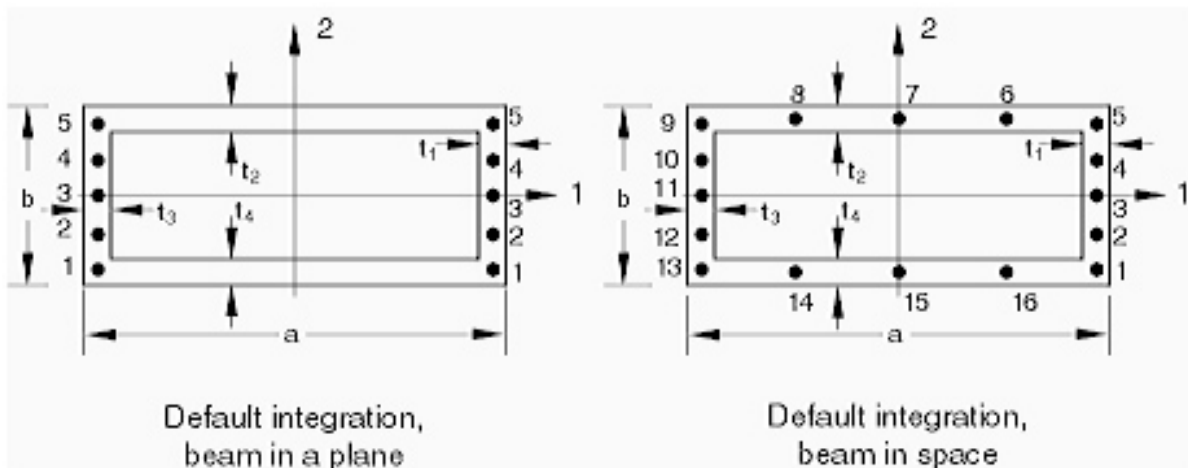


Figure 5.26: Section points for rectangular hollow section (RHS profile), beam in space. The four standard section points are 1, 5, 9 and 13 [10].

5.11.3 Scripting in Abaqus and Matlab

When the Abaqus/CAE GUI is used to create a model and to visualize the results, commands are issued internally by Abaqus/CAE after each user operation. The programming language called Python is used by the GUI to create the commands which are sent to the Abaqus/CAE kernel. Abaqus/CAE has the functionality to open and run custom scripts written in the Python language, and scripting thus represents a powerful tool which can automate many tasks which may be repetitive and time-consuming if done manually through the Abaqus/CAE GUI.

For this thesis, simple Python scripts have been used for extracting result data from the Output Database (ODB) file and writing these into a text file for further post-processing in Matlab. An Output Database file contains all the analysis results as requested by the user when setting up the analysis in Abaqus/CAE. The extracted result data from the ODB were the reaction forces (RF:*Magnitude, X-direction, Y-direction, Z-direction*) for all 23 supports (end connections) on the model, together with the Von-Mises stresses at critical locations on the model. This was done for all the static and the dynamic analyses.

A Matlab-script was written to calculate the DAF-values, using read-in data from the .dat files (text files) produced by the Abaqus Python script.

Reference is made to appendix D, E and I.

Chapter 6

Analysis results

This chapter presents the results from the parameter study performed on the pipe rack using both the static and the dynamic model. A major part of this chapter has been to investigate the behaviour of the structure *during* blast by comparing static and dynamic analysis models. Calculation of dynamic amplification factors (DAF) for both critical locations and end connections (support reactions) represents a way of understanding how the pipe rack responds to blast loads. The structural response will be described in terms of variation in stresses (Von-Mises, σ_{mises} [Pa]) and reaction forces (Newton, [N]). The DAF is calculated as the ratio between these parameters.

A parameter study has been performed on the pipe rack, where the following parameters have been accounted for:

- Blast load duration, T_d : 50, 100, 150 and 200 ms
- Blast load drag pressure level, P_d : 0.2 bar and 0.4 bar
- Structure and piping weight: Structure only, structure including piping arrangement 1, 2 and 3

6.1 Eigenmodes and eigenfrequencies

By using the linear perturbation feature in Abaqus, the eigenfrequencies are found corresponding to the first 10 eigenmodes. Four cases were studied; the first case took account for the bare structure (self-weight only), the rest involved the structure including piping arrangement 1, 2 and 3 as described in section 5.5. By studying the ratio between the eigenperiod and the duration of the blast, one can determine whether the responses should be classified as being in the *impulsive*, *dynamic* or *quasi-static* domain. According to Aker Solutions, the design blast load will be of duration between 50-200 ms. By

comparing these values with the obtained eigenperiods from Abaqus, the response range for the structure has been studied.

For a structure where both the self-weight and the piping are included in the analysis, it is seen that responses due to blast loads of duration between 50 and 100 ms are within the definition of a dynamic domain, according to the Blast and Fire Engineering Project [2]. According to J.Amdahl, blast durations between 50 and 150 ms are within the dynamic domain, with 200 ms blast duration in the transition zone between dynamic and quasi-static. For the bare structure (piping neglected), the responses are generally within the quasi-static domain for all blast durations. When the weight of the pipes are decreased (as described under section 5.5), the response range is expected to approach the quasi-static domain. Reference is made to appendix B.

As previously stated in section 1.3, a blast load problem within the dynamic domain, will require the pressure history to be idealised as triangular shaped loading functions. The peak value should be preserved as to capture the response of the structure in an accurate way. For the quasi-static domain, the load duration is not too important if the response is purely elastic. However, this becomes important when response is plastic (reference is made to figure 1.4). For the analyses done in this thesis, a triangular shaped loading function has been used for all cases.

6.2 Static analyses

Static analyses have been performed with the purpose of studying the static structural response for the simplified analysis model. The static model features a *static* drag pressure load. Because this static drag pressure is time independent, the effects on the structural response due to the duration of the blast are neglected.

It has been observed that the highest stress concentrations are found at element 614 for the cases with piping arrangement 1, 2 and 3. For the case with the bare structure only, element 702 is shown to experience the maximum stress. Element 614 is located at the connection between a larger (RHS350) and a smaller RHS profile (RHS200) beam. Element 702 is located at the connection between an angled brace and chord. Reference is made to figure 6.1 and 6.2. The maximum Von-Mises stress for each respective element is presented in table 6.1 for 0.2 bar drag load, and table 6.2 for the 0.4 bar drag load. It should be noted that all stresses are within the elastic range of the material.

Arrangement	$\sigma_{mises,max}$ (MPa), SP1	$\sigma_{mises,max}$ (MPa), SP2	Element number
1	55.6	55.3	614
2	49.0	48.7	614
3	33.4	33.0	614
No pipes	29.3	32.4	702

Table 6.1: Results from the static simplified model with 0.2 bar drag pressure for two different section points.

Arrangement	$\sigma_{mises,max}$ (MPa), SP1	$\sigma_{mises,max}$ (MPa), SP2	Element number
1	71.3	70.6	614
2	64.8	64.1	614
3	61.8	61.5	702
No pipes	59.5	63.0	702

Table 6.2: Results from the static simplified model with 0.4 bar drag pressure for two different section points.

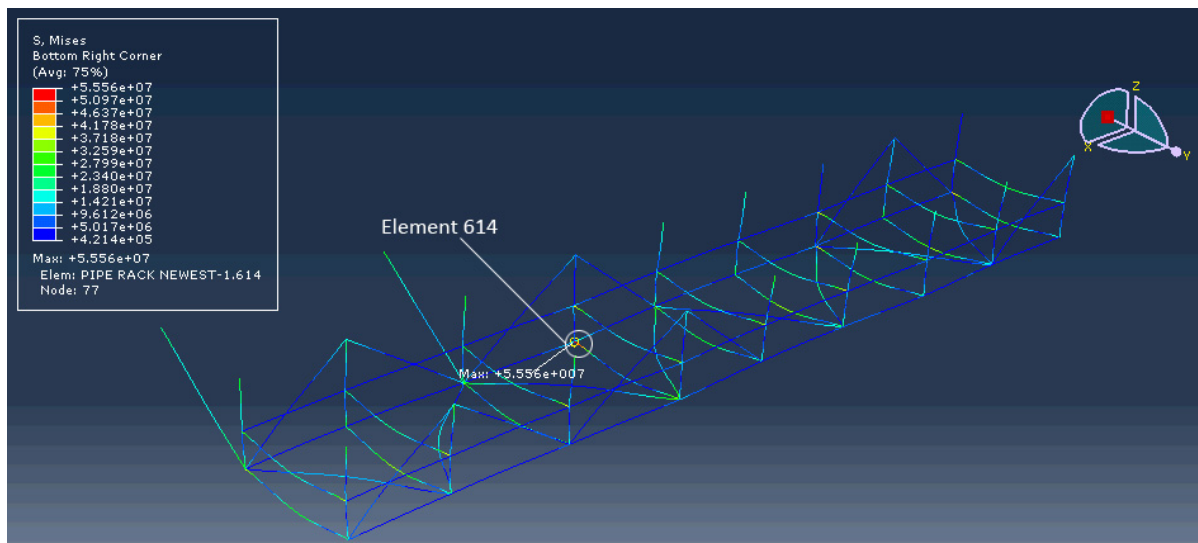


Figure 6.1: High stress area for the cases with pipe rack including piping arrangements 1,2 and 3.

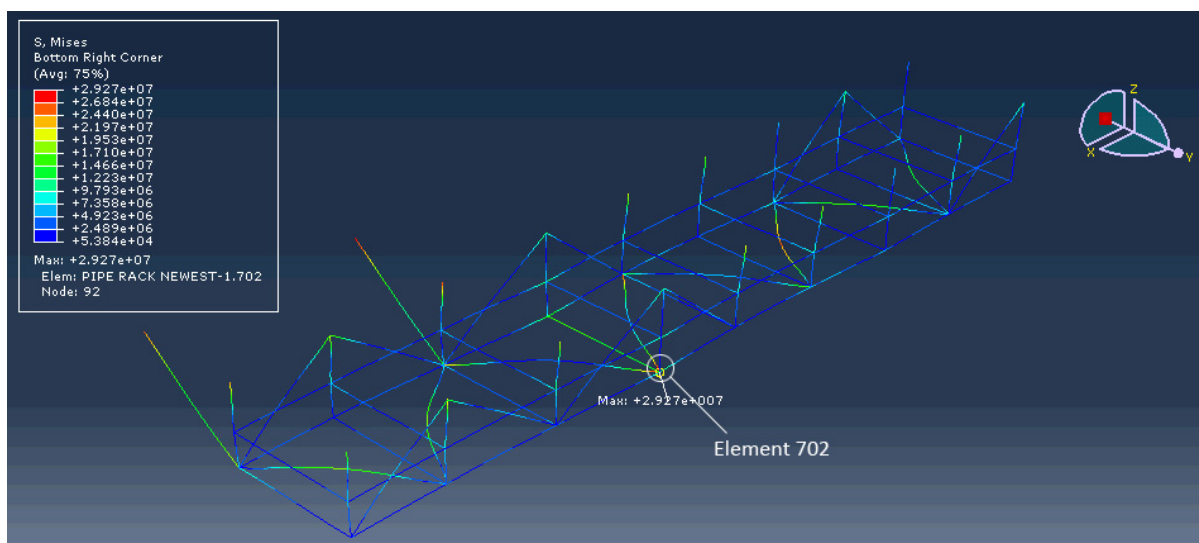


Figure 6.2: High stress area for the case with pipe rack only, no piping weight applied.

6.3 Dynamic analyses with simplified blast load model

Dynamic analyses have been performed with the purpose of studying the transient structural response. Because a blast case is of a dynamic nature, the structure is expected to react dynamically in a likewise manner.

The general response of the structure is observed to follow a common trend for the different blast cases. During the actual blast, the structure will see a slight lateral displacement in both positive and negative Y-direction (where the Y-direction represents the direction of the blast). This is due to the positive and negative contribution from the blast drag pressure. Figure 6.3 is provided for illustrative purposes. During post-blast, the horizontal beams which support the pipes will start to oscillate vertically. These oscillatory displacements are initiated by the response during the actual blast, and are driven by the piping weight. Hence, the heavier the pipes on the pipe racks are the higher stresses do they induce on the pipe rack. The highest stresses are found at the connection points where the vertical beams meet the horizontal beams supporting the pipes (see figure 6.4).

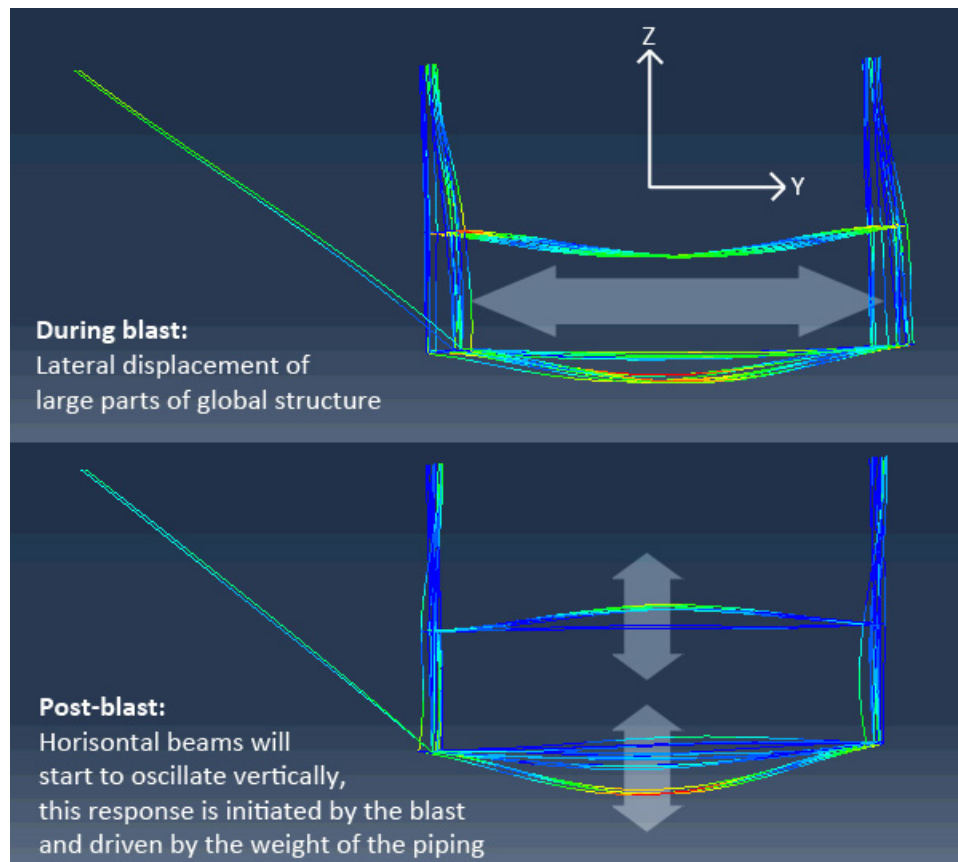


Figure 6.3: Illustration of the structural response during blast and post-blast.

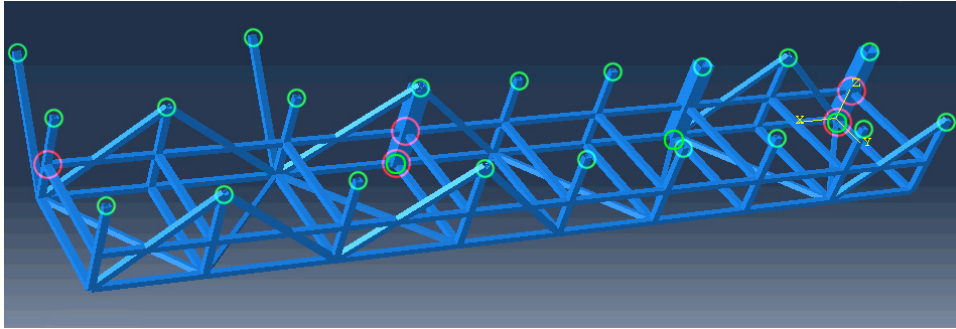


Figure 6.4: Stress (High stress areas marked red. Boundary conditions are marked green).

When observing the variation of Von-Mises stresses at selected elements on the structure, it is possible to capture the response during the actual blast as a characteristic peak. This is illustrated in figure 6.5. The differences in the response due to the different piping arrangements are clearly seen.

When observing the variation of reaction forces (RF) at selected nodes at the end connections, a similar response peak can be observed. The reactions forces will work against the direction of the blast load, and because the initial blast load direction is in the negative Y-direction, the positive drag pressure amplitude will give positive reaction forces, and vice versa for the negative drag pressure amplitude. This is illustrated in figure 6.6.

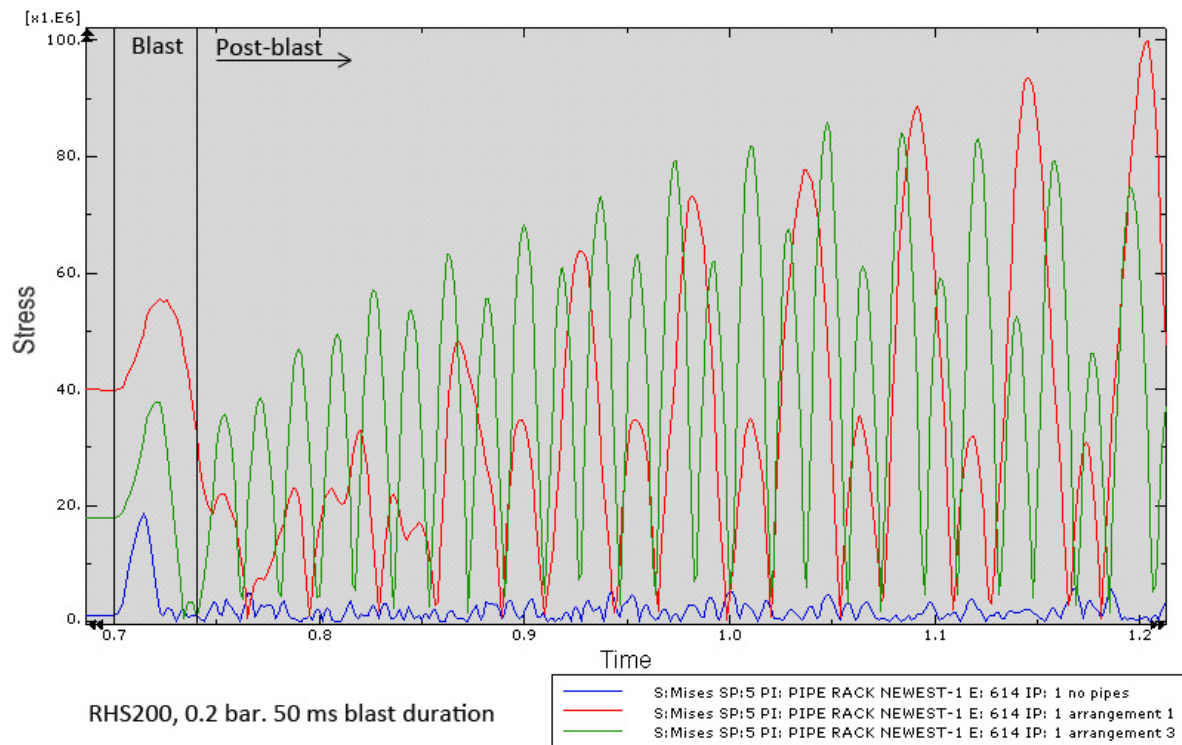


Figure 6.5: Dynamic response with respect to Von-Mises stresses on element 614 due to change in piping arrangement (Green curve represents arrangement 3, blue curve is the pipe rack without piping weight). The characteristic response peak is seen during the blast for all three cases.

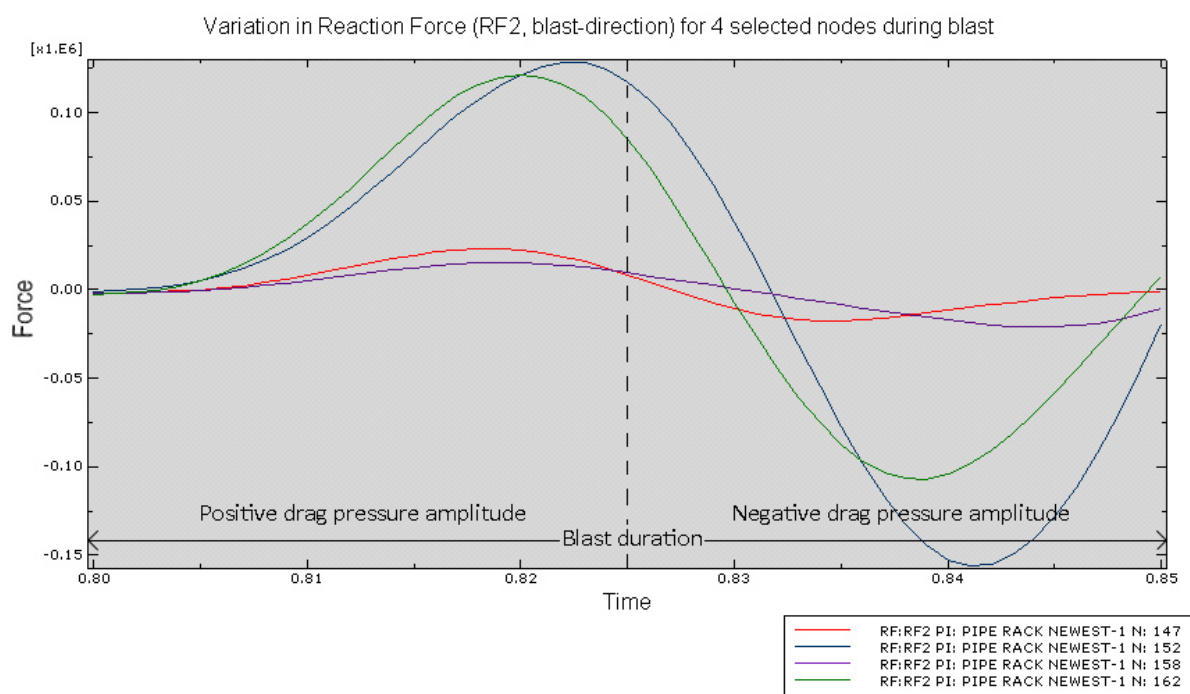


Figure 6.6: Variation of reaction force in Y-direction (blast-direction) for 4 selected nodes at end connections.

6.4 Dynamic Amplification Factors (DAF)

A dynamic load may have a significantly larger effect on the structure than a static load of the same magnitude due to the structure's inability to respond quickly to the loading. This is especially true for structural responses due to blast loads. The DAF reflects the increase of response due to a dynamic load, and is defined as the ratio between the dynamic response parameter (e.g Von Mises stress, reaction force, z-displacement etc.) and its respective static response parameter. This is seen from equation 6.1, for position or element i .

$$DAF_i = \frac{R_{dyn_i}}{R_{stat_i}} \quad (6.1)$$

The purpose of determining dynamic amplification factors is to try to find whether a relationship exists between a dynamic analysis model and its corresponding simplified static analysis model. In practice, the DAF will serve as a simple input for a structural engineer, as he or she will be able to quickly estimate stress values or reaction forces for the dynamic blast case by simply using a static analysis software.

Calculating DAF values involves comparing time independent analyses, i.e static analyses with time depending dynamic analyses. For dynamic analyses, the response of the structure in terms of stresses and reaction forces will change in time. This has been proven to be a challenge when trying to find the correct result values for calculation of DAFs for critical locations on the pipe rack. By creating a set of standard procedures for extracting stresses has thus proven practical, these methods are presented in section 6.4.1.

The most logic way of extracting stresses and reaction forces for determining DAFs would be to look at the response *during* the blast step. This is because the DAF is to be calculated by comparing the static blast model with its corresponding dynamic model. The static blast model with its static load represents a simplified blast model, in which the purpose is to model the structural response due to the blast only. Moving into the post-blast range will question the validity of comparing the static model with the dynamic model, the post-blast response is thus irrelevant for the calculation of DAF values.

6.4.1 Stress (Von-Mises) at critical locations

Dynamic amplification factors are to be calculated based on elements in the model which show a high degree of utilization, i.e high stress elements. Two approaches for calculating the DAF have been implemented. The first method starts with locating the element from the *static* analysis which experiences the highest stress, the DAF is calculated on the basis of this static stress together with the largest stress for this particular element over the blast-duration of its corresponding dynamic analysis.

The second approach starts with locating the element with the highest global stress over all blast-time steps in the *dynamic* analysis. Since the element with the highest stress changes its location through time, the particular element which has the highest stress during the blast may not be the same element which has the highest global stress initially from the static analysis. The DAF is calculated on the basis of the location of this element, also taking account for the same element in the static analysis. Figure 6.7 summarizes the different concepts behind method 1 and 2.

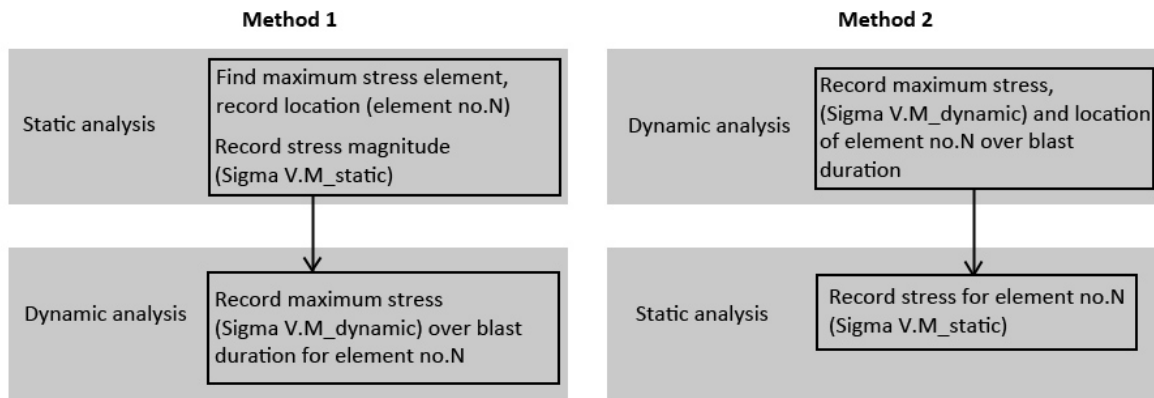


Figure 6.7: The difference between method 1 and method 2 for extracting stresses for calculating the DAF.

Because the element which experiences the largest stress throughout a *dynamic* analysis, may not be the same element which experiences the largest stress in the corresponding *static* analysis, it is expected that the DAF calculated using the second method will be somewhat higher than the first method. As the stress for one element is given for four different section points, it is seen that two section points always give the highest stresses. Reference is made to figure 6.8.

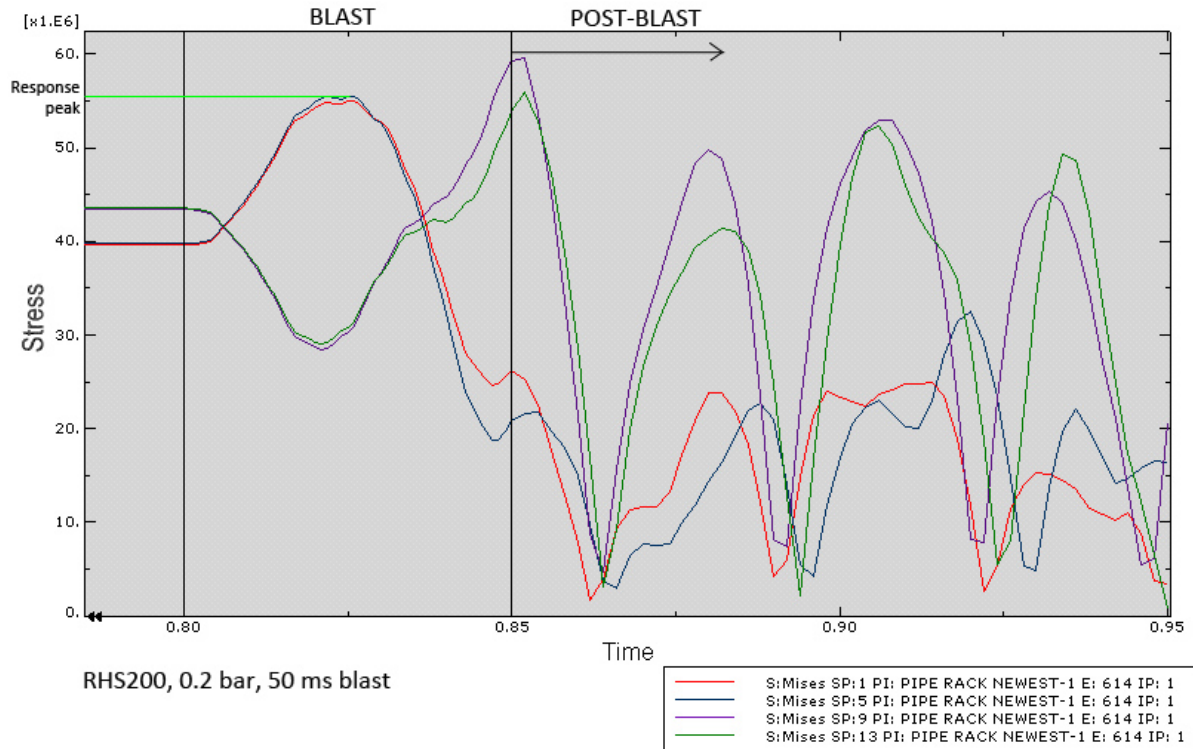


Figure 6.8: An example of maximum dynamic stress extraction from the blast step. Section points 1 and 5 (red and blue curve represent the highest stresses during the blast step).

By using method 1 and method 2, the DAF is plotted against blast duration. Not surprisingly, method 2 gives higher DAFs than method 1. The calculated DAF vary between 0.9 and 1.6 depending on blast duration. It can be observed that the DAF is significantly higher for the 50 ms blast duration than for the other cases, and with a reduction of DAF when the blast duration in increased. Again, it should be noted that *only one* stress value is extracted out from each blast case. Reference is made to figure 6.9 and appendix F.

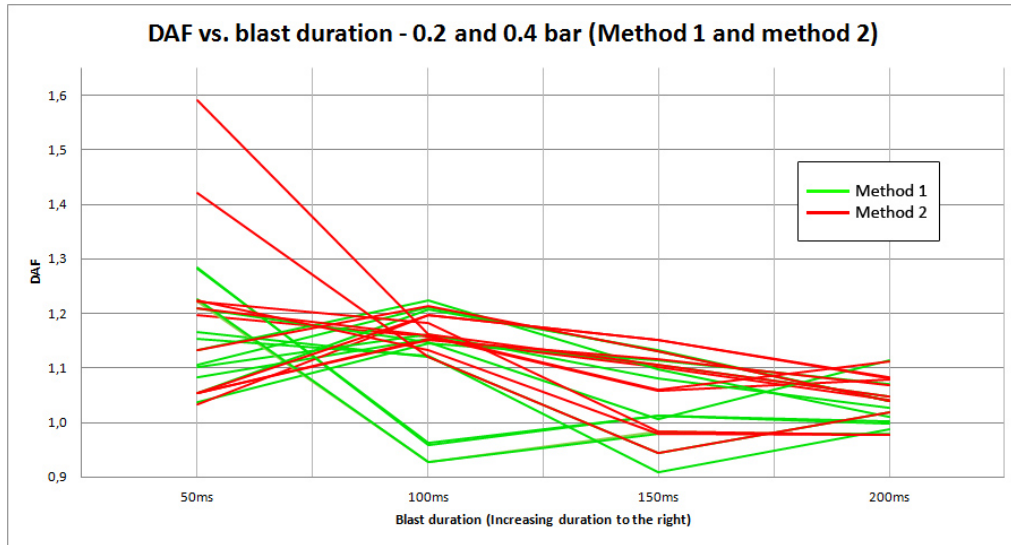


Figure 6.9: Variation of DAF with respect to blast duration for method 1 and 2.

Because the procedures for calculating the DAFs as previously presented involved extraction of only one stress value (from one element) per case, there may be a risk of ignoring other high stress elements which may be in the same magnitude as the maximum stress. To cope with this issue, a set of 12 elements from critical locations on the pipe rack structure has been selected for each blast case, and method 2 has been used for stress extraction for the calculation of DAFs. Reference is made to figure 6.10 for an overview over the location of these 12 elements.

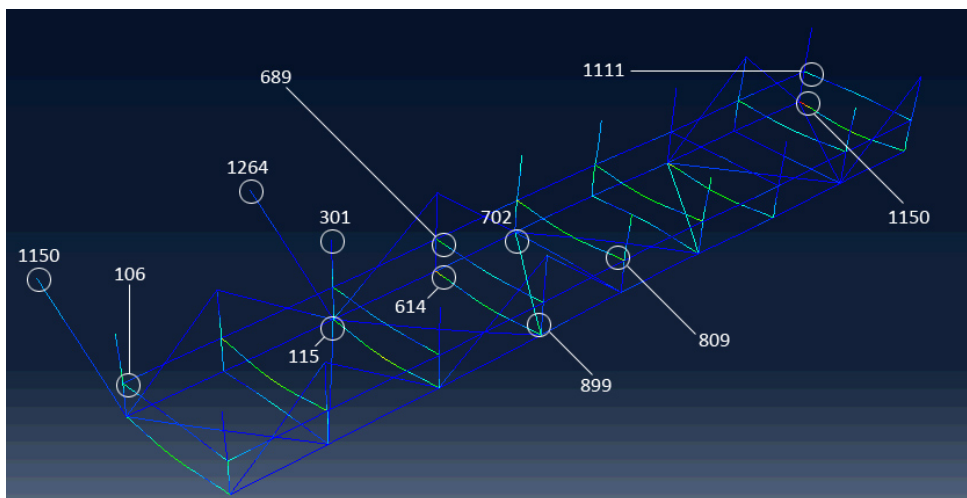


Figure 6.10: The locations of the 12 selected elements to be used for the extended DAF calculations.

Calculation of DAF for RHS200 0.2 bar 50 ms												
Arrangement 1												
Element number	106	115	301	614	689	702	809	899	1111	1150	1175	1264
DAF SP(1)	1,1	1,2	1,0	1,0	0,9	0,9	2,3	1,1	1,2	1,2	1,3	1,0
DAF SP(2)	1,1	1,1	1,0	1,0	10,7	12,3	0,8	1,1	1,2	1,3	1,2	1,0
DAF SP(3)	1,0	1,0	1,0	1,4	8,9	15,8	0,9	1,2	2,7	1,3	1,6	1,6
DAF SP(4)	1,0	1,1	1,2	1,2	1,1	0,9	2,1	1,1	2,8	1,4	2,1	1,5
Averaged:	1,0	1,1	1,0	1,1	5,4	7,5	1,5	1,2	2,0	1,3	1,5	1,3

Figure 6.11: An example of DAF values obtained from the 50 ms blast case, for arrangement 1. The DAFs are calculated for four section-points separately, in addition to the average of all section points.

The results from these calculations show the same trend as seen from previous graphs, that is the 50 ms blast being the most critical case. Element 689 and 702 consequently show high DAFs for all blast cases and arrangements, with the highest DAF being close to 100 for some analyses. This is highly unexpected. It should be noted that the DAFs for element 689 and 702 represent 8.3% of all calculated DAF values.

By plotting the variation of DAF with respect to blast duration, the contributions from element 689 and 702 are clearly seen. By removing these two contributions from the graphs, a more general picture is created of the response, these results will represent 91.7% of the calculated DAFs. Reference is made to figure 6.12 and 6.13.

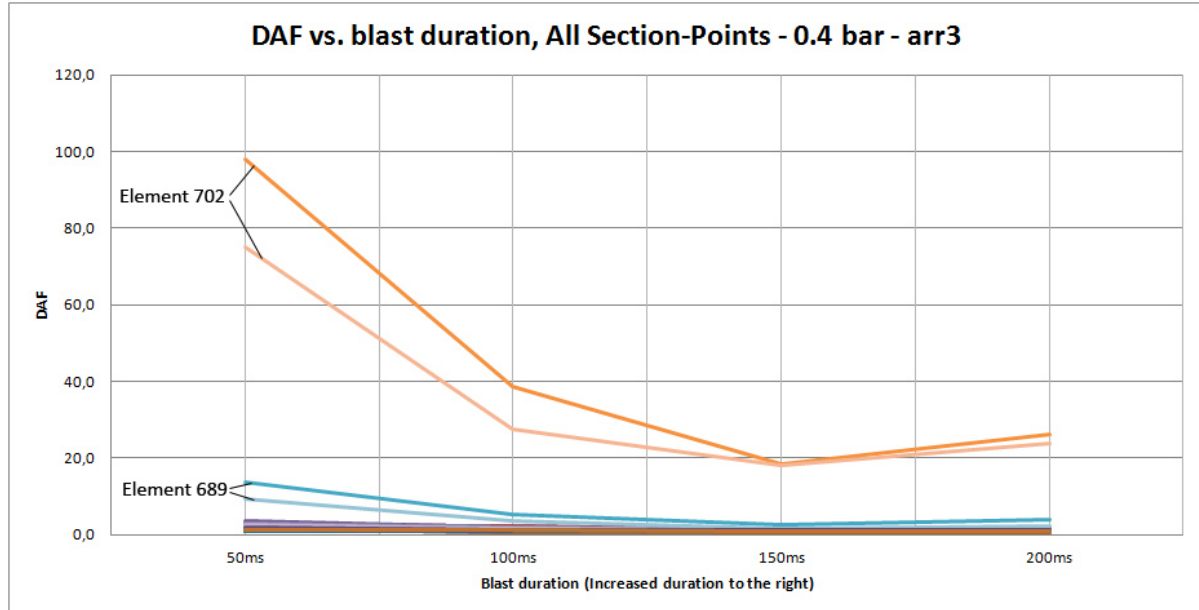


Figure 6.12: Plot of the variation of DAF with respect to blast duration, for all 4 section points for all 12 elements (0.4 bar, arrangement 3). The high DAFs represented by the response from element 689 and 702 are clearly expressed by the graph.

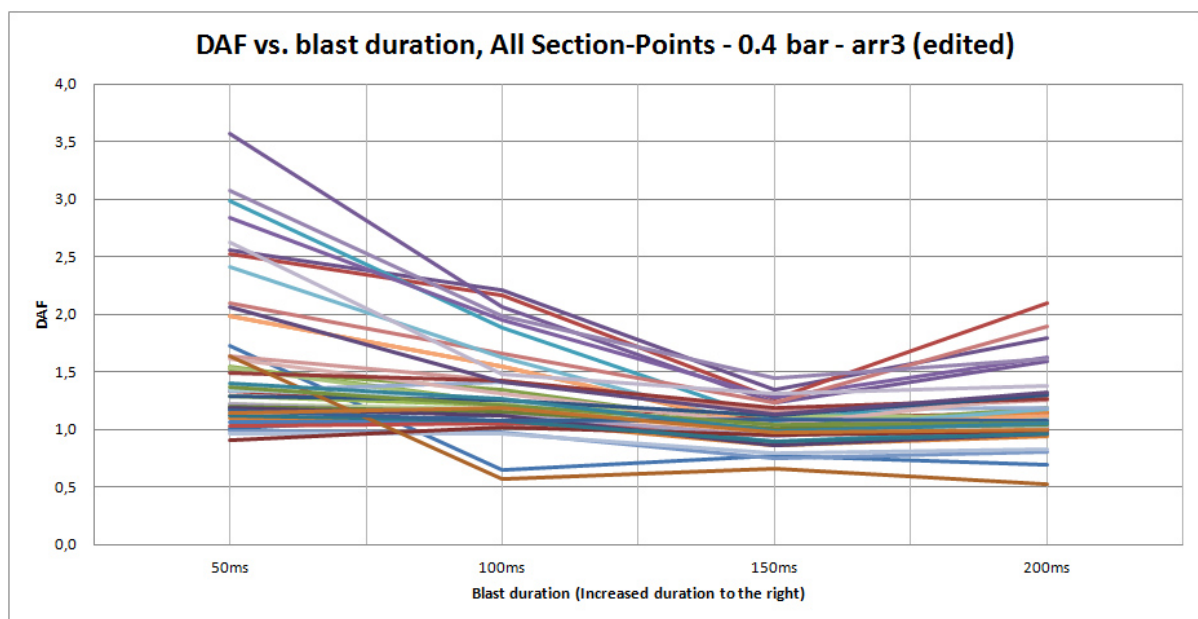


Figure 6.13: By removing the contribution from element 689 and 702, a more general picture of the response is seen. It should be emphasized that the response expressed by these DAFs represents 91.7% of the total number of DAFs for this particular piping arrangement.

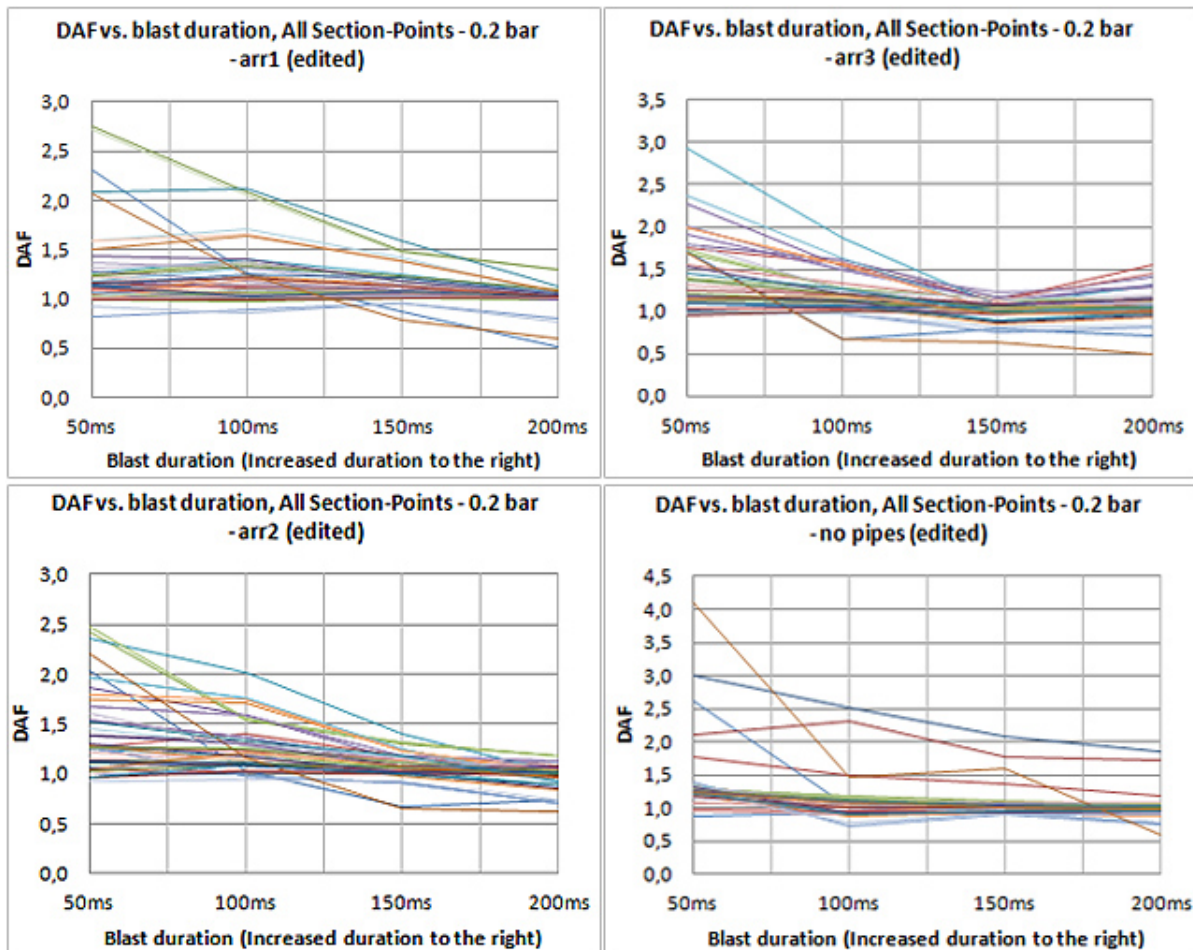


Figure 6.14: Plots of the variation of DAF with respect to blast duration for all section points, for the different piping arrangements. Blast drag pressure 0.2 bar. It is shown from these figures that the magnitude of the DAF decreases with increasing blast duration. It should be noted that the data points for element 689 and 702 have been removed in this figure.

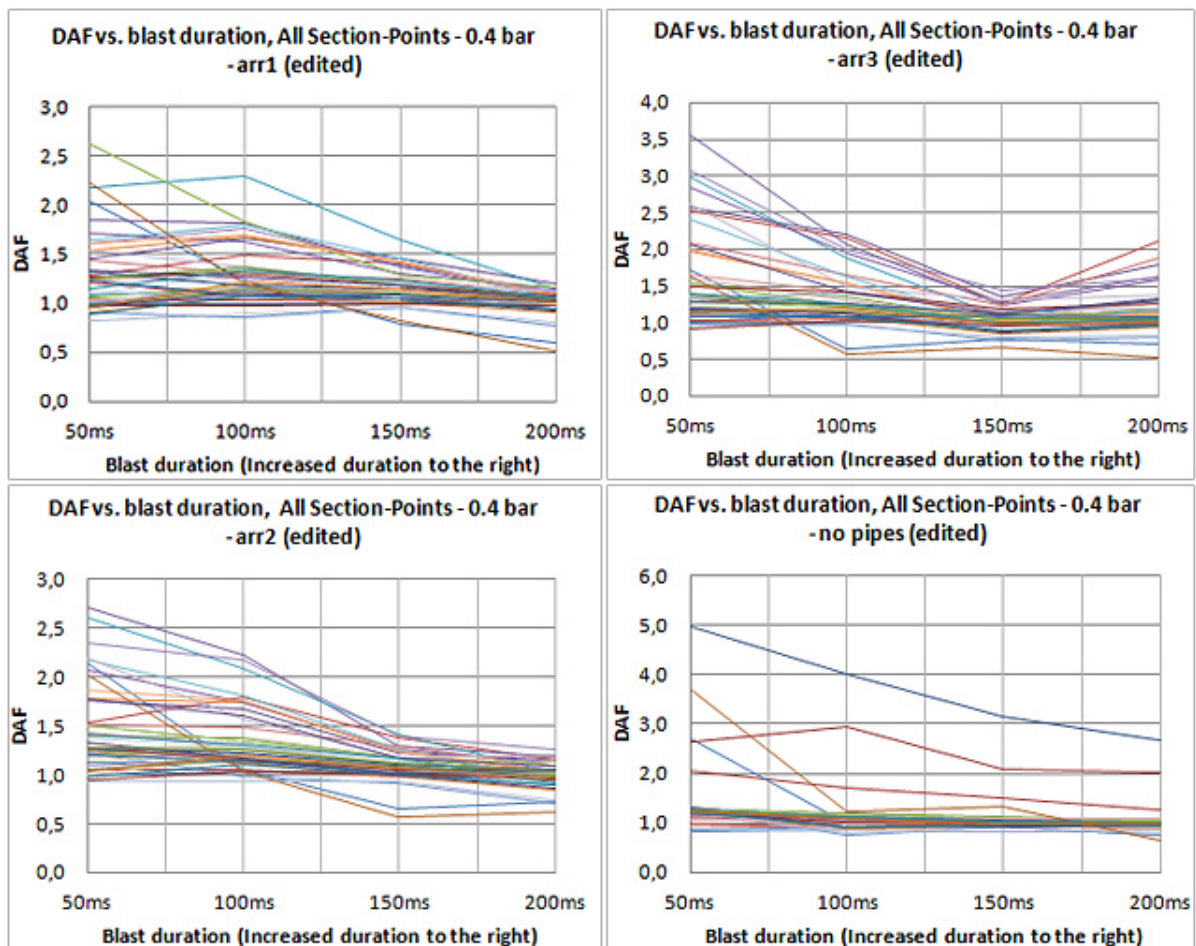


Figure 6.15: Plots of the variation of DAF with respect to blast duration for all section points, for the different piping arrangements (neglecting the DAFs from element 689 and 702). Blast drag pressure 0.4 bar. It should be noted that most DAF values are below 2, with exceptions of some elements in the 50 ms blast case. It is shown from these figures that the DAF decreases with increasing blast duration.

Averaging the DAF for all section points

As each data point on figure 6.14 and 6.15 represents a DAF for a certain element and section point, there is a certain scattering of data points for each blast duration. By combining the data from each arrangement into one figure, it is seen that the majority of DAF values are concentrated in the range between 0.5 and 2. Reference is made to figure 6.16. It proved to be a challenge when trying to determine a characteristic DAF for each blast duration; if the *highest* DAF is taken for each blast duration, this value may not characterize the majority of the DAFs calculated for the same duration, further wise there is a risk of obtaining too conservative values.

A solution to this issue is to assume that the DAF for each element can be taken as the average of the four DAFs for each section point. This reduced the number of data points for each element, thus reducing the scattering range for each blast duration case. The result of this are curves which describe the *general* change of DAF with respect to the blast duration in a much organized manner than previously. Reference is made to figure 6.17.

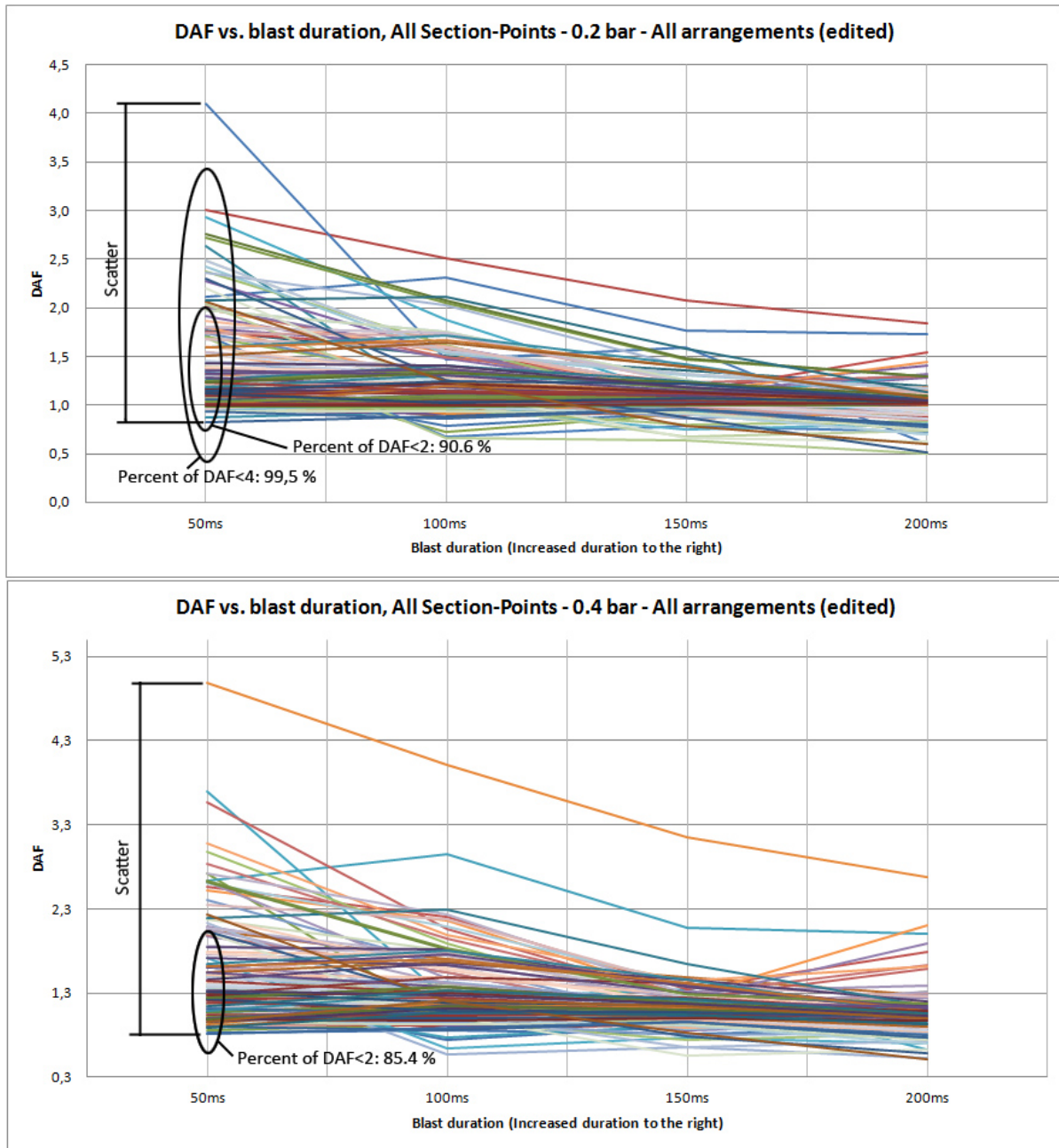


Figure 6.16: The following figure illustrates the scattering of data points for DAFs as line plots. The largest concentration of data points are located roughly between 0.5 and 2. The extreme DAF points only represent a small number of points. Please note that the range of scattering is largest for the 50 ms blast case. When looking at the 50 ms 0.2 bar blast case, 90.6% of the DAFs are below 2. For the 50 ms 0.4 bar blast case, 85.4% of the DAFs are below 2.

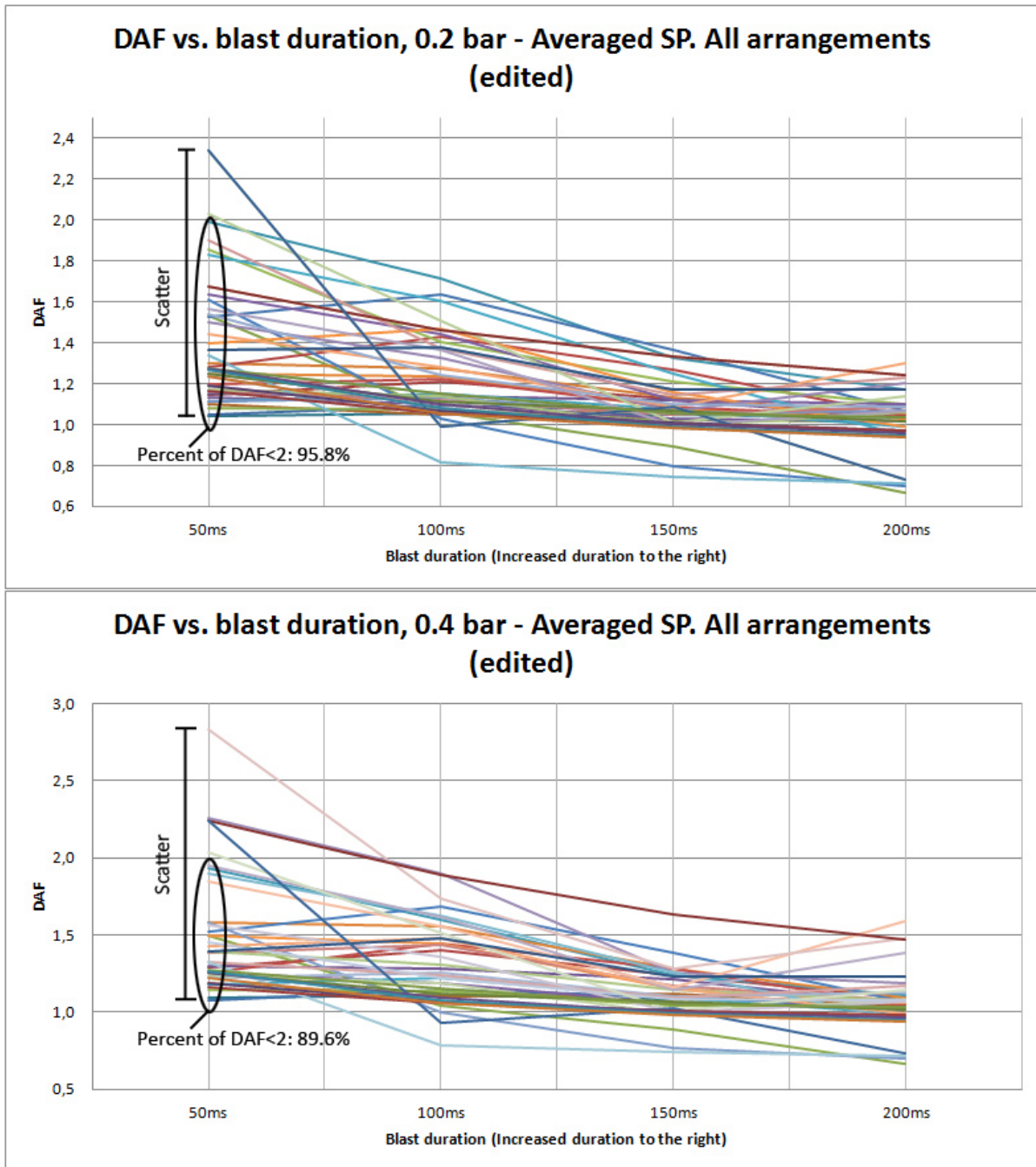


Figure 6.17: The following figure illustrates the scattering of data points for DAFs as line plots. The once four DAFs for each element is now reduced to one averaged DAF, this reduced the size of the scattering range of data points. Once again, it should be emphasized that the majority of DAFs are below the value of 2.

To investigate the possible relationship between the DAF and the blast duration, the variation of DAF is plotted against the blast duration for all elements except element 689 and 702. Reference is made to figure 6.18. It is shown that there is a clear relationship between the DAF and the blast duration, in which the DAF decreases with increased blast duration. The scattering range is consistently larger for the 0.4 bar than the 0.2 bar case.

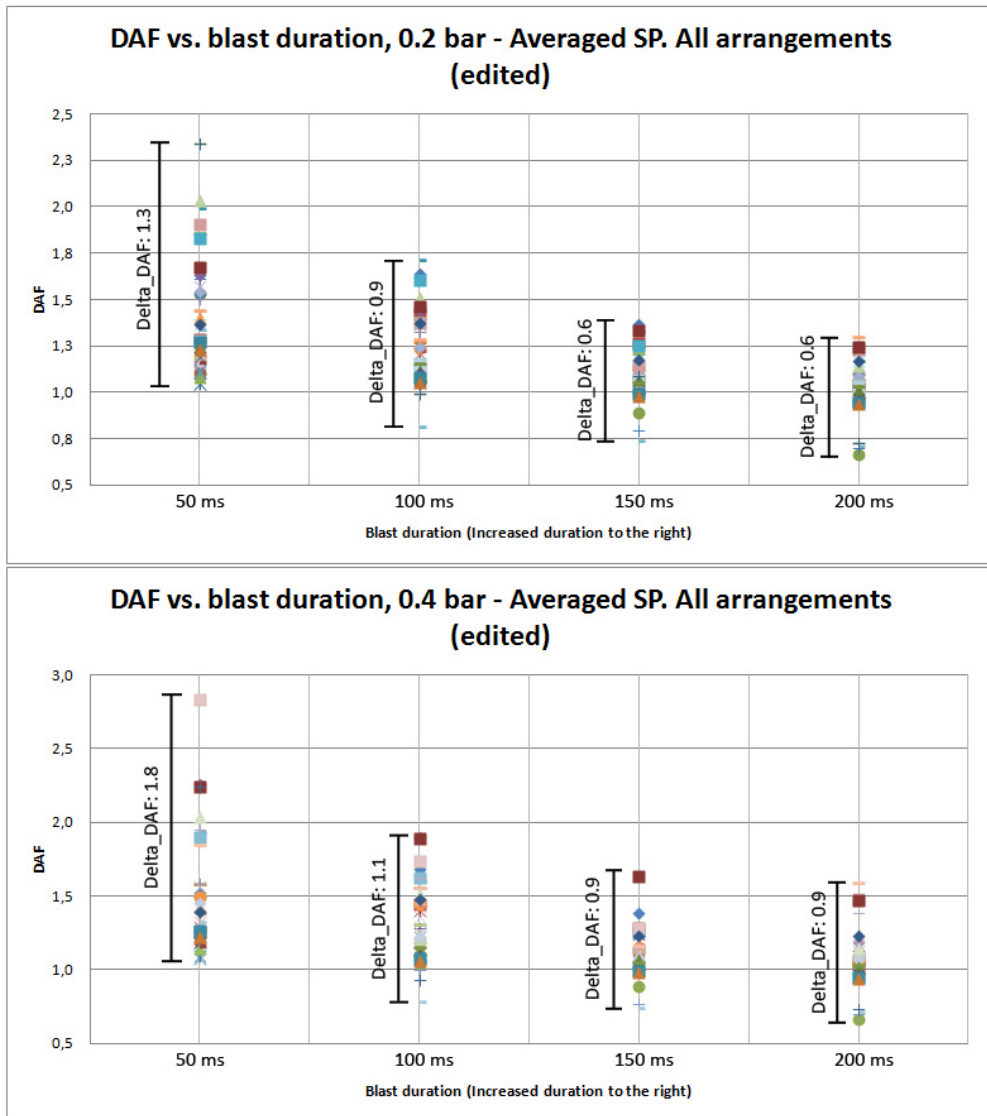


Figure 6.18: The following scatter plots illustrate the scattering of data points for DAFs (averaged section points). These plots do not contain the data points from element 689 and 702.

By averaging the DAF for all section-points on each element, and plotting the variation of DAF with respect to the *piping arrangement* using method 2 for the same critical points

on the structure, it is harder to see a relationship between the DAF and piping weight. This might indicate that the DAF will remain constant regardless of the change in piping weight (arrangement). The scattering range of DAF is between 2.1 and 1.2. Reference is made to figure 6.19 and appendix G. These results are further treated under section 7.2.

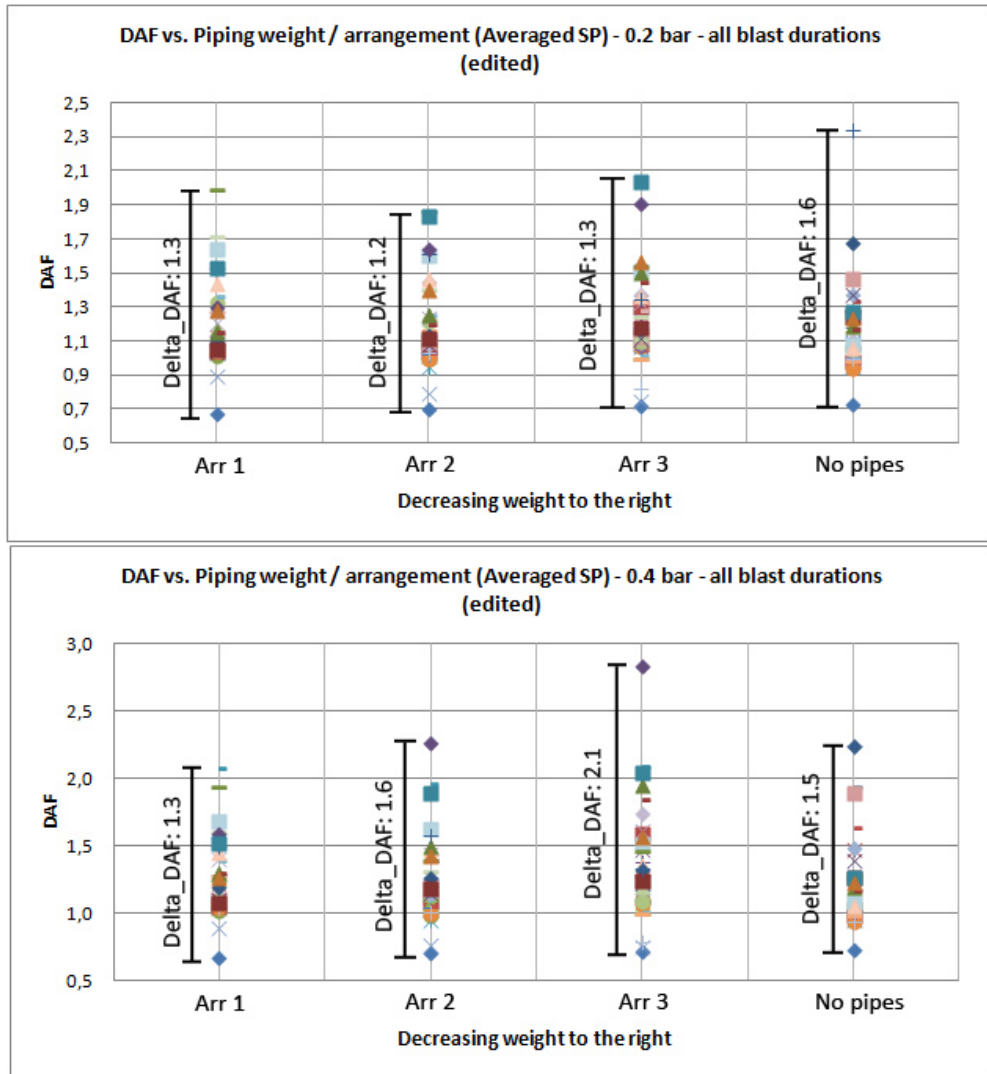


Figure 6.19: The variation of DAF plotted against piping weight (arrangement) as a scatter plot. The figure illustrates the scattering of data points. These plots do not contain the data points from element 689 and 702.

6.4.2 Reaction Forces (Support Reactions)

Dynamic amplification factors (DAFs) are to be calculated for all support reactions (end connections in the model). In Abaqus, these support reactions can be found by extracting

the nodal reaction forces (RF-forces) in the X, Y and Z-direction. There are in total 23 end connections in the model, figure 6.20 shows the location and node numbering for these.

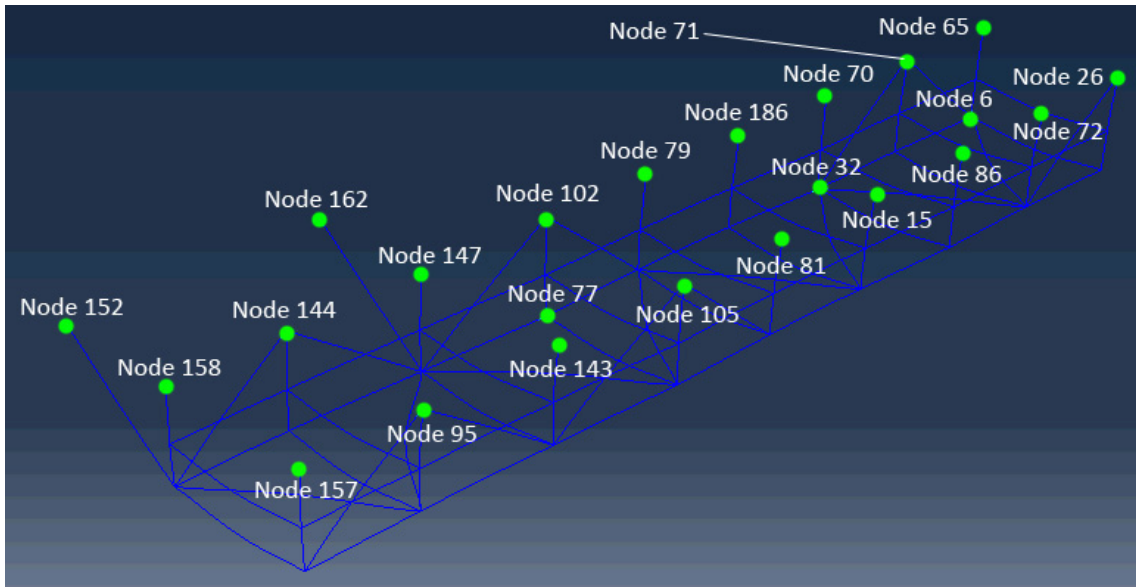


Figure 6.20: Location and node numbering for the extraction of reaction forces.

The DAF is calculated using expression 6.1, which involves a direct comparison between the dynamic and the static model. The reaction force from the dynamic case, is taken as the maximum reaction force during the blast load step. This is the same procedure as previously presented in section 6.4. If one assume that the DAF can be averaged over all arrangements, it is shown that the DAF will decrease with increased blast duration in the same manner as with the DAF for Von Mises stresses at critical locations on the pipe rack.

Investigation on the reaction forces in the Y- and Z-directions (RF2 and RF3) is of most importance, as these two forces represent the support reactions in the direction of the blast and gravity respectively. For reaction forces in the blast direction (RF2), the DAF is shown to be between 1.6 and 0.95. For the Z-direction (RF3) the DAF is found to be between 2 and 1. Reference is made to figure 6.23 and 6.24.

For the reaction forces in the X-direction (RF1), there are four nodes which show high DAF values up to 70. Reference is made to figure 6.22. The reason for this can be explained by the differences in the response between the static and dynamic analyses. In the static analyses, the external load working on the structure is the static blast load in the Y-direction. To fulfill static equilibrium, there will mainly be reaction forces in the Y-direction opposing this external load, thus, making the reaction force contribution from the X-direction minimal. For the corresponding dynamic analyses however, the structure will respond to the dynamic blast load in such a manner that it will see significant

displacements in the X-direction. The reaction forces in X-direction will reflect these directional changes, and thus give a significant contribution in the X-direction for the dynamic analyses. Since the DAF is calculated on the basis of the ratio between the contribution from the dynamic and the static analysis, the DAF value becomes high due to the significant differences between these two reaction force parameters. Figure 6.21 shows the coordinate system for the analysis models.

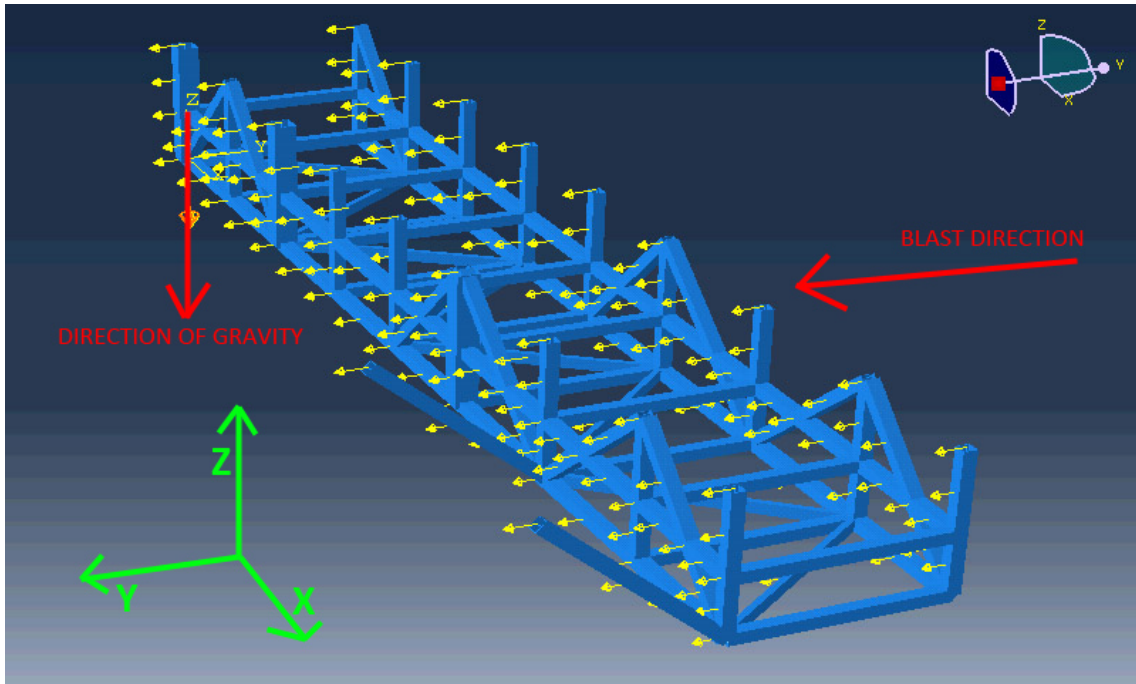


Figure 6.21: Coordinate system with respect to the direction of the blast, and the direction of the gravity.

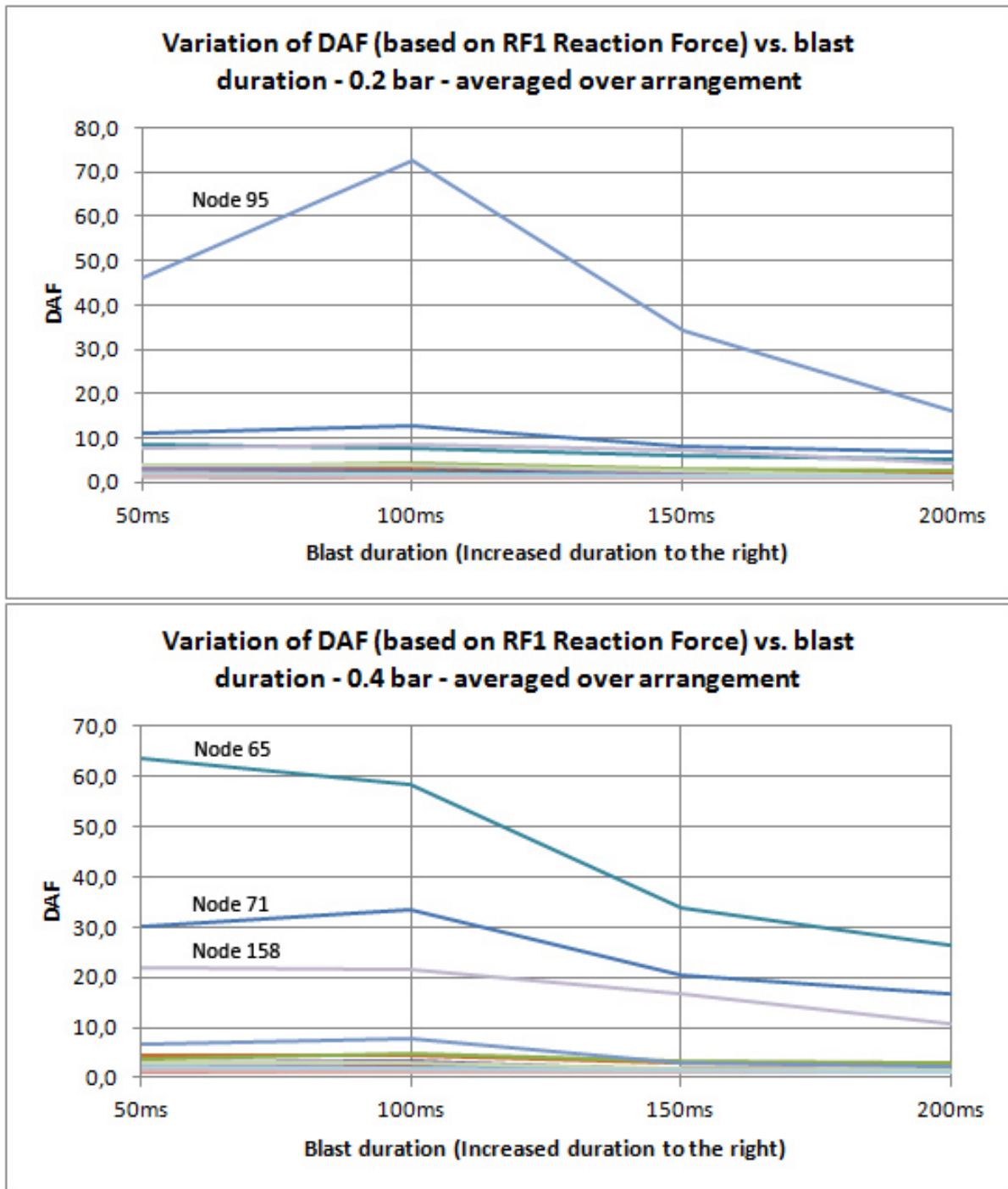


Figure 6.22: Variation of DAF (based on reaction force in X-direction) with respect to blast duration. Please note that most DAFs are below 10, with the exception of the DAF for nodes 65, 95, 71 and 158.

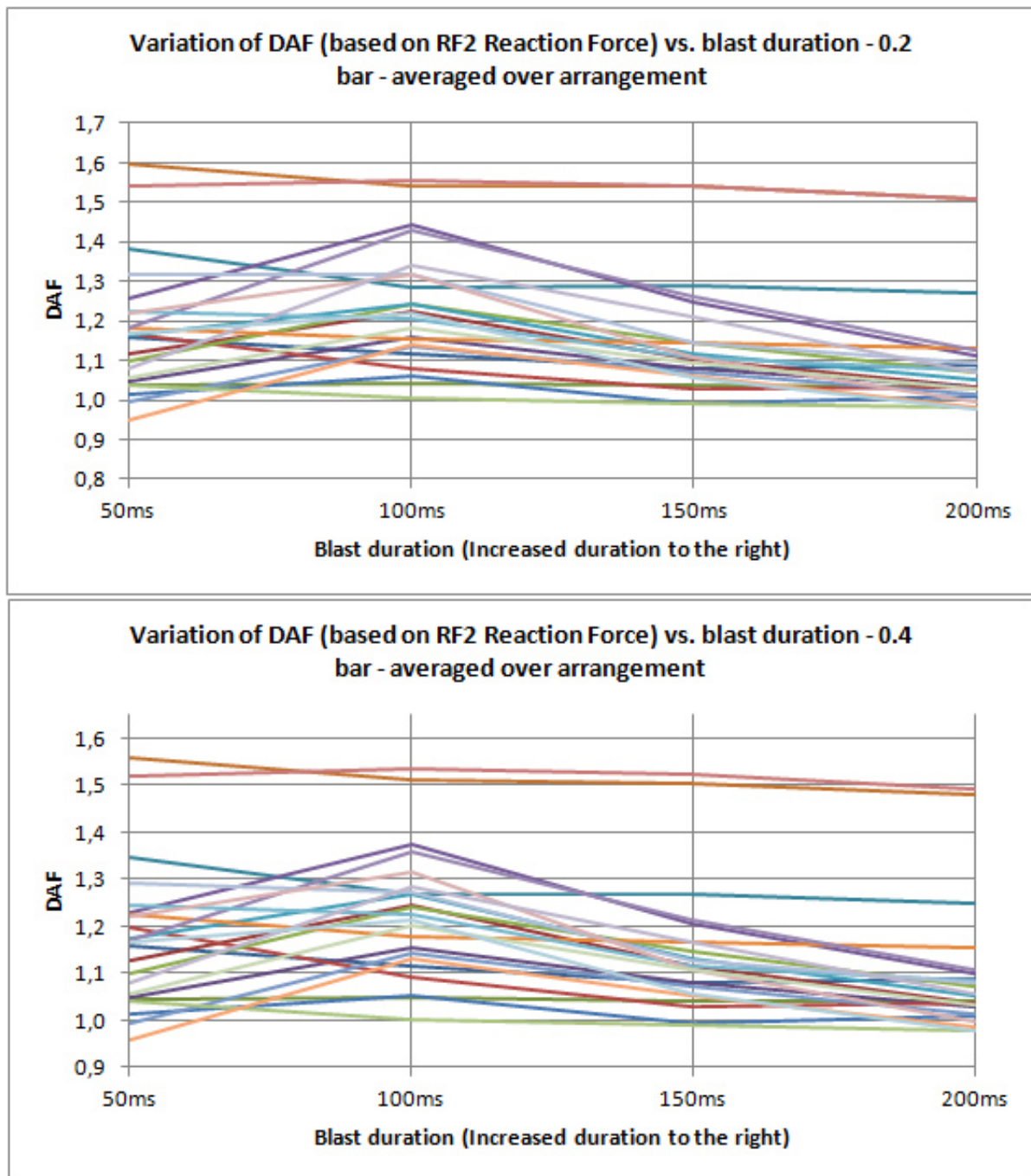


Figure 6.23: Variation of DAF (based on reaction force in Y-direction) with respect to blast duration. The Y-direction is the direction of the blast. The majority of the DAFs are found to be below 1.5.

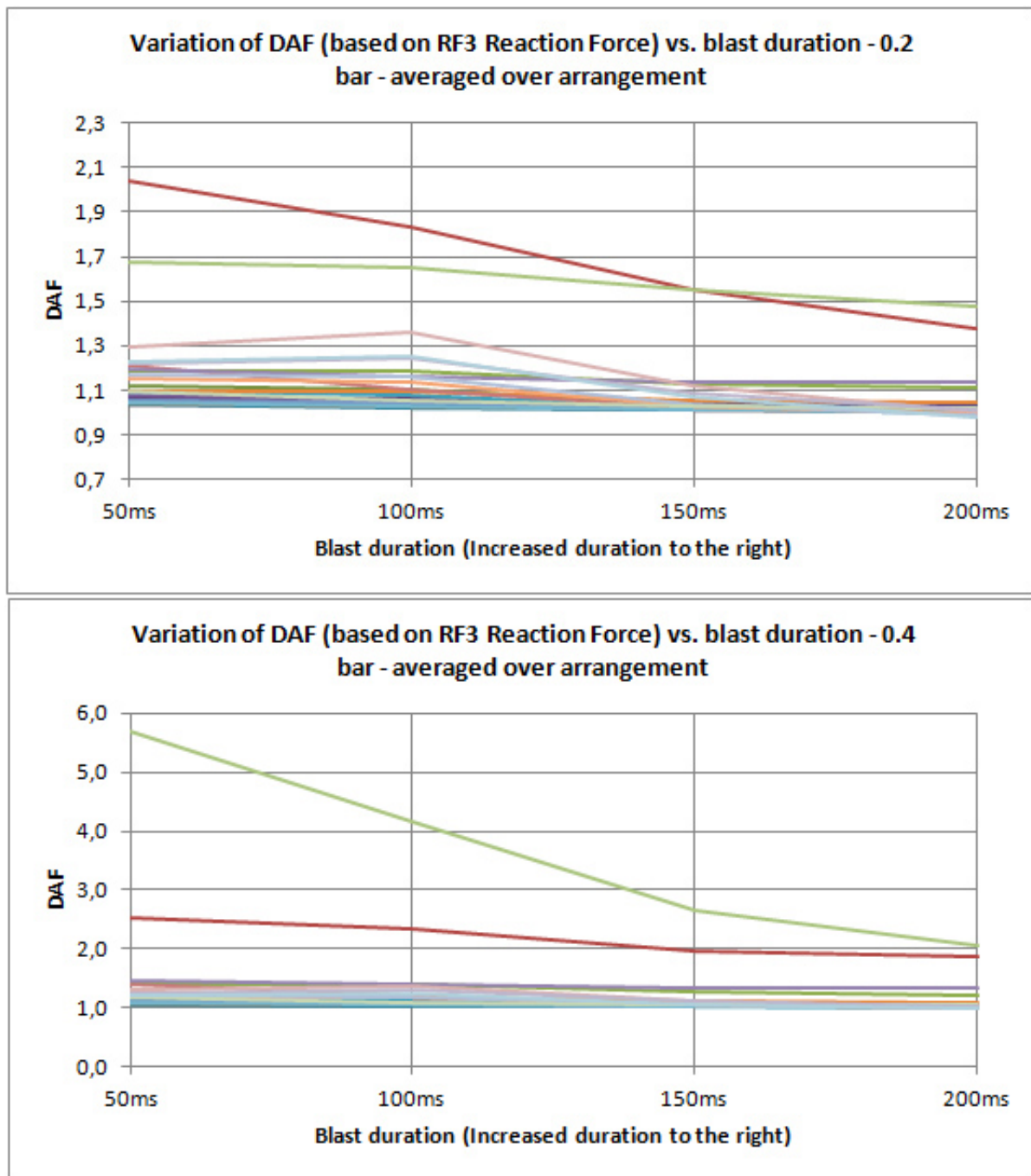


Figure 6.24: Variation of DAF (based on reaction force in Z-direction) with respect to blast duration. The Z-direction is the direction of the gravity. Please note that the majority of the DAFs are below 1.5.

Chapter 7

Discussion of results

In the following chapter, the results from the analyses will be discussed in able to understand the general response of the pipe rack, when being exposed to blast loads. The results will be further treated in able to obtain the final values as requested through the initial project scope, which was to find dimensioning DAF-values for critical locations on the pipe rack and support reactions.

7.1 Static and dynamic analyses

Both the static and dynamic analyses show that the stress variations on the structure are within the material's elastic range. One might think that blast loads will cause plastic deformations on the structure, which is indeed the case with blast walls and similar structures as seen from for instance the research paper by L.A Louca and R.M.Mohamed Ali [11]. However, for a truss work structure as the pipe rack being modelled, each structural member is of a small area presented to the explosion. Due to this fact, the direct overpressure loading on the pipe rack is of relatively small magnitude. In these circumstances, the dynamic pressure, or drag load is to be considered. Because the dynamic pressure is calculated based on the projected area of a member, the resulting pressure load was not of such a magnitude that it resulted in any plastic response of the structure.

Because the main project scope was to investigate the dynamic amplification of the structure by comparing dynamic analyses against static analyses, it is merely the ratio between stresses which are of interest, and not the stress value itself.

The dynamic analyses showed the effect of the structural blast- and post-blast response due to the positive and negative drag pressure contribution from the blast load. For most elements, the blast-response was captured as a stress peak during the blast. Reference is made to figure 7.1. Due to the lack of a damping model, the stress levels in the post-blast

response range represented a great uncertainty. For the project scope however, this proved to be irrelevant as the blast-response was the main focus.

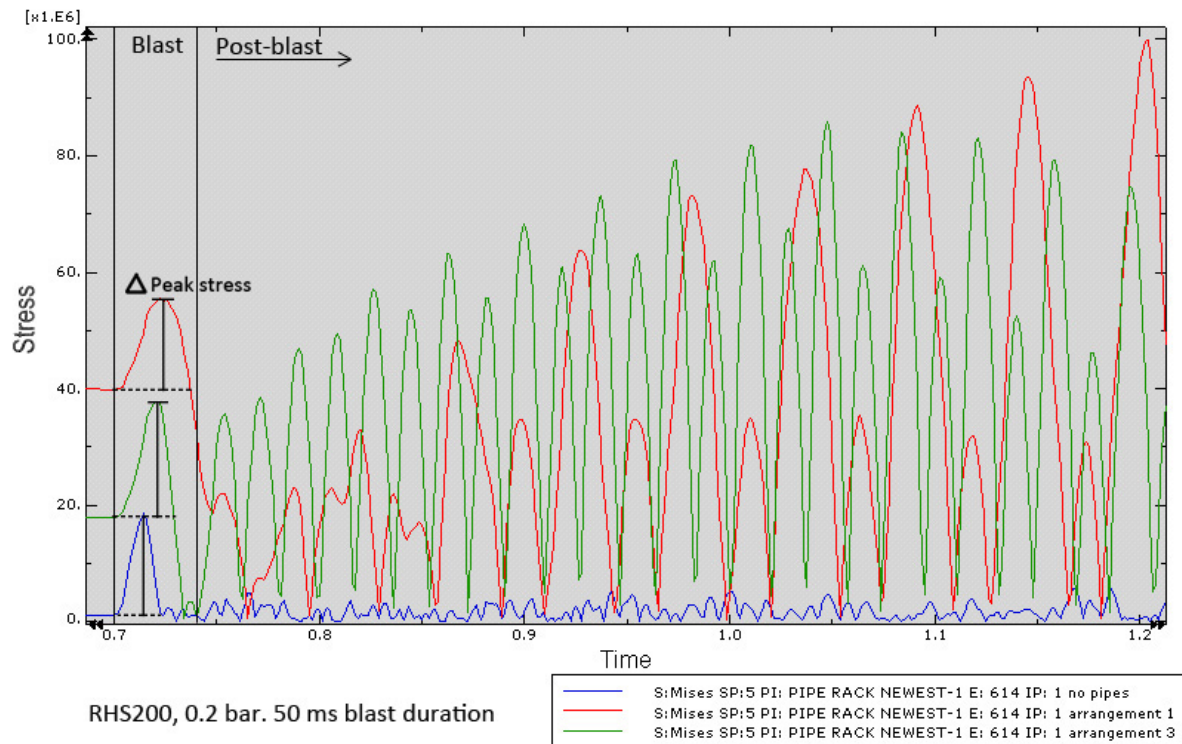


Figure 7.1: Showing the response stress peak observed under blast. The figure also show that the differences between the lowest and highest stresses (Delta peak stress) remain almost constant for the different piping weights during the blast. This indicates that the stress response *during* the blast may be independent of the piping weight.

7.2 DAF for critical locations on the pipe rack

Dynamic amplification factors have been found based on the change of Von-Mises stresses on the structure for the static and dynamic analyses. Results show that the DAF varies with the blast duration, in addition to this, there is also a significant amount of scattering of data points for each blast duration, this is due to each critical element on the pipe rack having different DAFs. Two elements (689 and 702) stand out because they have DAFs up to 100. Seen from a general perspective, the DAFs represented by these two elements stand for only a small percentage of the total DAFs, this makes up for an argument for not taking account for these two elements in further calculations, if one is to study the *general* response.

As the main task is to find *general* DAF values which are to characterize critical locations on the pipe rack, certain assumptions and simplifications must be made to obtain any reasonable results. A few suggestions on the approach of determining general, dimensioning DAF-values for critical locations on the pipe rack are given below in section 7.2.1, 7.3.2 and 7.2.3.

7.2.1 Using the upper bound (Method A)

If the high DAFs from element 689 and 702 can be ignored, and if it is assumed that the once four DAFs for each section point in an element can be replaced with one averaged DAF, the upper bound values can be taken as to represent the DAFs for the critical locations on the pipe rack. This is hereby referred to as method A. Reference is made to figure 7.2 and 7.3.

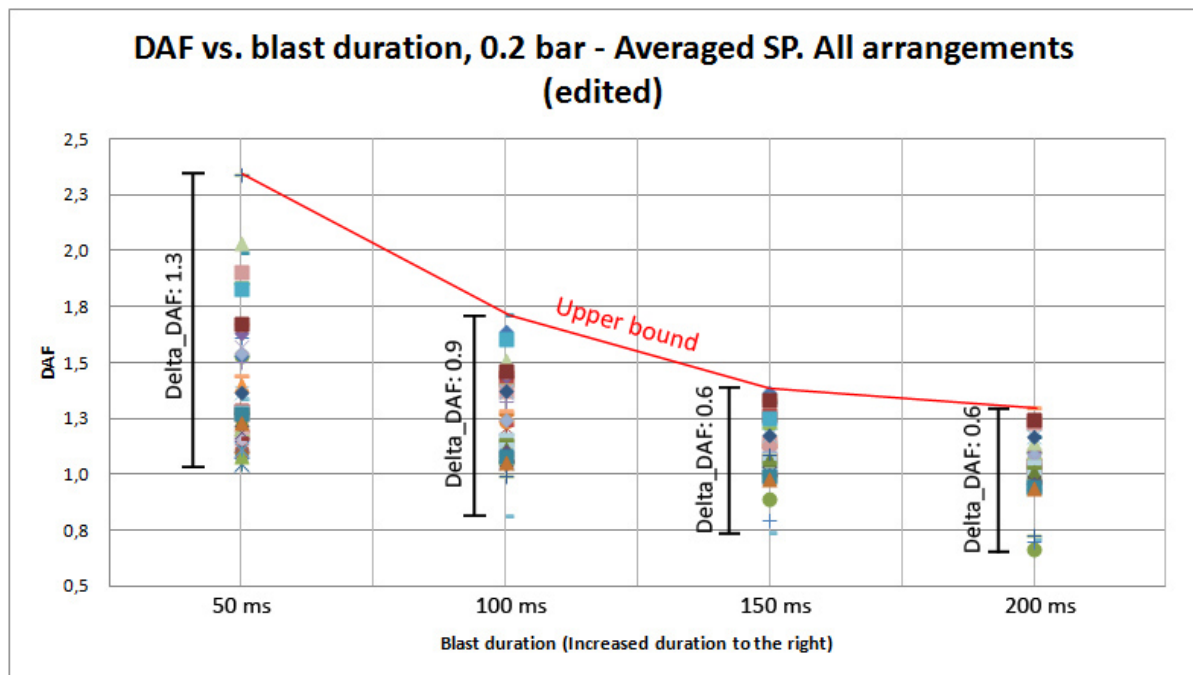


Figure 7.2: Upper bound values for DAF, method A. 0.2 bar blast pressure (not including data points from element 689 and 702).

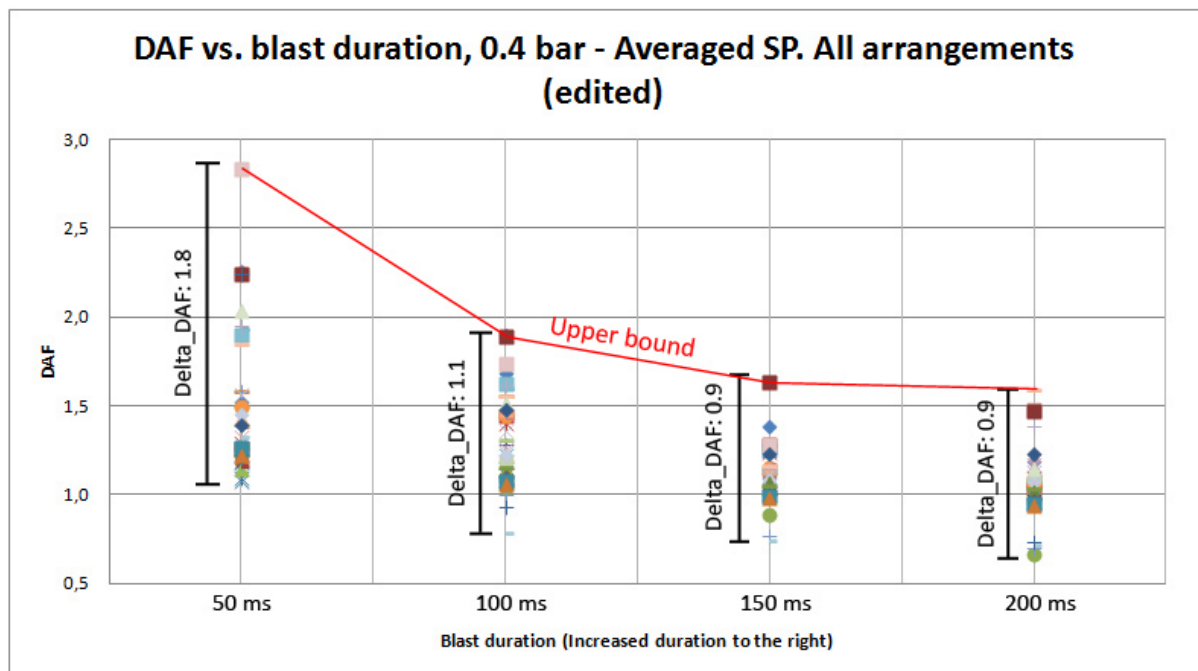


Figure 7.3: Upper bound values for DAF, method A. 0.4 bar blast pressure (not including data points from element 689 and 702).

7.2.2 Averaging over all elements, use the upper bound (Method B)

Method B involves taking the average of the DAFs over all section points *and* elements for each blast duration. This reduced the number of DAFs to only one value per blast duration. The upper bound is then taken for the remaining data points. This is illustrated in figure 7.4 and 7.5.

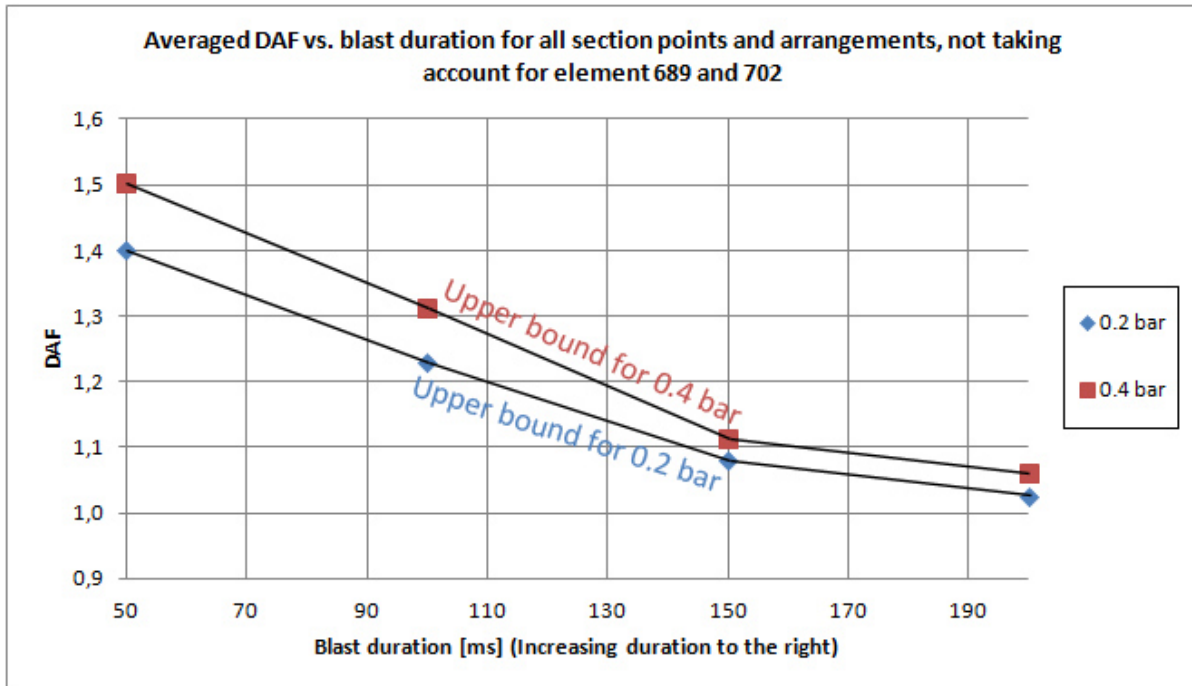


Figure 7.4: Upper bound values for DAF, method B. 0.2 bar blast pressure.

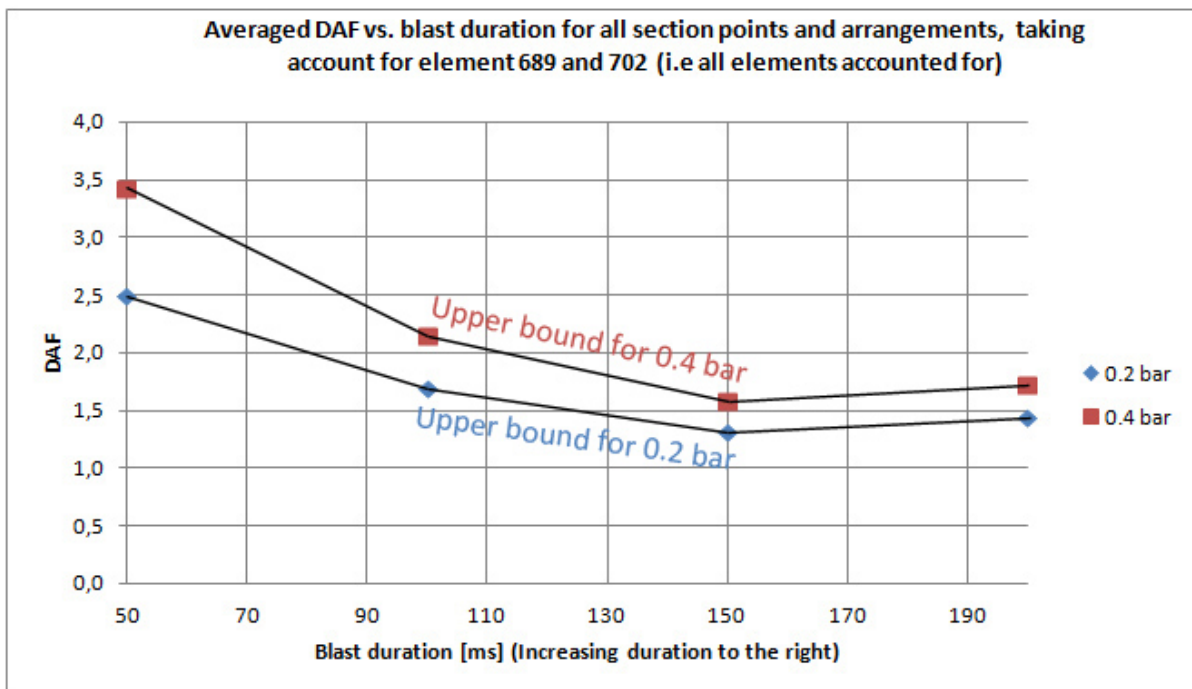


Figure 7.5: Upper bound values for DAF, method B. 0.4 bar blast pressure.

7.2.3 Averaging over all elements, use curve fit techniques (Method C)

Method C involved averaging the data points for all section points *and* elements for each blast duration, in the same manner as for method B. Linear or nonlinear least squares regression is then used to a curve to the remaining data points. The mathematical expression for this curve will express the variation of DAF over the blast duration. The benefit of using method C is that any DAF can be calculated using the resulting equation given a particular input parameter (e.g blast duration).

DAF vs. blast duration

It is seen that the data points and the variation of DAF with respect to the blast duration are fitted best to a logarithmic curve.

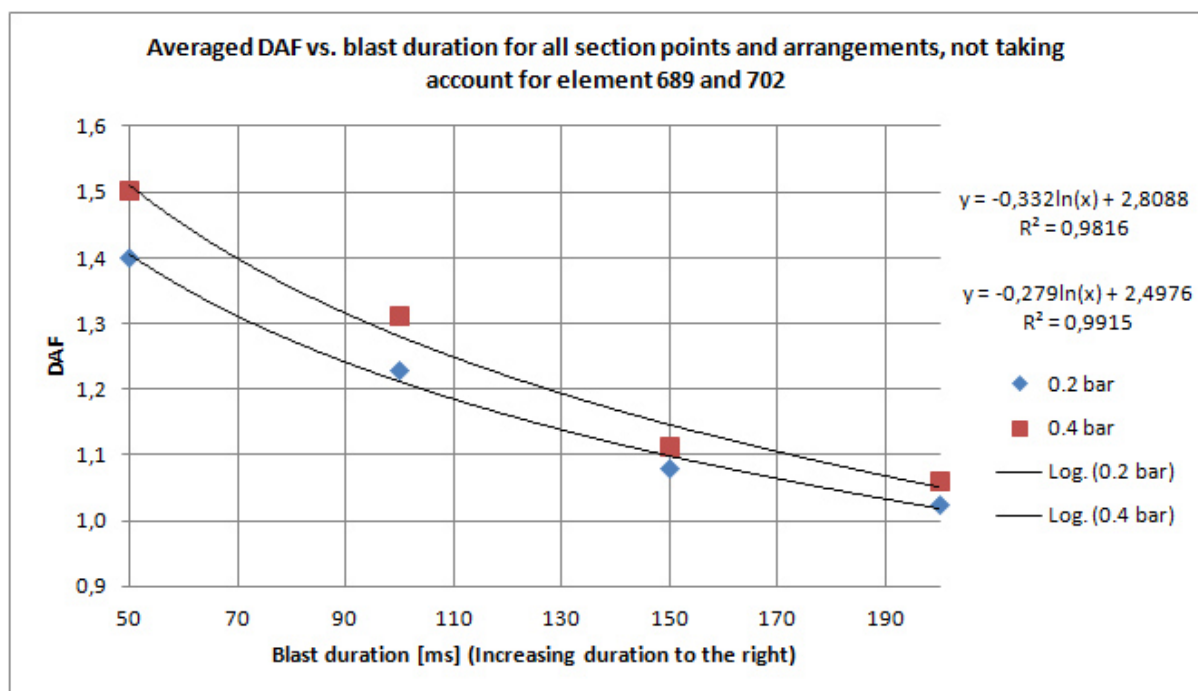


Figure 7.6: Variation of DAF with respect to blast duration, method C. Please note that this graph does not include the averaged data points from element 689 and 702.

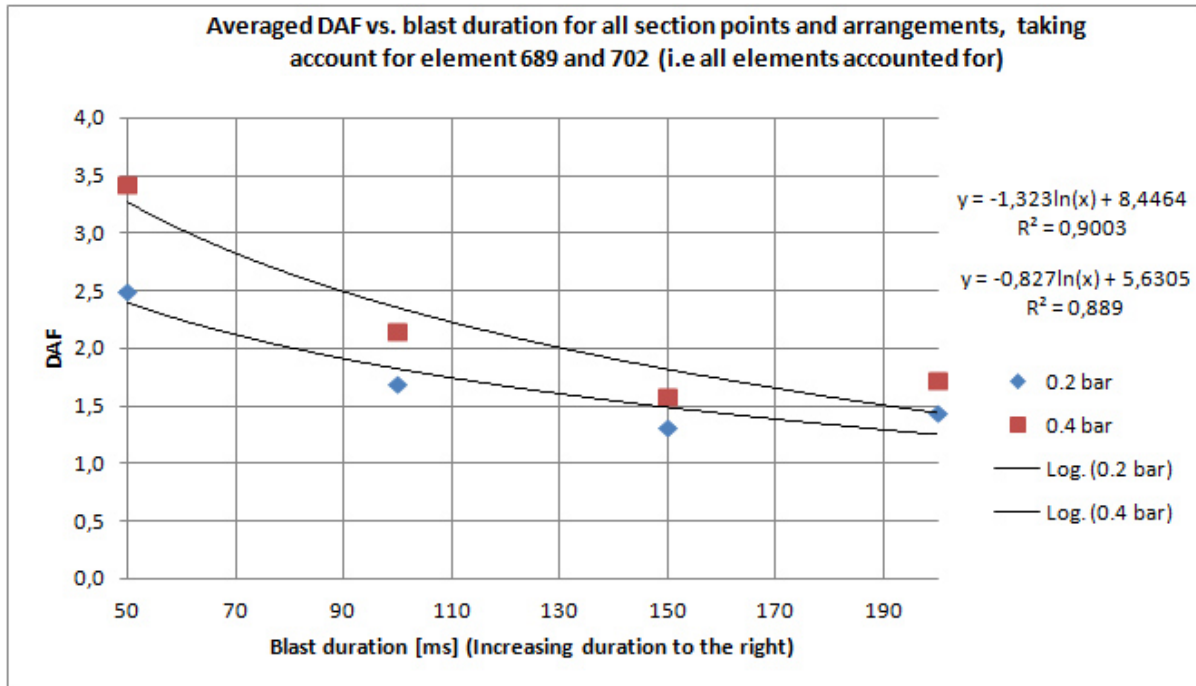


Figure 7.7: Variation of DAF with respect to blast duration, method C. The following graph includes the averaged data points from element 689 and 702.

DAF vs. piping arrangement (piping weight)

By plotting the DAF over the piping arrangement using method C, very small variations of the DAF was seen for varying piping arrangements. An exception is for arrangement 3 which showed deviation from the general trend, however by using linear regression to fit a curve to the remaining data points, it shown that the variation of DAF is very small, if not constant. For the case with element 689 and 702 accounted for, the DAF was found to be between 1.7-1.8 and 2.2-2.3 for the 0.2 and 0.4 bar cases respectively. If element 689 and 702 were *not* accounted for, the DAF seemed to have a near constant value of 1.2 for the 0.2 bar case, and a varying DAF between 1.2-1.3 for the 0.4 bar case. Reference is made to figure 7.9 and 7.8.

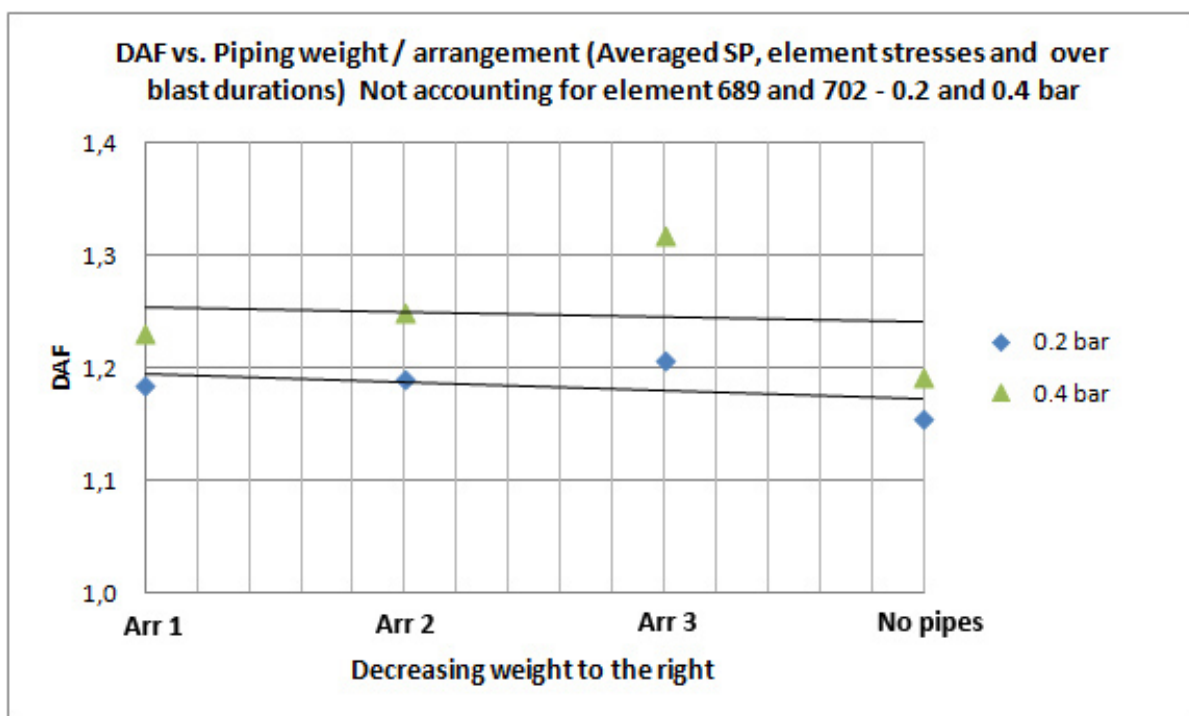


Figure 7.8: Variation of DAF with respect to arrangement (piping weight), method C. The following graph does not include the averaged data points from element 689 and 702.

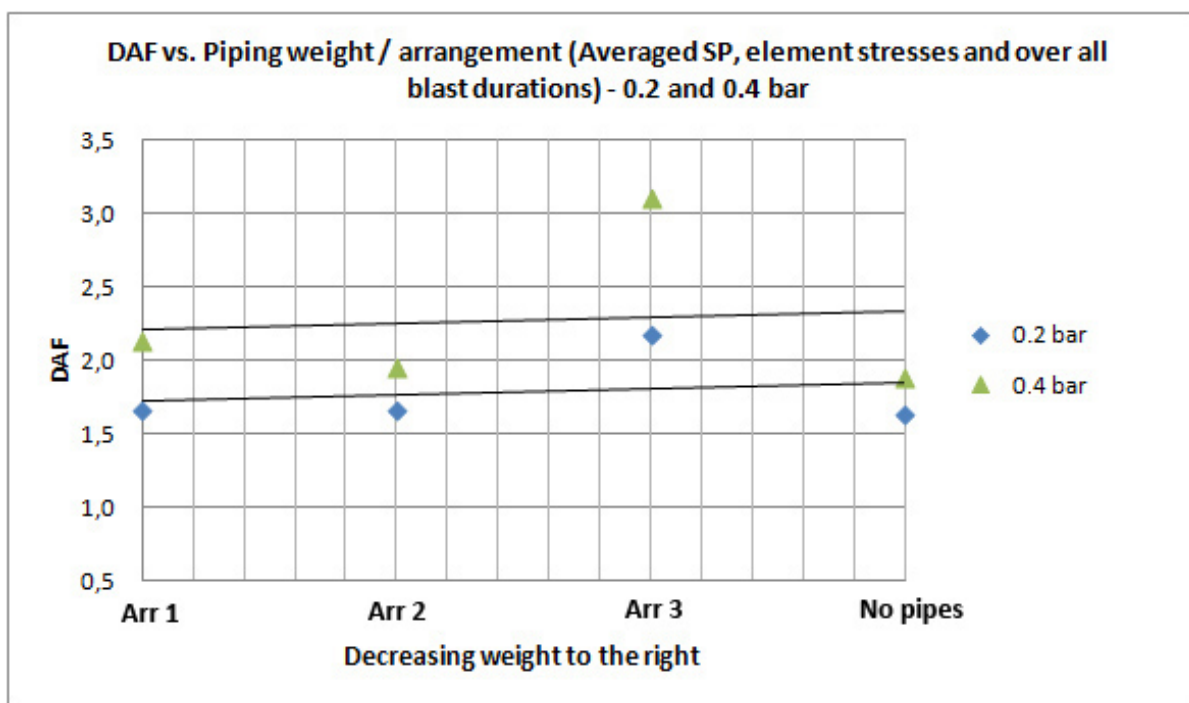


Figure 7.9: Variation of DAF with respect to arrangement (piping weight), method C. The following graph includes the averaged data points from element 689 and 702.

7.2.4 Summary

It is seen that different methods for obtaining the DAF for critical locations on the pipe rack, give different results. Results which include the data points from element 689 and 702 give noticeable higher DAF-values than for results without these two elements accounted for. The DAF values representing the 0.4 bar drag pressure are also higher than those for 0.2 bar drag pressure. While the DAF decreases with increased blast duration, it seems to remain constant with respect to piping weight (arrangement). Table 7.1, 7.2 and 7.3 summarize the DAF values found using the different methods.

Blast duration	DAF Method A	DAF Method B	DAF Method C
50 ms	2.3 (-)	1.4 (2.5)	1.4 (2.4)
100 ms	1.7 (-)	1.2 (1.7)	1.2 (1.8)
150 ms	1.4 (-)	1.1 (1.3)	1.1 (1.5)
200 ms	1.3 (-)	1.0 (1.4)	1.0 (1.3)

Table 7.1: DAF for 0.2 bar drag pressure (DAF vs. blast duration). The values in parentheses are the DAF accounted for element 689 and 702.

Blast duration	DAF Method A	DAF Method B	DAF Method C
50 ms	2.8 (-)	1.5 (3.4)	1.5 (3.3)
100 ms	1.9 (-)	1.3 (2.1)	1.3 (2.4)
150 ms	1.6 (-)	1.1 (1.6)	1.2 (1.8)
200 ms	1.6 (-)	1.1 (1.7)	1.1 (1.4)

Table 7.2: DAF for 0.4 bar drag pressure (DAF vs. blast duration). The values in parentheses are the DAF accounted for element 689 and 702.

Arrangement	0.2 bar	0.4 bar
1	1.2 (1.7)	1.3 (2.2)
2	1.2 (1.7)	1.2 (2.2)
3	1.2 (1.7)	1.2 (2.2)
No pipes	1.2 (1.8)	1.2 (2.3)

Table 7.3: DAF for different piping arrangements found by method C. Arrangement 1 being the heaviest loaded condition. The values in parentheses are the DAFs accounted for element 689 and 702.

7.3 DAF for support reactions

The different methods for determining DAF for support reactions are the same as previously presented in section 7.2 for critical locations on the pipe rack.

7.3.1 Using the upper bound (Method A)

By using the upper bound from the results (see figure 6.22, 6.23 and 6.24) the DAF values could be taken directly from the graphs for each case. An example of this is shown in figure 7.10.

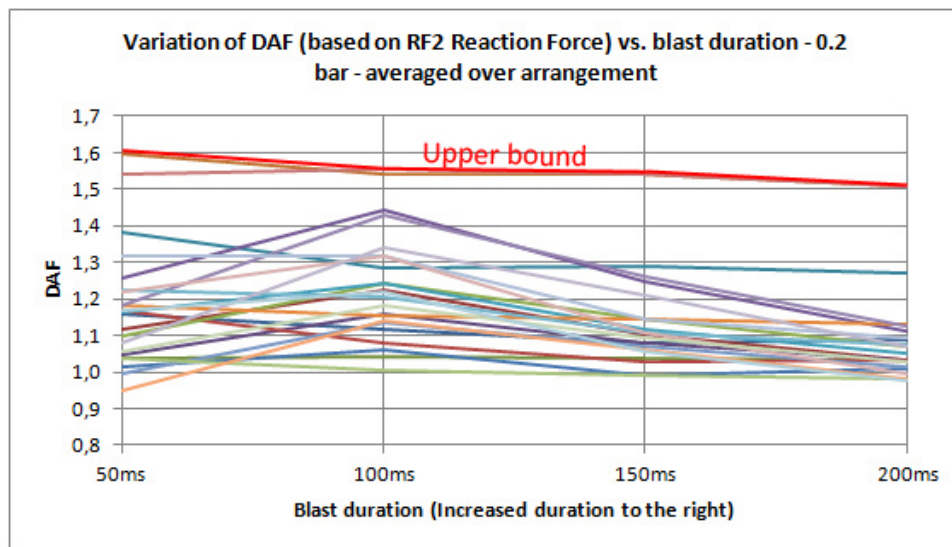


Figure 7.10: According to method A, the DAF value can be taken directly from the upper bound.

7.3.2 Averaging over all nodes, use the upper bound (Method B)

Method B involved taking the average of the DAFs over all nodes for each blast duration. This reduced the number of DAFs to only one value per blast duration. The upper bound was then taken for the remaining data points. This is illustrated in figure 7.11.

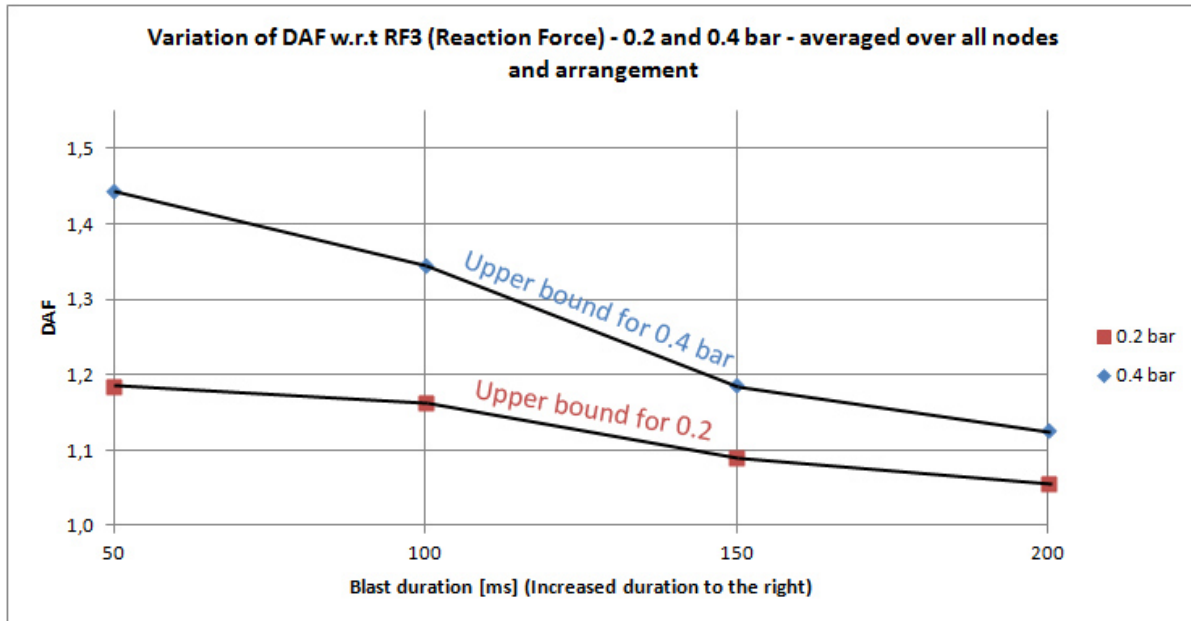


Figure 7.11: According to method B, the DAF value can be taken directly from the upper bound from the averaged DAF over all nodes.

7.3.3 Averaging over all nodes, use linear curve fit (Method C)

DAF vs. blast duration

From the results of the variation of DAF for reaction forces represented by figure 6.22, 6.23 and 6.24, scattering of data points are observed for each blast duration. A generalization has been done in the same manner as with the DAFs for critical locations on the pipe rack; by assuming that all DAFs for all nodes can be reduced to one generalized, averaged DAF. The data points are thus reduced to one DAF value per blast duration.

A study of the results showed that the DAF decreases with increased blast duration in such a way that a linear curve can be fitted to the data points. Linear least squares regression has been used to generate curves which show the relationship between the DAF and the blast duration. The best fit (i.e the curve which has the R^2 -value closest to 1) is obtained from the results from the reaction forces in Z-direction, which is the direction of the gravity. Reference is made to figure 7.14.

Another observation made is that the two curves for the reaction forces in Y-direction (each representing the 0.2 and 0.4 bar drag pressure) almost coincide with each other. This indicates that the reaction forces in Y-direction are independent of the magnitude of the blast. Reference is made to figure 7.13.

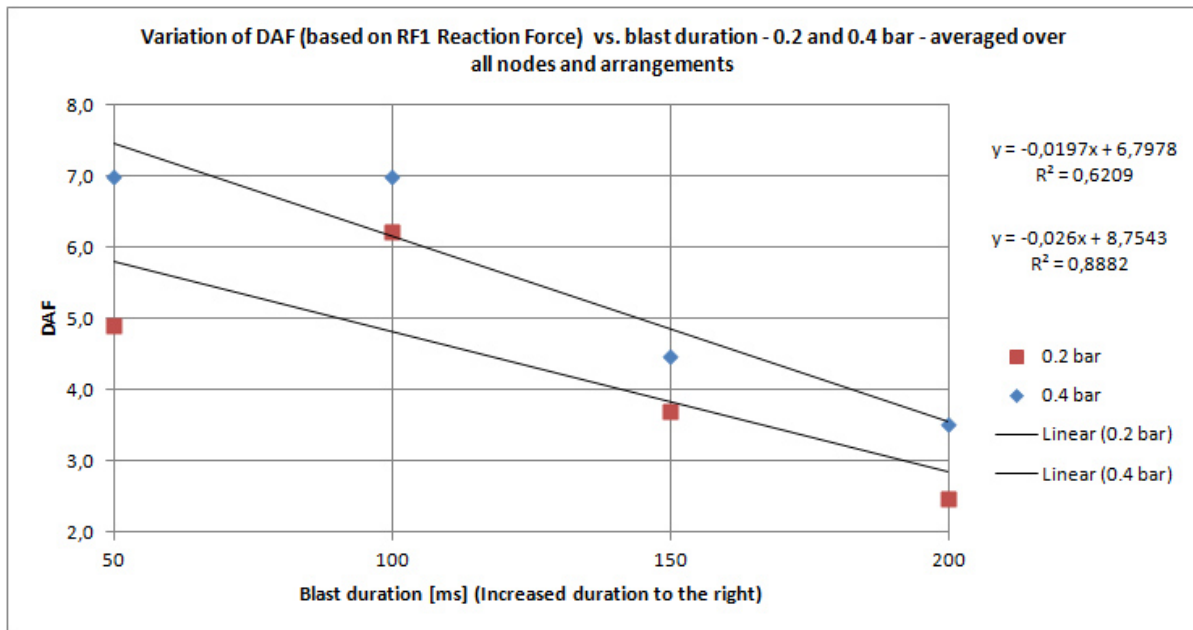


Figure 7.12: Linear least squared curve fit for the data points of RF1 (Reaction force in X-direction), DAF vs. blast duration.

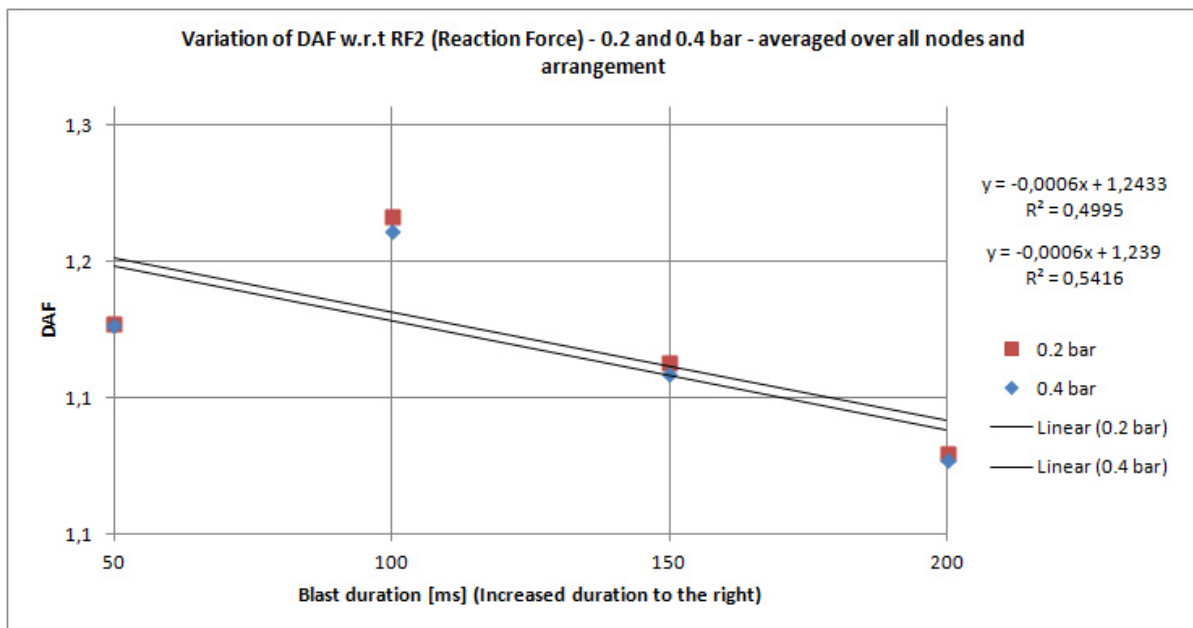


Figure 7.13: Linear least squared curve fit for the data points of RF2 (Reaction force in Y-direction; direction of blast), DAF vs. blast duration.

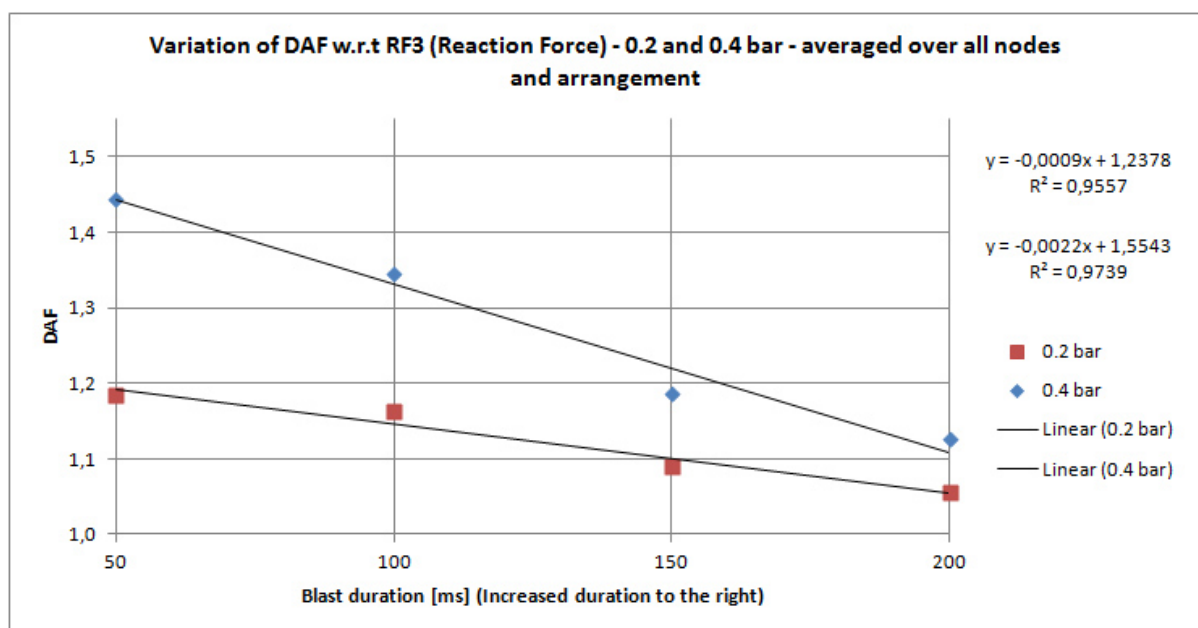


Figure 7.14: Linear least squared curve fit for the data points of RF3 (Reaction force in Z-direction; direction of gravity), DAF vs. blast duration.

DAF vs. piping arrangement (piping weight)

Method C was utilized, and the data points for each DAF were reduced to one value per piping arrangement. The change of DAF with respect to piping arrangement was then plotted. For the reaction forces in the X-direction, linear curves were fitted to the data points. These showed a decrease in DAF for reduced piping weight for both the 0.2 and the 0.4 bar cases. Reference is made to figure 7.15.

For the reaction forces in the Y-direction, the change of DAF is between 1.1 and 1.2. The DAF is decreasing with reduced piping weight for both 0.2 and 0.4 bar cases in the same manner as with the X-direction. Reference is made to figure 7.16.

The reaction forces in the Z-direction were fitted to second order polynomial curves. For this direction, the DAF increases with reduced piping weight for both the 0.2 and 0.4 cases. Reference is made to figure 7.17.

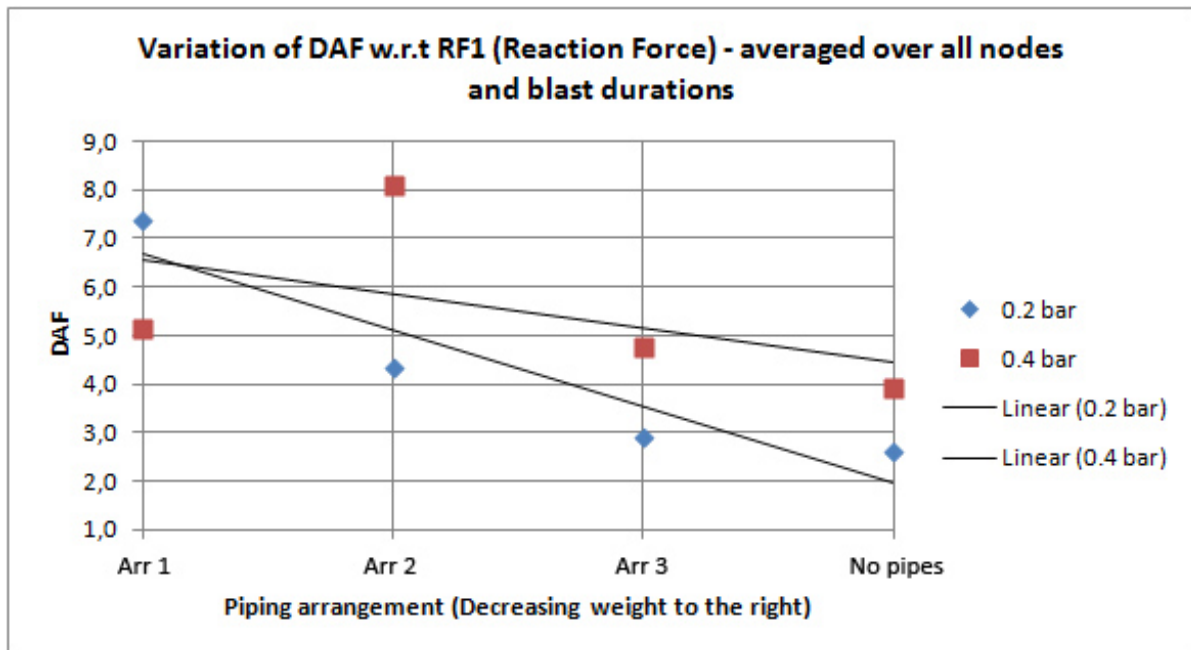


Figure 7.15: Linear least squared curve fit for the data points of RF1 (Reaction force in X-direction), DAF vs. piping arrangement.

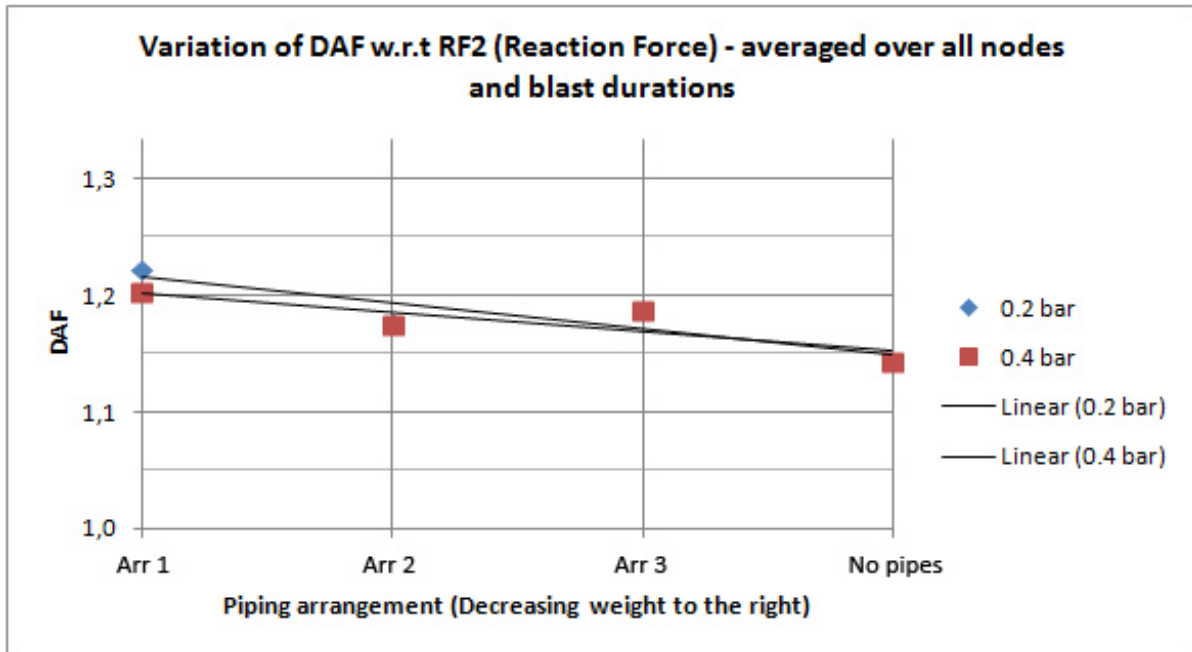


Figure 7.16: Linear least squared curve fit for the data points of RF2 (Reaction force in Y-direction; direction of gravity), DAF vs. piping arrangement.

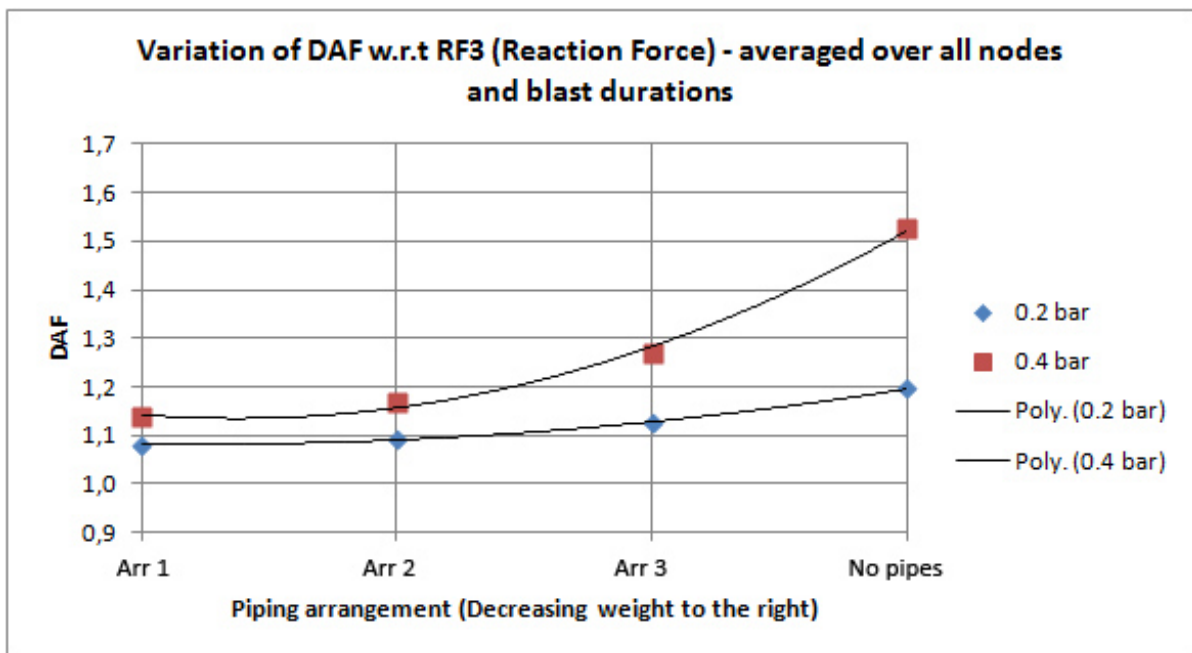


Figure 7.17: Nonlinear least squared curve fit for the data points of RF3 (Reaction force in Z-direction; direction of gravity), DAF vs. piping arrangement.

7.3.4 Summary

As with section 7.2.4, it is seen that different methods for obtaining DAF for support reactions (reaction forces) on the pipe rack, give different results. It should be noted that the DAF values for the support reactions (reaction forces) in the Y-direction (i.e the direction of the blast) seem to be constant, this indicates that the DAF for this direction is independent of the magnitude of the drag pressure.

Table 7.4, 7.5 and 7.6 summarize the obtained results of the DAF with respect to the blast duration for the different methods. Table 7.7, 7.8 and 7.9 summarize the obtained results of the DAF with respect to the piping arrangement for the different methods.

Blast duration	DAF Method A	DAF Method B	DAF Method C
50 ms	45.9 (63.7)	4.9 (7.0)	5.8 (7.5)
100 ms	72.8 (58.5)	6.2 (7.0)	4.8 (6.2)
150 ms	34.4 (33.8)	3.7 (4.5)	3.8 (4.9)
200 ms	16.1 (26.3)	2.5 (3.5)	2.9 (3.6)

Table 7.4: DAF values for support reactions (reaction forces) in X-direction. The values in parentheses are the DAF for 0.4 bar drag pressure.

Blast duration	DAF Method A	DAF Method B	DAF Method C
50 ms	1.6 (1.6)	1.2 (1.2)	1.2 (1.2)
100 ms	1.6 (1.5)	1.2 (1.2)	1.2 (1.2)
150 ms	1.5 (1.5)	1.2 (1.1)	1.2 (1.2)
200 ms	1.5 (1.5)	1.1 (1.1)	1.1 (1.1)

Table 7.5: DAF values for support reactions (reaction forces) in Y-direction (direction of the blast). The values in parentheses are the DAF for 0.4 bar drag pressure.

Blast duration	DAF Method A	DAF Method B	DAF Method C
50 ms	2.0 (5.7)	1.2 (1.4)	1.2 (1.4)
100 ms	1.8 (4.1)	1.2 (1.3)	1.2 (1.3)
150 ms	1.5 (2.7)	1.1 (1.2)	1.1 (1.2)
200 ms	1.5 (2.1)	1.1 (1.1)	1.1 (1.1)

Table 7.6: DAF values for support reactions (reaction forces) in Z-direction (direction of the gravity). The values in parentheses are the DAF for 0.4 bar drag pressure.

Arrangement	DAF Method A	DAF Method B	DAF Method C
1	188.3 (51.7)	7.4 (5.2)	6.7 (6.6)
2	87.3 (180.1)	4.4 (8.1)	5.1 (5.9)
3	18.6 (45.4)	2.9 (4.8)	3.5 (5.2)
No pipes	16.7 (55.7)	2.6 (3.9)	2.0 (4.4)

Table 7.7: DAF values for support reactions (reaction forces) in X-direction. The values in parentheses are the DAFs for 0.4 bar drag pressure.

Arrangement	DAF Method A	DAF Method B	DAF Method C
1	1.8 (1.6)	1.2 (1.2)	1.2 (1.2)
2	1.6 (1.6)	1.2 (1.2)	1.2 (1.2)
3	1.6 (1.6)	1.2 (1.2)	1.2 (1.2)
No pipes	1.6 (1.6)	1.1 (1.1)	1.1 (1.1)

Table 7.8: DAF values for support reactions (reaction forces) in Y-direction. The values in parentheses are the DAFs for 0.4 bar drag pressure.

Arrangement	DAF Method A	DAF Method B	DAF Method C
1	1.5 (1.8)	1.1 (1.1)	1.1 (1.1)
2	1.5 (2.5)	1.1 (1.2)	1.1 (1.2)
3	1.9 (4.2)	1.1 (1.3)	1.1 (1.3)
No pipes	3.4 (17.8)	1.1 (1.5)	1.2 (1.5)

Table 7.9: DAF values for support reactions (reaction forces) in Z-direction. The values in parentheses are the DAFs for 0.4 bar drag pressure.

Chapter 8

Conclusion and further work

8.1 Conclusion

This paper has been an investigation on the phenomenon of hydrocarbon explosions, the resulting blast load, and the structural response following such an event. Although a hydrocarbon explosion is considered a rare accidental event, effort should be made to reduce the amount of structural damage if an explosion was to occur. If blast load scenarios are not considered for critical structural elements close to a processing area, an initial blast accident can easily cause further escalation of damage, especially if pipes containing hydrocarbon liquid or gases rupture. A literature study has been done to gather as much relevant information about the topic as possible. Although similar work has been done by various sources such as The British Gas Research and Technology (ERS) [2], Hamdan [23], Christian Michelsen Research (CMR) Programme [41] and Scheler EA. et al.[30], none of these sources focus on the practical implementation of the dynamic drag/overpressure on the actual structure. The different sources deal mostly with the structural response of blast walls (confined spaces) and thick support beams. There are also a lot of uncertainties in the different sources concerning the drag effects of the dynamic pressure, this is an effect of more importance for truss works and open frame structures than for instance blast walls and other structures with large surfaces.

A pipe rack (truss) structure which is located outside a topside hydrocarbon processing area has been the object of the study. The blast scenario is assumed to be causing a drag pressure acting perpendicular to the longitudinal direction of the pipe rack and its pipes. In order to fully understand the dynamic response of the pipe rack structure *during* the blast, a parameter study has been performed by varying the blast load and duration. Further on, dynamic amplification factors (DAFs) have been calculated for critical locations on the pipe rack and at end connections by comparing dynamic and static analysis models. These dimensioning DAFs are to reflect the dynamic nature of the structural response during blast. Because the main project scope is to investigate

the dynamic amplification of the structure by comparing dynamic analyses against static analyses, it is merely the ratio between stresses which are of interest. With this said, the uncertainties regarding the determination of the magnitude of the drag load on the structure is greatly reduced.

Familiarization with the dynamic features in Abaqus/Explicit (especially concerning performing analyses of an impulsive character) and the post-processing of time dependent data have been emphasized. A simplified beam model of the pipe rack structure was created, in this model, connection (joint) eccentricities have been neglected. A mesh sensitivity (stress convergence) study was performed, and the mesh density was determined based on a consideration of a trade-off between computational time and relative accuracy of results. The piping weights on the pipe rack have been taken account for by using inertia masses, but the physical effects of the drag pressure on the pipes have been ignored for the sake of simplification. This simplification was based on assuming that the pipes are connected to the pipe rack with simple U-braces, which makes the piping stiffness-contribution to the overall structure negligible. Damping has been neglected as it is shown not to affect the responses to any large degree for blast analyses.

It should be noted by the reader that the structural responses due to the blast loading were within the material's elastic range, and no permanent deformations were observed. If plastic deformations have been observed, a ductility level analysis as presented under section 4.4 would have been performed. Three different methods were used to determine the general, dimensioning DAF for each blast case, and the results from all methods were presented.

Final results showed that the dimensioning DAF is dependent on both the blast duration *and* the weight of the pipes on the structure. For critical locations on the pipe rack, the DAF decreased with increased blast duration. The DAF remained almost constant regardless of change in piping weight.

For the end connections (support reactions), the DAF decreased with increased blast duration in the X- and Z-direction, while remaining almost constant for the Y-direction (blast direction) regardless of both changes in blast duration and piping weight. The DAF decreased with reduced piping weight in the X-direction, while it increased with reduced piping weight in the Z-direction.

8.2 Recommendations for future work

Further work should focus on analysing pipe rack structures of different sizes, RHS-profiles and designs as to obtain more DAF-values, such that a more *general* picture of the structural response of pipe racks can be obtained. Further work should also focus on investigating the effects of connection eccentricity on the structure with respect to the DAF, this will require a new model to be created. A parameter study with additional

drag pressure levels and blast durations may also be considered. In addition to this, variable mesh densities should be introduced, as to better capture the stresses near joints and critical areas.

CFD analyses, simulating the dispersion of the pressure and its effect on the pipes and structure, including possible shielding or blocking effects may be studied. A more accurate drag coefficient C_D for the drag pressure equation (as from equation 4.1) should be calculated. However, this may require familiarization with specialized CFD-software used to simulate explosions, i.e FLACS or Kameleon FireEx (KFX).

Bibliography

- [1] Ir. W.P.M Merx. *Methods for the determination of possible damage to people and objects resulting from releases of hazardous materials*. CPR 16E, TNO, first edition, 1992.
- [2] British Gas Research and Technology (ERS). *Blast and fire engineering project for topside structures, Work package No.BR2*. 1991.
- [3] W.Clough. R and Penzien. J. *Dynamics of Structures*. McGraw-Hill International Editions, second edition, 1993.
- [4] Amdahl J. *Lecture notes in subject TMR 4195 Design of Offshore Structures, Dept. Marine Structures, Norwegian Institute of Technology, Trondheim*. 2011.
- [5] *Orcaflex Manual 9.4a*. Orcina Ltd., 2010.
- [6] <http://www.offshoretechnology.com/projects/britannia/>.
- [7] Cirak. F. *Lectures in Plates and Shells: Theory and Computations*. Structural Mechanics Lab, Department of Engineering, University of Cambridge, 1999.
- [8] Zhong. W et al. Yao. W. *Symplectic Elasticity*. World Scientific Publishing Co. Pte. Ltd., 2009.
- [9] Abaqus/CAE 6.10-2 Documentation. *Getting Started with Abaqus: Interactive Edition*, publisher =.
- [10] Abaqus/CAE 6.10-2 Documentation. *User Manual: 26.3.8 Beam element library*. Dassault Systemes Simulia Corp., 2010.
- [11] L.A. Louca and R.M Mohamed Ali. *Improving the ductile behaviour of offshore topside structures under extreme loads*. Elsevier/Department of Civil and Environmental Engineering, Imperial College London UK, 1994.
- [12] Task Committee on Blast Resistant Design Society of Civil Engineers. *Design of Blast Resistant buildings in petrochemical facilities*. ASCE Publications, 1997.
- [13] Madenci E. and Guven I. *The Finite Element Method and Applications in Engineering using ANSYS*. Springer Science+Business Media, LLC, 2006.

- [14] Walter C. Hurty and Moshe F. Rubinstein. *Dynamics of Structures*. Prentice-Hall Series in Engineering of the Physical Sciences, 1964.
- [15] Abaqus/CAE 6.10-2 Documentation. *User Manual: Section 23.1.1 Material damping*. Dassault Systemes Simulia Corp., 2010.
- [16] Edward L. Wilson. *Three-Dimensional Static and Dynamic Analysis of Structures: A Physical Approach with Emphasis on Earthquake Engineering*. Computers and Structures, Inc., 1999.
- [17] Senthil S. Vel Brian P. Baillargeon and Jeffery S. Koplik. *Utilizing ABAQUS to Analyze the Active Vibration Suppression of Structural Systems*. ABAQUS Users' Conference, 2004.
- [18] ABS Consulting Ltd. *Design, materials and connections for blast-loaded structures, Research Report 205*. Health and Safety Executive (UK), 2006.
- [19] Buick Davison and Graham W. Owens. *Steel Designer's Manual 6th Edition*. Blackwell Publishing, 2006.
- [20] H. Bachmann et al. *Vibration Problems in Structures*. Birkhauser Verlag, Berlin, 1995.
- [21] Moan T. *TMR4305, Advanced Structural Analysis, Chapter 12 - Nonlinear Analysis*. 2011.
- [22] Abaqus/CAE 6.10-2 Documentation. *Theory Manual*. Dassault Systemes Simulia Corp., 2010.
- [23] Hamdan F. *Structural strengthening of offshore topsides structures as part of explosion risk reduction methods*. The Steel Construction Institute, Research Report 489, 2006.
- [24] NORSOK N-003. *Action and Action effects; 8.2 Fires and explosions*. Standards Norway (Norsk Standard), second edition, 2007.
- [25] FABIG. *FABIG Technical Note 2: Explosion Mitigation Systems*. The Steel Construction Institute, 1994.
- [26] Tam V. et. al Walker S., Corr B. *New Guidance on Fire and Explosion Engineering*. 21st International Conference on Offshore Mechanics and Arctic Engineering (OMAE 2002), 2002.
- [27] Det Norske Veritas. *DNV-RP-C204 Design Against Accidental Loads*. DNV, Det Norske Veritas, 2010.
- [28] Technical Staff of General Monitors. *A Guide to the Characteristics of Combustible Gases and Applicable Detection Technologies*. General Monitors.
- [29] Demeter G. Fertis. *Dynamics and Vibration of Structures*. John Wiley & Sons Inc, 1973.

- [30] Valdivieso JB Wood BJ. Scheler EA, Salter HS. *The modeling of gas explosions and the response of topside structures SPE*,. First International Conference on Health, Safety and Environment (Hague), 1991.
- [31] Yasseri S. Iso-damage diagrams for blast resistant design. *FABIG Newsletter Issue 42*, 2005.
- [32] Abaqus/CAE 6.10-2 Documentation. *Section 12, The Property Module*. Dassault Systemes Simulia Corp., 2010.
- [33] Abaqus/CAE 6.10-2 Documentation. *Section 20.2.3, Rate-dependent yield*. Dassault Systemes Simulia Corp., 2010.
- [34] Michael L. Berins. *SPI plastics engineering handbook of the Society of the Plastics Industry, Inc.* Kluwer Academic Publishers, fifth edition, 2002.
- [35] Irgens. F. *Formelsamling i Mekanikk*. Tapir Akademisk Forlag, third edition, 1999.
- [36] Abaqus/CAE 6.10-2 Documentation. *User Manual: Section 32.1 Defining inertia*. Dassault Systemes Simulia Corp., 2010.
- [37] Hong Chen and J. Y. Richard Liew. *Explosion and Fire Analysis of Steel Frames Using Mixed Element Approach*. JOURNAL OF ENGINEERING MECHANICS © ASCE/JUNE 2005, 2005.
- [38] M. Gough and E. Yandzio. *Protection of Buildings Against Explosions*. The Steel Construction Institute, 1999.
- [39] Abaqus/CAE 6.10-2 Documentation. *User Manual: Section 6.3.3 Explicit dynamic analysis*. Dassault Systemes Simulia Corp., 2010.
- [40] Sverre Steen and Jan V.Aarsnes. *TMR7 Experimental Methods in Marine Hydrodynamics Compendium*. Institutt for Marin Teknikk, 2010.
- [41] Wingerden K.V. Bjerketvedt, Bakke J.R. *GEXCON Gas Explosion Handbook*. Gas Safety Programme 1990-1992.

Appendix A

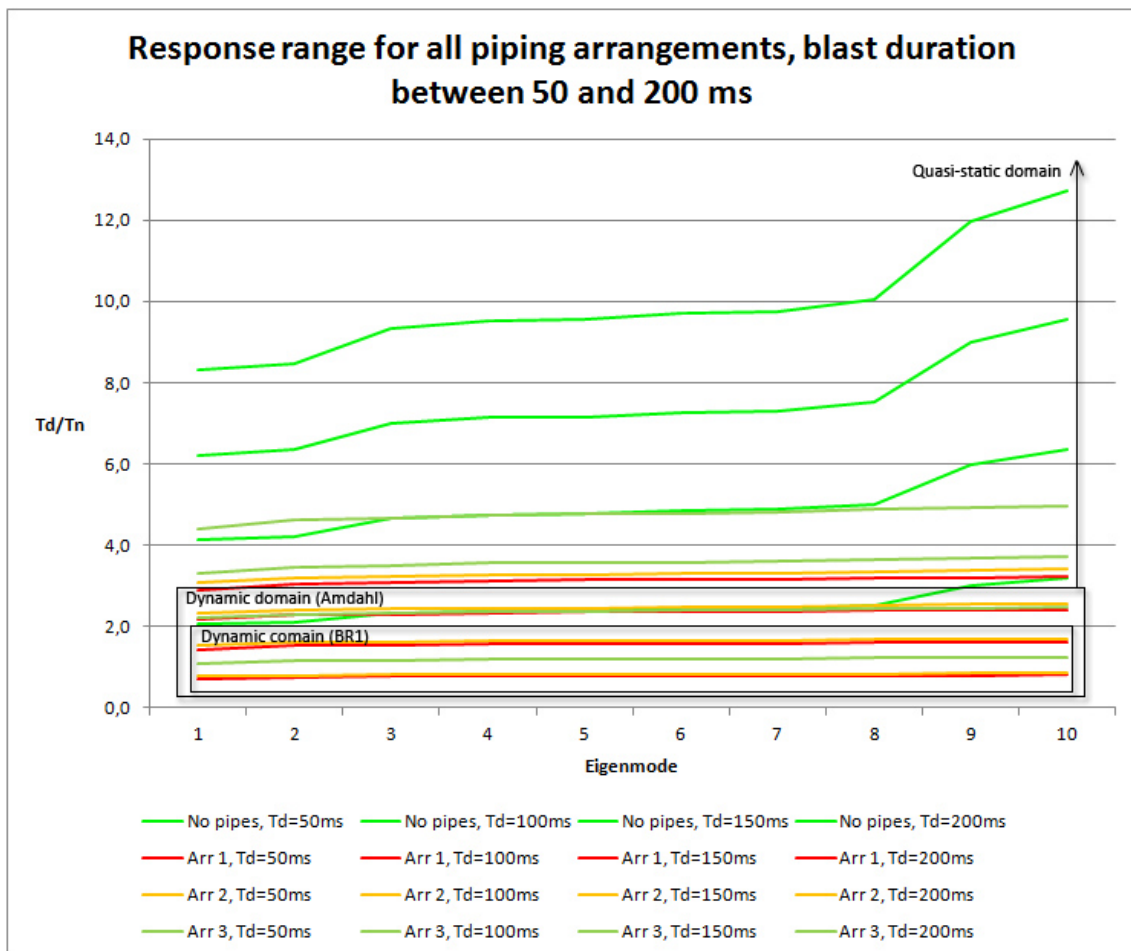
Piping weight

Piping weight from Span Chart for stainless steel lines/alloy steel lines								
*All weights are taken for the pipe with largest thickness (i.e which gives the largest weight)								
Note: All piping weights are assumed to attack as a point load (evenly distributed over the number of connection brackets on the pipe rack)								
Pipe assuming spanning over the whole length of the pipe rack, e.g 19 m								
Pipe no.	Pipe type	Max allowable span [m]	Span [m] (Approx)	Weight [N/m] (Pipe+liquid+insulation)	Total weight* [N]	No. Connection brackets	Point weight [N]	Point mass (approx)
1	DN1000	13,6	19	10209	193971	9	21552	2155
2	DN800	19,5	19	6782	128858	9	14318	1432
3	DN700	16,8	19	8648	164312	9	18257	1826
4	DN600	14,4	19	4622	87818	9	9758	976
5	DN500	13,4	19	3446	65474	9	7275	727
6	DN450	12,9	19	2918	55442	9	6160	616
7	DN400	11,9	19	2167	41173	9	4575	457
8	DN350	11,3	19	1755	33345	9	3705	371
9	DN300	10,3	19	1727	32813	9	3646	365
10	DN250	9,6	19	1345	25555	9	2839	284
11	DN200	9,7	19	1083	20577	9	2286	229

Figure A.1: Piping weight recalculated as concentrated masses in Excel.

Appendix B

Response range corresponding to eigenmodes



Appendix C

Pipe span chart

SPAN CHART FOR STAINLESS STEEL LINES / ALLOY STEEL LINES										
NOMINAL PIPE SIZE (IN.)	PIPE SIZE	SCH / W THK	PIPE ONLY		PIPE & LIQUID		PIPE + LIQUID + INSULATION		PIPE + VAPOUR + INSULATION	
			SPAN (M)	WEIGHT (N/M)	SPAN (M)	WEIGHT (N/M)	SPAN (M)	WEIGHT (N/M)	SPAN (M)	WEIGHT (N/M)
NPS 12	DN 300	10S	12.0	363	9.1	1126	8.9	1189	11.4	450
		40S	11.9	739	10.1	1455	10.0	1518	11.6	824
		80S 30	11.9 13.1	978 656	10.4 10.9	1664 1383	10.3 10.7	1727 1446	11.6 12.7	1062 741
NPS 14	DN 350	5S	12.6	348	9.1	1279	9.0	1348	11.9	445
		10S	12.6	417	9.4	1359	9.3	1408	12.0	513
		30	13.7	814	11.4	1687	11.3	1755	13.3	909
NPS 16	DN 400	5S	13.5	418	9.6	1638	9.5	1716	12.7	532
		10S	13.5	477	9.8	1690	9.7	1767	12.8	591
		30	14.7	933	12.0	2089	11.9	2167	14.3	1045
NPS 18	DN 450	5S	14.3	471	9.9	2023	9.8*	2109	13.4	603
		10S	14.3	537	10.2	2081	10.1	2169	13.5	670
		30	15.5	1396	13.0	2832	12.9	2918	15.2	1525
NPS 20	DN 500	5S	15.1	598	10.5	2512	10.4	2606	14.2	750
		10S	15.1	684	10.8	2587	10.7	2682	14.3	836
		30	16.4	1557	13.5	3351	13.4	3446	16.0	1703
NPS 24	DN 600	5S	16.5	823	11.4	3587	11.3*	3699	15.7	1018
		10S	16.5	956	11.8	3704	11.7	3816	15.8	1150
		30	18.0	1877	14.5	4510	14.4	4622	17.6	2068
NPS 28	DN 700	30 mm	19.2	5056	16.9	8400	16.8	8648	18.9	5403
NPS 32	DN 800	9.53 mm	19.5	1925	14	6782				
NPS 40	DN 1000	7.9 mm	23.4	1971	13.8*	9864	13.6*	10209	21.9	2547

NOTES: These spans are based on pipe containing fluid with specific gravity of 1.0 with temperature as specified in piping specification and maximum material stress 30 Mpa or maximum deflection 7 mm. 20 Mpa for CuNi pipes. * When stress is the critical value.

Figure C.1: Span chart provided by Aker Solutions

Appendix D

Python Script for extracting RF (Magnitude)

```
#Script for extracting Reaction Forces from 23 Nodes (at end connections) on the pipe rack:  
#(The numerical symbol 'firkant' is the comment symbol in Python)
```

```
from abaqus import *  
from abaqusConstants import *  
  
o1 = session.openOdb(name='C:/Temp/RHS200_02bar_50ms_arr1.odb')  
session.viewports['Viewport: 1'].setValues(displayedObject=o1)  
odb = session.odbs['C:/Temp/RHS200_02bar_50ms_arr1.odb']  
session.xyDataListFromField(odb=odb, outputPosition=NODAL, variable=((('RF',  
NODAL, ((INVARIANT, 'Magnitude'), )), ), nodePick=((('PIPE RACK NEWEST-1',  
23, ('[#82004020 #0 #402150e1 #20000120 #3084c000 #2 ]', )), ), )  
  
x0 = session.xyDataObjects['RF:Magnitude PI: PIPE RACK NEWEST-1 N: 6']  
x1 = session.xyDataObjects['RF:Magnitude PI: PIPE RACK NEWEST-1 N: 15']  
x2 = session.xyDataObjects['RF:Magnitude PI: PIPE RACK NEWEST-1 N: 26']  
x3 = session.xyDataObjects['RF:Magnitude PI: PIPE RACK NEWEST-1 N: 32']  
x4 = session.xyDataObjects['RF:Magnitude PI: PIPE RACK NEWEST-1 N: 65']  
x5 = session.xyDataObjects['RF:Magnitude PI: PIPE RACK NEWEST-1 N: 70']  
x6 = session.xyDataObjects['RF:Magnitude PI: PIPE RACK NEWEST-1 N: 71']  
x7 = session.xyDataObjects['RF:Magnitude PI: PIPE RACK NEWEST-1 N: 72']  
x8 = session.xyDataObjects['RF:Magnitude PI: PIPE RACK NEWEST-1 N: 77']  
x9 = session.xyDataObjects['RF:Magnitude PI: PIPE RACK NEWEST-1 N: 79']  
x10 = session.xyDataObjects['RF:Magnitude PI: PIPE RACK NEWEST-1 N: 81']  
x11 = session.xyDataObjects['RF:Magnitude PI: PIPE RACK NEWEST-1 N: 86']  
x12 = session.xyDataObjects['RF:Magnitude PI: PIPE RACK NEWEST-1 N: 95']  
x13 = session.xyDataObjects['RF:Magnitude PI: PIPE RACK NEWEST-1 N: 102']  
x14 = session.xyDataObjects['RF:Magnitude PI: PIPE RACK NEWEST-1 N: 105']
```

```
x15 = session.xyDataObjects['RF:Magnitude PI: PIPE RACK NEWEST-1 N: 126']
x16 = session.xyDataObjects['RF:Magnitude PI: PIPE RACK NEWEST-1 N: 143']
x17 = session.xyDataObjects['RF:Magnitude PI: PIPE RACK NEWEST-1 N: 144']
x18 = session.xyDataObjects['RF:Magnitude PI: PIPE RACK NEWEST-1 N: 147']
x19 = session.xyDataObjects['RF:Magnitude PI: PIPE RACK NEWEST-1 N: 152']
x20 = session.xyDataObjects['RF:Magnitude PI: PIPE RACK NEWEST-1 N: 157']
x21 = session.xyDataObjects['RF:Magnitude PI: PIPE RACK NEWEST-1 N: 158']
x22 = session.xyDataObjects['RF:Magnitude PI: PIPE RACK NEWEST-1 N: 162']
session.writeXYReport(fileName='C:/Temp/RHS200_02bar_50ms_arr1.rpt', xyData=(x0, x1, x2,
x3, x4, x5, x6, x7, x8, x9, x10, x11, x12, x13, x14, x15, x16, x17, x18,
x19, x20, x21, x22))
```

Appendix E

Python Script for extracting RF (X, Y and Z-direction)

#Script for extracting Reaction Forces from 23 Nodes (at end connections) on the pipe rack:

```
from abaqus import *
from abaqusConstants import *

o1 = session.openOdb(name='C:/Temp/RHS200_02bar_50ms_arr1.odb')
session.viewports['Viewport: 1'].setValues(displayedObject=o1)
odb = session.odbs['C:/Temp/RHS200_02bar_50ms_arr1.odb']
session.xyDataListFromField(odb=odb, outputPosition=NODAL, variable=((('RF',
NODAL, ((COMPONENT, 'RF1'), (COMPONENT, 'RF2'), (COMPONENT, 'RF3'), )), ),
nodePick=((('PIPE RACK NEWEST-1', 23, (
'#82004020 #0 #402150e1 #20000120 #3084c000 #2 ]', )), ), )

x0 = session.xyDataObjects['RF:RF1 PI: PIPE RACK NEWEST-1 N: 6']
x1 = session.xyDataObjects['RF:RF1 PI: PIPE RACK NEWEST-1 N: 15']
x2 = session.xyDataObjects['RF:RF1 PI: PIPE RACK NEWEST-1 N: 26']
x3 = session.xyDataObjects['RF:RF1 PI: PIPE RACK NEWEST-1 N: 32']
x4 = session.xyDataObjects['RF:RF1 PI: PIPE RACK NEWEST-1 N: 65']
x5 = session.xyDataObjects['RF:RF1 PI: PIPE RACK NEWEST-1 N: 70']
x6 = session.xyDataObjects['RF:RF1 PI: PIPE RACK NEWEST-1 N: 71']
x7 = session.xyDataObjects['RF:RF1 PI: PIPE RACK NEWEST-1 N: 72']
x8 = session.xyDataObjects['RF:RF1 PI: PIPE RACK NEWEST-1 N: 77']
x9 = session.xyDataObjects['RF:RF1 PI: PIPE RACK NEWEST-1 N: 79']
x10 = session.xyDataObjects['RF:RF1 PI: PIPE RACK NEWEST-1 N: 81']
x11 = session.xyDataObjects['RF:RF1 PI: PIPE RACK NEWEST-1 N: 86']
x12 = session.xyDataObjects['RF:RF1 PI: PIPE RACK NEWEST-1 N: 95']
x13 = session.xyDataObjects['RF:RF1 PI: PIPE RACK NEWEST-1 N: 102']
x14 = session.xyDataObjects['RF:RF1 PI: PIPE RACK NEWEST-1 N: 105']
```

APPENDIX E. PYTHON SCRIPT FOR EXTRACTING RF (X, Y AND Z-DIRECTION)E. 2

```
x15 = session.xyDataObjects['RF:RF1 PI: PIPE RACK NEWEST-1 N: 126']
x16 = session.xyDataObjects['RF:RF1 PI: PIPE RACK NEWEST-1 N: 143']
x17 = session.xyDataObjects['RF:RF1 PI: PIPE RACK NEWEST-1 N: 144']
x18 = session.xyDataObjects['RF:RF1 PI: PIPE RACK NEWEST-1 N: 147']
x19 = session.xyDataObjects['RF:RF1 PI: PIPE RACK NEWEST-1 N: 152']
x20 = session.xyDataObjects['RF:RF1 PI: PIPE RACK NEWEST-1 N: 157']
x21 = session.xyDataObjects['RF:RF1 PI: PIPE RACK NEWEST-1 N: 158']
x22 = session.xyDataObjects['RF:RF1 PI: PIPE RACK NEWEST-1 N: 162']
x23 = session.xyDataObjects['RF:RF2 PI: PIPE RACK NEWEST-1 N: 6']
x24 = session.xyDataObjects['RF:RF2 PI: PIPE RACK NEWEST-1 N: 15']
x25 = session.xyDataObjects['RF:RF2 PI: PIPE RACK NEWEST-1 N: 26']
x26 = session.xyDataObjects['RF:RF2 PI: PIPE RACK NEWEST-1 N: 32']
x27 = session.xyDataObjects['RF:RF2 PI: PIPE RACK NEWEST-1 N: 65']
x28 = session.xyDataObjects['RF:RF2 PI: PIPE RACK NEWEST-1 N: 70']
x29 = session.xyDataObjects['RF:RF2 PI: PIPE RACK NEWEST-1 N: 71']
x30 = session.xyDataObjects['RF:RF2 PI: PIPE RACK NEWEST-1 N: 72']
x31 = session.xyDataObjects['RF:RF2 PI: PIPE RACK NEWEST-1 N: 77']
x32 = session.xyDataObjects['RF:RF2 PI: PIPE RACK NEWEST-1 N: 79']
x33 = session.xyDataObjects['RF:RF2 PI: PIPE RACK NEWEST-1 N: 81']
x34 = session.xyDataObjects['RF:RF2 PI: PIPE RACK NEWEST-1 N: 86']
x35 = session.xyDataObjects['RF:RF2 PI: PIPE RACK NEWEST-1 N: 95']
x36 = session.xyDataObjects['RF:RF2 PI: PIPE RACK NEWEST-1 N: 102']
x37 = session.xyDataObjects['RF:RF2 PI: PIPE RACK NEWEST-1 N: 105']
x38 = session.xyDataObjects['RF:RF2 PI: PIPE RACK NEWEST-1 N: 126']
x39 = session.xyDataObjects['RF:RF2 PI: PIPE RACK NEWEST-1 N: 143']
x40 = session.xyDataObjects['RF:RF2 PI: PIPE RACK NEWEST-1 N: 144']
x41 = session.xyDataObjects['RF:RF2 PI: PIPE RACK NEWEST-1 N: 147']
x42 = session.xyDataObjects['RF:RF2 PI: PIPE RACK NEWEST-1 N: 152']
x43 = session.xyDataObjects['RF:RF2 PI: PIPE RACK NEWEST-1 N: 157']
x44 = session.xyDataObjects['RF:RF2 PI: PIPE RACK NEWEST-1 N: 158']
x45 = session.xyDataObjects['RF:RF2 PI: PIPE RACK NEWEST-1 N: 162']
x46 = session.xyDataObjects['RF:RF3 PI: PIPE RACK NEWEST-1 N: 6']
x47 = session.xyDataObjects['RF:RF3 PI: PIPE RACK NEWEST-1 N: 15']
x48 = session.xyDataObjects['RF:RF3 PI: PIPE RACK NEWEST-1 N: 26']
x49 = session.xyDataObjects['RF:RF3 PI: PIPE RACK NEWEST-1 N: 32']
x50 = session.xyDataObjects['RF:RF3 PI: PIPE RACK NEWEST-1 N: 65']
x51 = session.xyDataObjects['RF:RF3 PI: PIPE RACK NEWEST-1 N: 70']
x52 = session.xyDataObjects['RF:RF3 PI: PIPE RACK NEWEST-1 N: 71']
x53 = session.xyDataObjects['RF:RF3 PI: PIPE RACK NEWEST-1 N: 72']
x54 = session.xyDataObjects['RF:RF3 PI: PIPE RACK NEWEST-1 N: 77']
x55 = session.xyDataObjects['RF:RF3 PI: PIPE RACK NEWEST-1 N: 79']
x56 = session.xyDataObjects['RF:RF3 PI: PIPE RACK NEWEST-1 N: 81']
x57 = session.xyDataObjects['RF:RF3 PI: PIPE RACK NEWEST-1 N: 86']
x58 = session.xyDataObjects['RF:RF3 PI: PIPE RACK NEWEST-1 N: 95']
x59 = session.xyDataObjects['RF:RF3 PI: PIPE RACK NEWEST-1 N: 102']
```

APPENDIX E. PYTHON SCRIPT FOR EXTRACTING RF (X, Y AND Z-DIRECTION)E. 3

```
x60 = session.xyDataObjects['RF:RF3 PI: PIPE RACK NEWEST-1 N: 105']
x61 = session.xyDataObjects['RF:RF3 PI: PIPE RACK NEWEST-1 N: 126']
x62 = session.xyDataObjects['RF:RF3 PI: PIPE RACK NEWEST-1 N: 143']
x63 = session.xyDataObjects['RF:RF3 PI: PIPE RACK NEWEST-1 N: 144']
x64 = session.xyDataObjects['RF:RF3 PI: PIPE RACK NEWEST-1 N: 147']
x65 = session.xyDataObjects['RF:RF3 PI: PIPE RACK NEWEST-1 N: 152']
x66 = session.xyDataObjects['RF:RF3 PI: PIPE RACK NEWEST-1 N: 157']
x67 = session.xyDataObjects['RF:RF3 PI: PIPE RACK NEWEST-1 N: 158']
x68 = session.xyDataObjects['RF:RF3 PI: PIPE RACK NEWEST-1 N: 162']
session.writeXYReport(fileName='RHS200_02bar_50ms_arr1.rpt', xyData=(x0,
x1, x2, x3, x4, x5, x6, x7, x8, x9, x10, x11, x12, x13, x14, x15, x16, x17,
x18, x19, x20, x21, x22, x23, x24, x25, x26, x27, x28, x29, x30, x31, x32,
x33, x34, x35, x36, x37, x38, x39, x40, x41, x42, x43, x44, x45, x46, x47,
x48, x49, x50, x51, x52, x53, x54, x55, x56, x57, x58, x59, x60, x61, x62,
x63, x64, x65, x66, x67, x68))
```

Appendix F

Variation of DAF against blast duration.

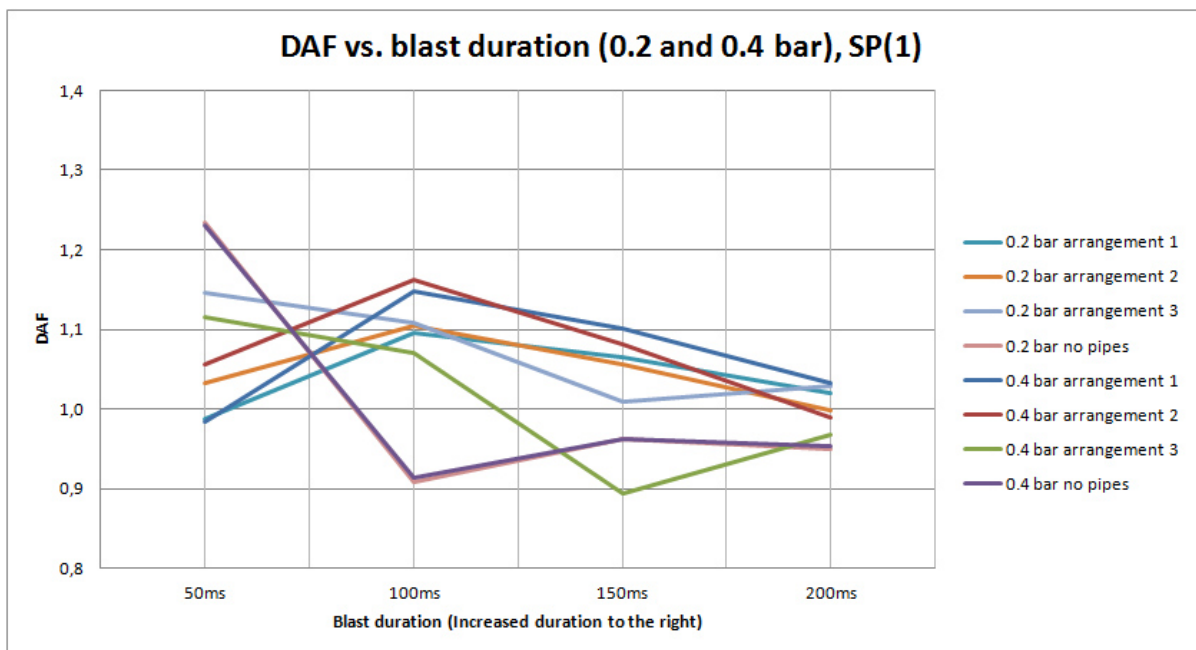


Figure F.1: The following graph shows the variation of DAF for the first section points with respect to blast duration, using method 1 to extract the stresses. Stress is taken for one element per case only

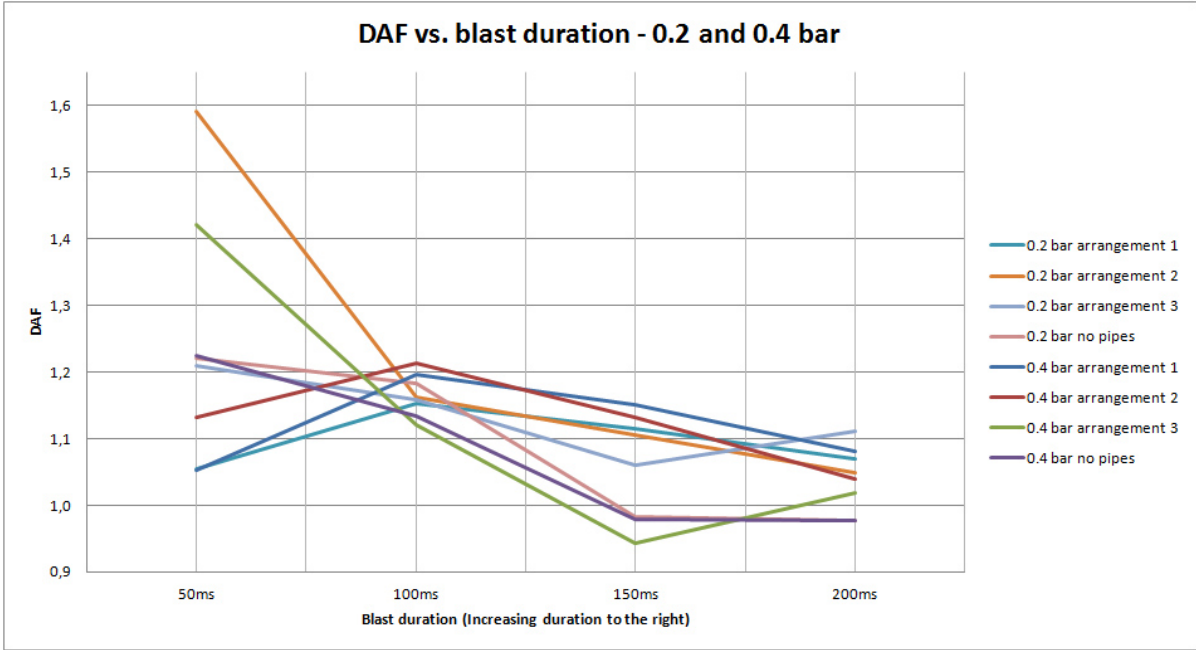


Figure F.2: The following graph shows the variation of DAF for the first section points with respect to blast duration, using method 2 to extract the stresses. Stress is taken for one element per case only

Appendix G

Variation of DAF against piping weight (arrangement).

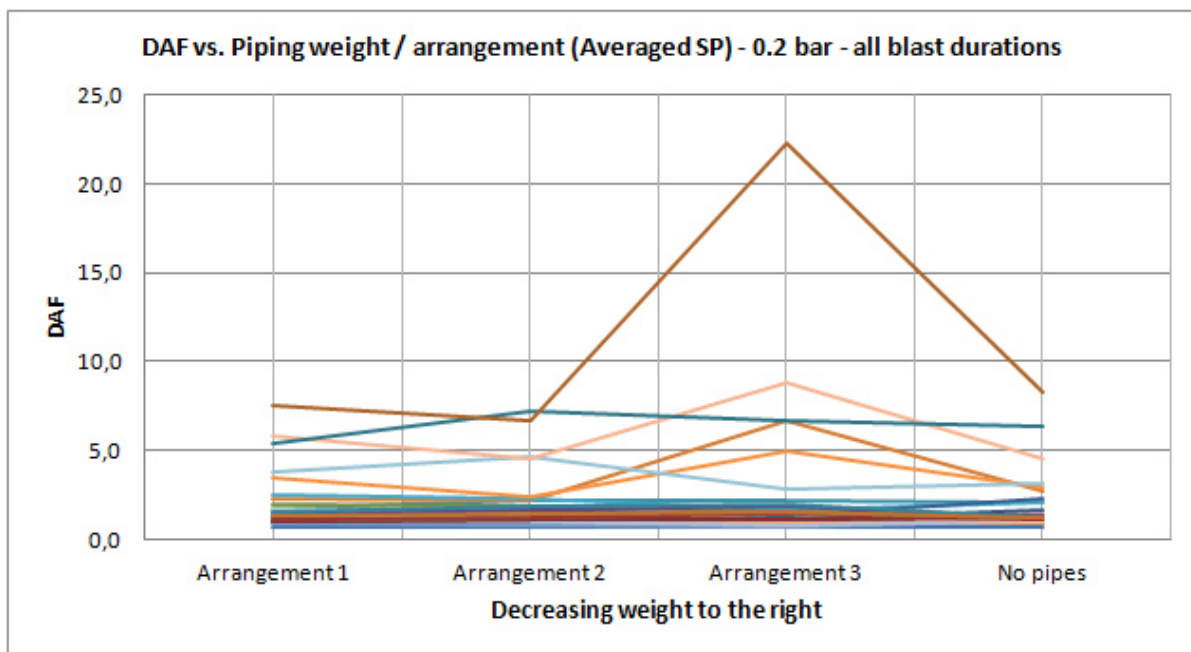


Figure G.1: Averaged DAF plotted against piping weight (arrangement) for all elements. 0.2 bar blast drag pressure.

APPENDIX G. VARIATION OF DAF AGAINST PIPING WEIGHT (ARRANGEMENT). G. 2

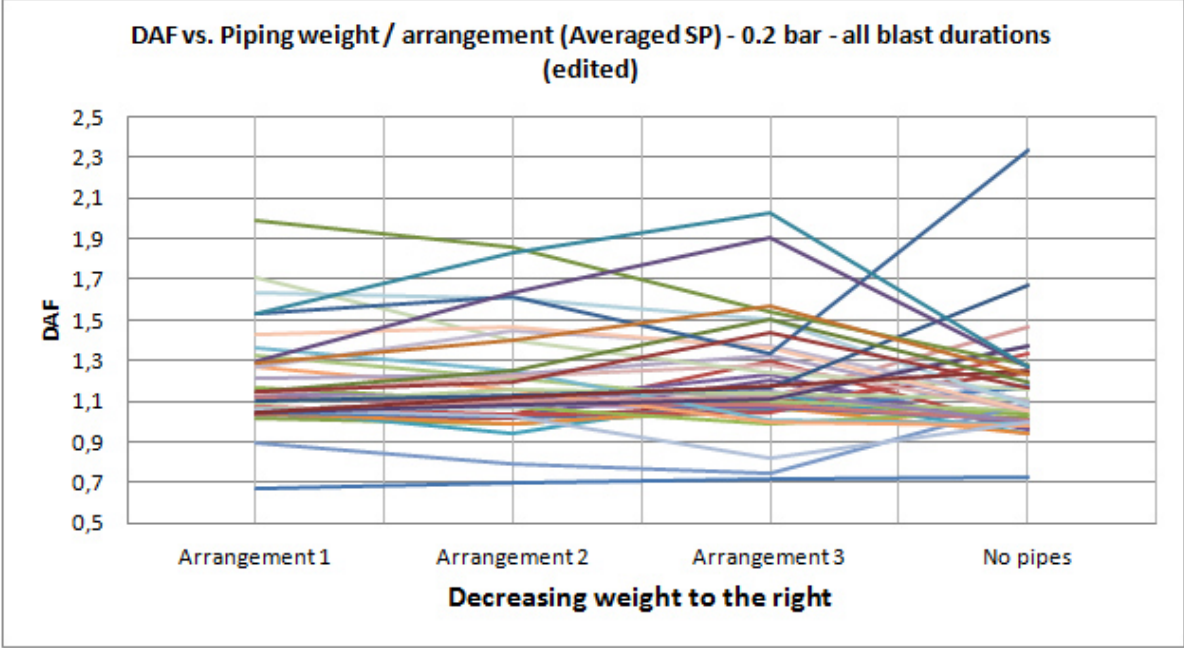


Figure G.2: Averaged DAF plotted against piping weight (arrangement) neglecting the data points for element 689 and 702. 0.2 bar blast drag pressure.

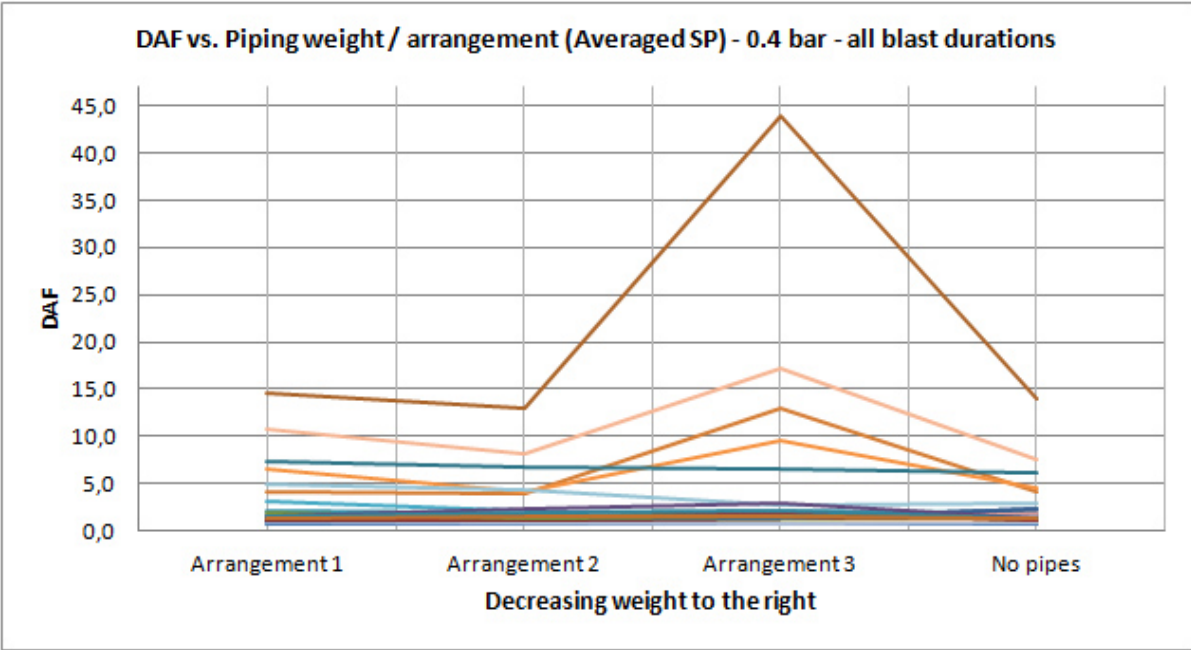


Figure G.3: Averaged DAF plotted against piping weight (arrangement) for all elements. 0.4 bar blast drag pressure.

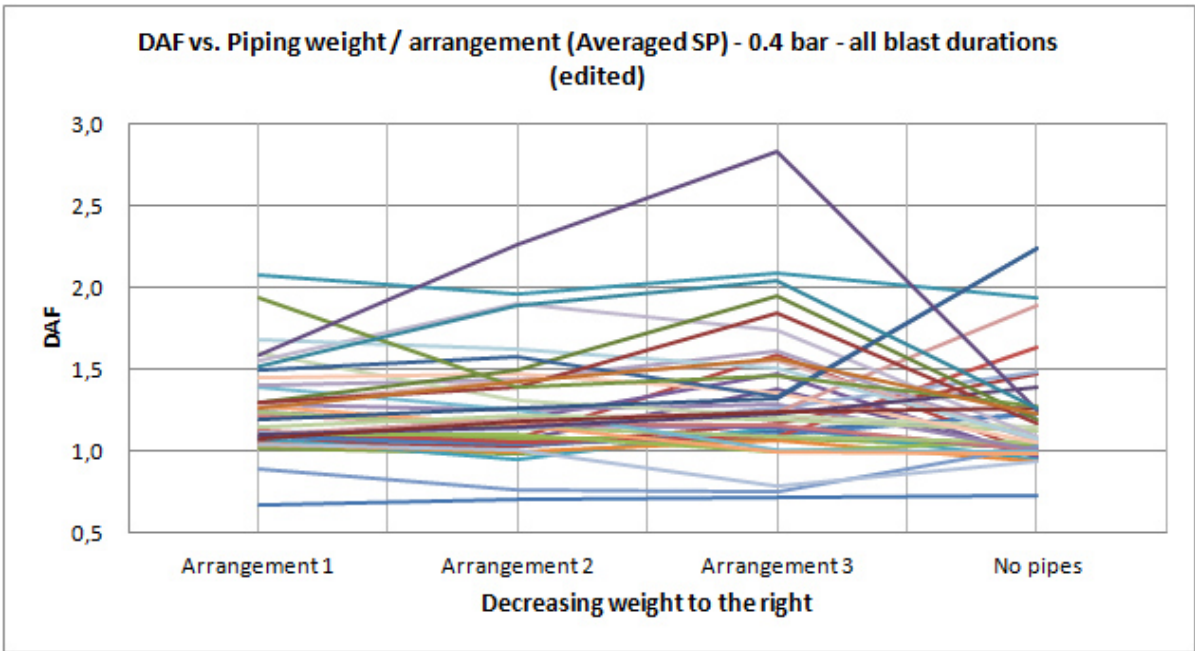


Figure G.4: Averaged DAF plotted against piping weight (arrangement) neglecting the data points for element 689 and 702. 0.4 bar blast drag pressure.

Appendix H

Variation of V.M stresses along path/beam.

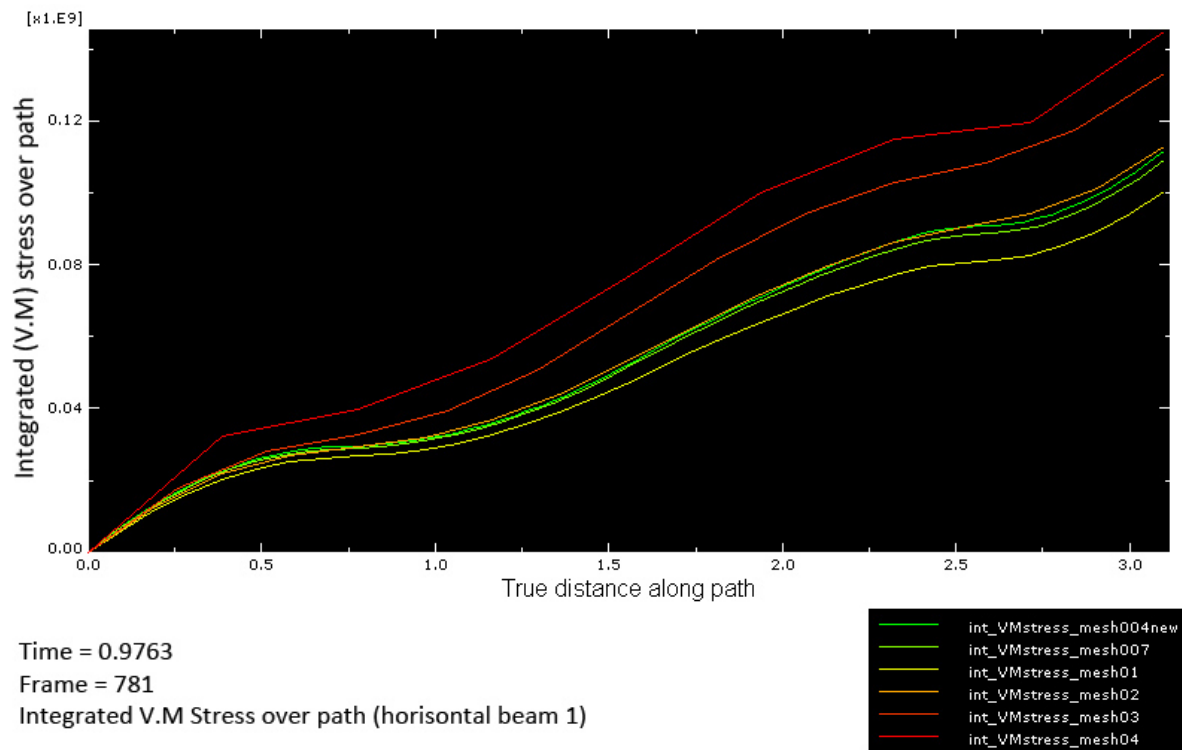


Figure H.1: Integrated Von-Mises stress along path, horizontal beam 1.

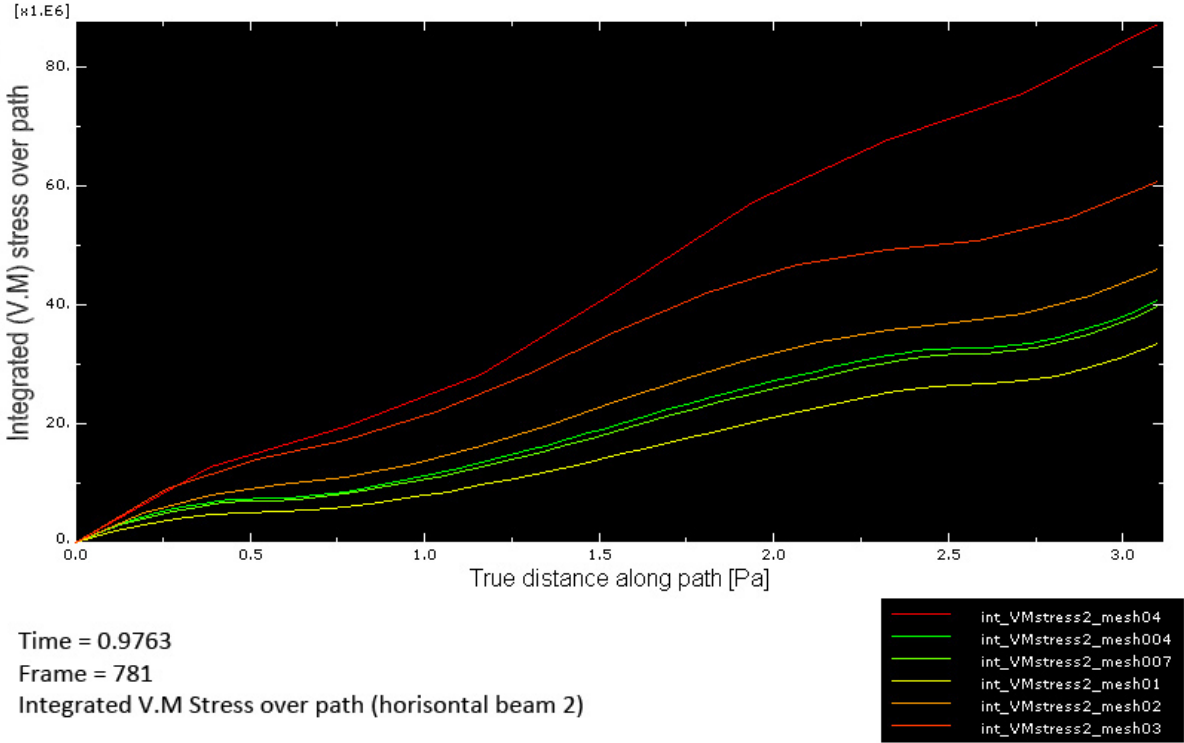


Figure H.2: Integrated Von-Mises stress along path, horisontal beam 2.

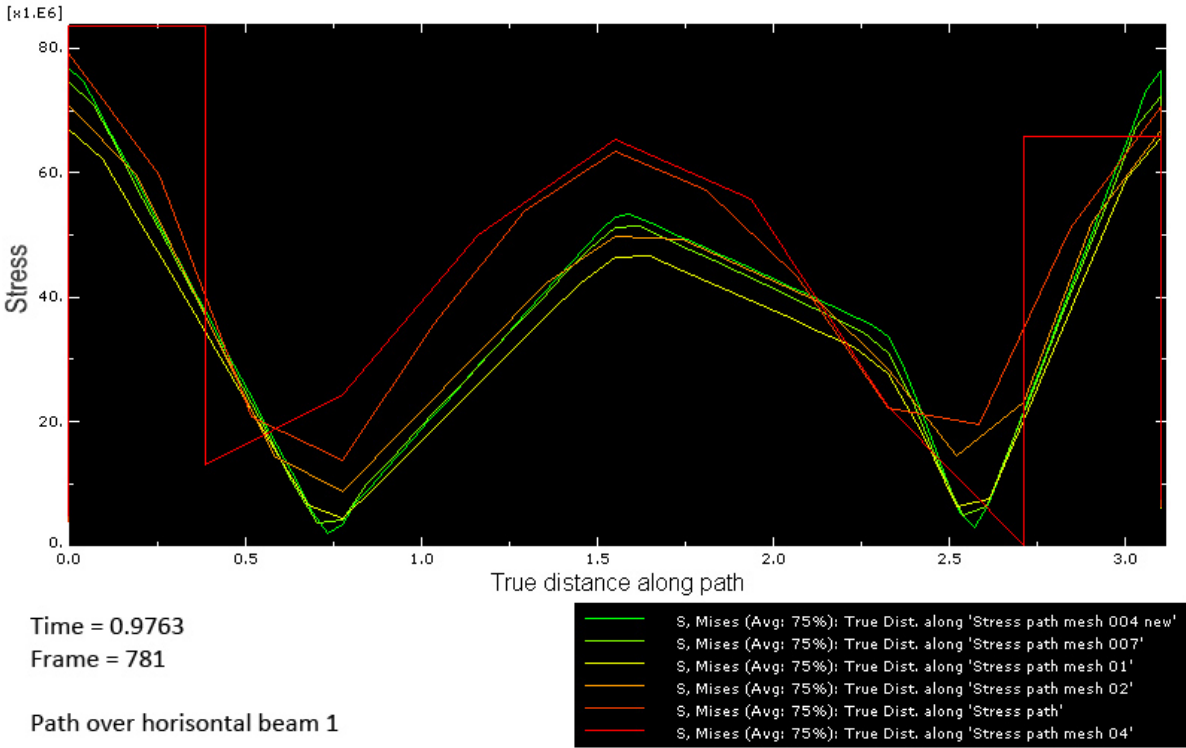


Figure H.3: Von-Mises stress variation along path, horizontal beam 1.

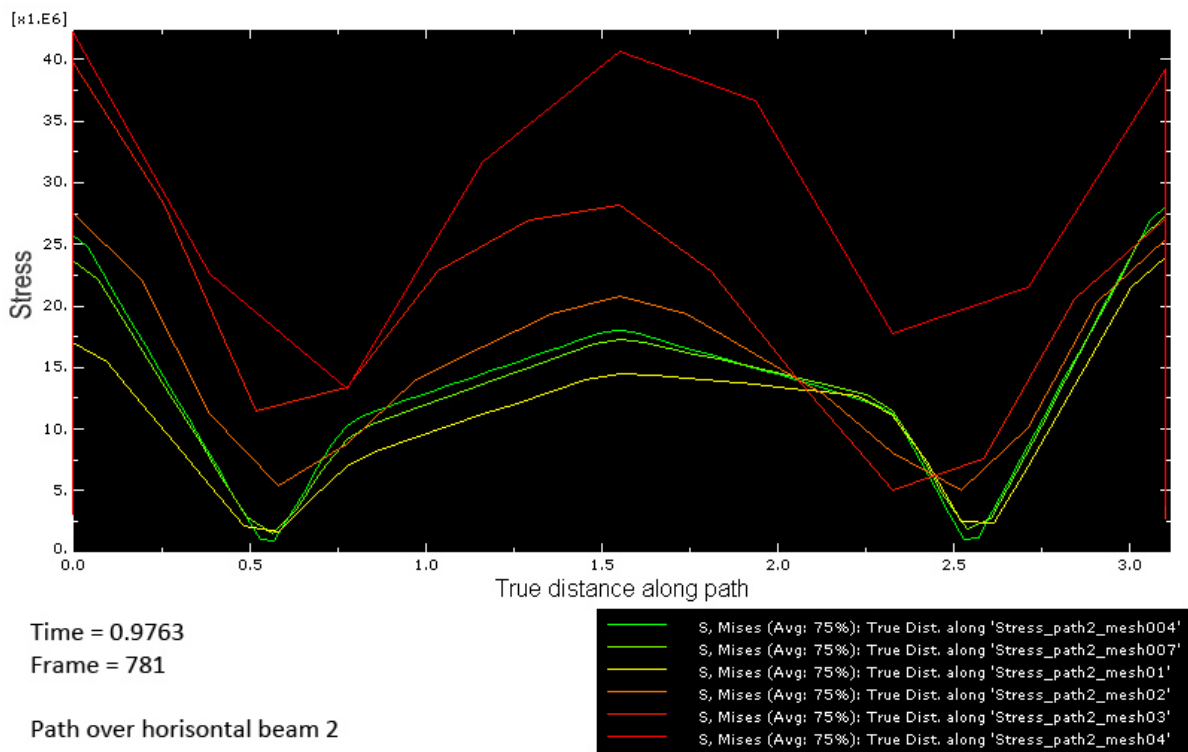


Figure H.4: Von-Mises stress variation along path, horizontal beam 2.

Appendix I

Matlab script: Read in data and calculate DAF.

```
1 %Master Thesis spring 2012 for Stud.Techn. Aiwei Su.
2 %The following file is to be used to calculate DAF (Dynamic ...
   amplification
3 %factors) based on RF (Reaction forces) on end connections on pipe ...
   racks:
4 %DAF=dynamic_RF_max/static_RF_max
5
6 infile1='RHS200_02bar_50ms_arr1.dat'; %Name of ODB result file, ...
   dynamic case
7 infile2='RHS200_02bar_static_arr1.dat'; %Name of ODB result file, ...
   static case
8 rows1=51;
9 rows2=2;
10 DAF=zeros(5,12);
11 DAF_SP1=zeros(2,12);
12 DAF_SP2=zeros(2,12);
13 DAF_SP3=zeros(2,12);
14 DAF_SP4=zeros(2,12);
15
16 %Writing the element numbers into the first row in the DAF matrix ...
   for the
17 %different section points.
18 Elem=[106,115,301,614,689,702,809,899,1111,1150,1175,1264];
19 DAF(1,:)=Elem;
20 DAF_SP1(1,:)=Elem;
21 DAF_SP2(1,:)=Elem;
22 DAF_SP3(1,:)=Elem;
23 DAF_SP4(1,:)=Elem;
24
```



```

25 %Using textread-function to read in the reaction forces (RF) over ...
    the blast
26 %duration. Each node (end connection) is denoted ...
    RFdyn_N'nodenumber'. Dynamic
27 %and static case:
28 [time1,dynE106_SP1,dynE115_SP1,dynE301_SP1,dynE614_SP1,dynE689_SP1,
29 dynE702_SP1,dynE809_SP1,dynE899_SP1,dynE1111_SP1,dynE1150_SP1,
30 dynE1175_SP1,dynE1264_SP1,dynE106_SP2,dynE115_SP2,dynE301_SP2,
31 dynE614_SP2,dynE689_SP2,dynE702_SP2,dynE809_SP2,dynE899_SP2,
32 dynE1111_SP2,dynE1150_SP2,dynE1175_SP2,dynE1264_SP2,dynE106_SP3,
33 dynE115_SP3,dynE301_SP3,dynE614_SP3,dynE689_SP3,dynE702_SP3,
34 dynE809_SP3,dynE899_SP3,dynE1111_SP3,dynE1150_SP3,dynE1175_SP3,
35 dynE1264_SP3,dynE106_SP4,dynE115_SP4,dynE301_SP4,dynE614_SP4,
36 dynE689_SP4,dynE702_SP4,dynE809_SP4,dynE899_SP4,dynE1111_SP4,
37 dynE1150_SP4,dynE1175_SP4,dynE1264_SP4] = textread(infile1,'%f\t
38 %f\t %f\t %f\t %f\t %f\t %f\t %f\t %f\t %f\t %f\t %f\t %f\t
39 %f\t %f\t %f\t %f\t %f\t %f\t %f\t %f\t %f\t %f\t %f\t %f\t
40 %f\t %f\t %f\t %f\t %f\t %f\t %f\t %f\t %f\t %f\t %f\t %f\t
41 %f\t %f\t %f\t %f\t %f\t %f\t %f\t %f\t %f\t %f',rows1,'headerlines',5);
42 [time2,statE106_SP1,statE115_SP1,statE301_SP1,statE614_SP1,
43 statE689_SP1,statE702_SP1,statE809_SP1,statE899_SP1,statE1111_SP1,
44 statE1150_SP1,statE1175_SP1,statE1264_SP1,statE106_SP2,statE115_SP2,
45 statE301_SP2,statE614_SP2,statE689_SP2,statE702_SP2,statE809_SP2,
46 statE899_SP2,statE1111_SP2,statE1150_SP2,statE1175_SP2,statE1264_SP2,
47 statE106_SP3,statE115_SP3,statE301_SP3,statE614_SP3,statE689_SP3,
48 statE702_SP3,statE809_SP3,statE899_SP3,statE1111_SP3,statE1150_SP3,
49 statE1175_SP3,statE1264_SP3,statE106_SP4,statE115_SP4,statE301_SP4,
50 statE614_SP4,statE689_SP4,statE702_SP4,statE809_SP4,statE899_SP4,
51 statE1111_SP4,statE1150_SP4,statE1175_SP4,statE1264_SP4] = textread(
52 infile2,'%f\t %f\t %f\t %f\t %f\t %f\t %f\t %f\t %f\t %f\t %f\t %f\t
53 %f\t %f\t %f\t %f\t %f\t %f\t %f\t %f\t %f\t %f\t %f\t %f\t %f\t
54 %f\t %f\t %f\t %f\t %f\t %f\t %f\t %f\t %f\t %f\t %f\t %f\t %f\t
55 %f\t %f\t %f\t %f\t %f\t %f\t %f\t %f\t %f\t %f',rows2,'headerlines',5);
56
57 %Calculating the DAF for SP1:
58 DAF_SP1(2,1) = max(dynE106_SP1)/max(statE106_SP1);
59 DAF_SP1(2,2) = max(dynE115_SP1)/max(statE115_SP1);
60 DAF_SP1(2,3) = max(dynE301_SP1)/max(statE301_SP1);
61 DAF_SP1(2,4) = max(dynE614_SP1)/max(statE614_SP1);
62 DAF_SP1(2,5) = max(dynE689_SP1)/max(statE689_SP1);
63 DAF_SP1(2,6) = max(dynE702_SP1)/max(statE702_SP1);
64 DAF_SP1(2,7) = max(dynE809_SP1)/max(statE809_SP1);
65 DAF_SP1(2,8) = max(dynE899_SP1)/max(statE899_SP1);
66 DAF_SP1(2,9) = max(dynE1111_SP1)/max(statE1111_SP1);
67 DAF_SP1(2,10) = max(dynE1150_SP1)/max(statE1150_SP1);
68 DAF_SP1(2,11) = max(dynE1175_SP1)/max(statE1175_SP1);
69 DAF_SP1(2,12) = max(dynE1264_SP1)/max(statE1264_SP1);
70
71 %Calculating the DAF for SP2:
72 DAF_SP2(2,1) = max(dynE106_SP2)/max(statE106_SP2);
73 DAF_SP2(2,2) = max(dynE115_SP2)/max(statE115_SP2);

```

```

74 DAF_SP2(2,3) = max(dynE301_SP2)/max(stateE301_SP2);
75 DAF_SP2(2,4) = max(dynE614_SP2)/max(stateE614_SP2);
76 DAF_SP2(2,5) = max(dynE689_SP2)/max(stateE689_SP2);
77 DAF_SP2(2,6) = max(dynE702_SP2)/max(stateE702_SP2);
78 DAF_SP2(2,7) = max(dynE809_SP2)/max(stateE809_SP2);
79 DAF_SP2(2,8) = max(dynE899_SP2)/max(stateE899_SP2);
80 DAF_SP2(2,9) = max(dynE1111_SP2)/max(stateE1111_SP2);
81 DAF_SP2(2,10) = max(dynE1150_SP2)/max(stateE1150_SP2);
82 DAF_SP2(2,11) = max(dynE1175_SP2)/max(stateE1175_SP2);
83 DAF_SP2(2,12) = max(dynE1264_SP2)/max(stateE1264_SP2);
84
85 %Calculating the DAF for SP3:
86 DAF_SP3(2,1) = max(dynE106_SP3)/max(stateE106_SP3);
87 DAF_SP3(2,2) = max(dynE115_SP3)/max(stateE115_SP3);
88 DAF_SP3(2,3) = max(dynE301_SP3)/max(stateE301_SP3);
89 DAF_SP3(2,4) = max(dynE614_SP3)/max(stateE614_SP3);
90 DAF_SP3(2,5) = max(dynE689_SP3)/max(stateE689_SP3);
91 DAF_SP3(2,6) = max(dynE702_SP3)/max(stateE702_SP3);
92 DAF_SP3(2,7) = max(dynE809_SP3)/max(stateE809_SP3);
93 DAF_SP3(2,8) = max(dynE899_SP3)/max(stateE899_SP3);
94 DAF_SP3(2,9) = max(dynE1111_SP3)/max(stateE1111_SP3);
95 DAF_SP3(2,10) = max(dynE1150_SP3)/max(stateE1150_SP3);
96 DAF_SP3(2,11) = max(dynE1175_SP3)/max(stateE1175_SP3);
97 DAF_SP3(2,12) = max(dynE1264_SP3)/max(stateE1264_SP3);
98
99 %Calculating the DAF for SP4:
100 DAF_SP4(2,1) = max(dynE106_SP4)/max(stateE106_SP4);
101 DAF_SP4(2,2) = max(dynE115_SP4)/max(stateE115_SP4);
102 DAF_SP4(2,3) = max(dynE301_SP4)/max(stateE301_SP4);
103 DAF_SP4(2,4) = max(dynE614_SP4)/max(stateE614_SP4);
104 DAF_SP4(2,5) = max(dynE689_SP4)/max(stateE689_SP4);
105 DAF_SP4(2,6) = max(dynE702_SP4)/max(stateE702_SP4);
106 DAF_SP4(2,7) = max(dynE809_SP4)/max(stateE809_SP4);
107 DAF_SP4(2,8) = max(dynE899_SP4)/max(stateE899_SP4);
108 DAF_SP4(2,9) = max(dynE1111_SP4)/max(stateE1111_SP4);
109 DAF_SP4(2,10) = max(dynE1150_SP4)/max(stateE1150_SP4);
110 DAF_SP4(2,11) = max(dynE1175_SP4)/max(stateE1175_SP4);
111 DAF_SP4(2,12) = max(dynE1264_SP4)/max(stateE1264_SP4);
112
113 %Collecting all DAFs for for an element (i.e SP1,2,3 and 4) in one ...
    place:
114 DAF(2,:) = DAF_SP1(2,:);
115 DAF(3,:) = DAF_SP2(2,:);
116 DAF(4,:) = DAF_SP3(2,:);
117 DAF(5,:) = DAF_SP4(2,:);
118
119 %xlswrite('DAF_temp.xlsx',DAF) %Writing the result matrix into Excel ...
    file.

```